THERMAL PERFORMANCE OF HELIUM-COOLED DIVERTORS FOR MAGNETIC FUSION APPLICATIONS

A Thesis
Presented to
The Academic Faculty

by

James Brandon Weathers

In Partial Fulfillment
of the Requirements for the Degree
Master of Science in the
School of Mechanical Engineering

Georgia Institute of Technology
August 2007

THERMAL PERFORMANCE OF HELIUM-COOLED DIVERTORS FOR MAGNETIC FUSION APPLICATIONS

Approved by:

Dr. Said I. Abdel-Khalik, Advisor
School of Mechanical Engineering
Georgia Institute of Technology

Dr. Minami Yoda
School of Mechanical Engineering
Georgia Institute of Technology

Dr. S. Mostafa Ghiaasiaan
School of Mechanical Engineering
Georgia Institute of Technology

Date Approved: June 11, 2007

ACKNOWLEDGEMENTS

I would like to thank my advisor, Dr. Said Abdel-Khalik for his guidance and support throughout this thesis. I will always be grateful of the opportunity that he provided for me to work with his research group during my time at Georgia Tech. I would also like to thank my committee members, Dr. Minami Yoda and Dr. Mostafa Ghiaasiaan for their contributions to this thesis.

The time and advice that Lorenzo Crosatti provided to this project has been invaluable. I greatly appreciate his willingness and enthusiasm to work with me throughout this project.

The expertise of Mr. Dennis Sadowski in the design and construction of the experimental test section is sincerely appreciated. His efforts were a cornerstone to the timely completion of this project.

Furthermore, I would like to thank the Forschungszentrum Karlsruhe for their funding in support of this research project. I particularly appreciate the support of Regina Kruessmann.

I would also like to thank all of my laboratory colleagues for their advice and support: Chih-Cheih Hu, Tim Koehler, Celine Lascar, and Bo Lu.

Most importantly, I am grateful for the support of my family. All that I may achieve will be built on the foundation of their efforts and labor. The example that has been set by my parents and especially my grandfather, James M. Weathers Sr., has been an important source of guidance for my life.

TABLE OF CONTENTS

LIST OF TABLES

LIST OF FIGURES

LIST OF SYMBOLS AND ABBREVIATIONS

A	Area (m^2, mm^2)
c	Specific heat (J/(kg-K))
D	Diameter (m, mm)
dP	Pressure drop across the test section (kPa, MPa, psi)
HTC	Heat transfer coefficient ($W/(m^2-K)$)
k	Thermal conductivity (W/(m-K))
m	Mass flow rate (g/s)
Ma	Mach number
MFR	Mass flow rate (g/s)
Nu	Nusselt number
P	Pressure (kPa, psi)
Q	Heater power input (W)
q"	Heat flux (MW/m^2)
Re	Reynolds number
SS	Stainless steel
T	Temperature (^oC, K)
TI	Thermocouple reference location 1
T2	Thermocouple reference location 2
T3	Thermocouple reference location 3
T4	Thermocouple reference location 4
T5	Thermocouple reference location 5

T6	Thermocouple reference location 6
T7	Thermocouple reference location 7
T8	Thermocouple reference location 8
T9	Thermocouple reference location 9
U	Uncertainty

Greek Letters

Θ	Azimuthal angular position (degrees)
μ	Dynamic viscosity (kg/(m-s))
ρ	Density (kg/m^3)
σ	Standard deviation

Subscripts

Brazing	Brazing surface of the copper heater block and brass thimble
Embedded	Physical thermocouple location in the brass thimble
Experimental	Experimentally measured/calculated quantity
f	Film
In	Inlet
Jet	Central jet
Jets	All jets
max	Maximum
nominal	No heat loss due to convection

Out	Outlet
Surface	Projected thermocouple location on the "cooled surface" of the brass thimble

SUMMARY

The heat transfer performance of the Helium-cooled Multi-jet (HEMJ) divertor was investigated. The HEMJ design uses impinging jets to significantly enhance its heat transfer capability. The convective heat transfer coefficient predicted by computational fluid dynamics software packages is on the order of 50,000 W/(m^2-K). The high predicted values of the convective heat transfer coefficient necessitated experimental validation, which was the focus of this investigation.

A test section which simulates the thermal performance of the HEMJ divertor was designed, constructed, and instrumented for testing an in air flow loop. The operating conditions of the air flow loop were chosen to match the non-dimensional operating conditions expected for the HEMJ divertor in a post-ITER fusion power plant. The air flow loop experiments were performed for mass flow rates of 2.0 g/s to 8.0 g/s and with incident nominal heat fluxes of 0.8 MW/m^2 and 1.0 MW/m^2. The angular variation of the heat transfer coefficient was also investigated. Numerical simulations which matched the experimental operating conditions were performed using the computational fluid dynamics software package, FLUENT® 6.2. Comparisons of the experimental and numerical pressure drop, temperature, and heat transfer coefficient were made. The experimental results agreed with the numerical predictions for all operating conditions in this investigation. This provided a strong degree of confidence in using the FLUENT® software package to analyze the HEMJ divertor design.

CHAPTER I

INTRODUCTION

1.1 Motivation and Objectives

1.1.1 Magnetic Confinement Fusion Energy

Generating electricity through the process of fusion has many desirable attributes that justify its continued research. If the fusion process can economically generate a net power output, it would do so using an abundant fuel source and without emitting greenhouse gas byproducts. The premise of releasing energy by fusion is that low atomic weight elements are brought together at high temperature and density such that they form a heavier element and release energy. The reaction involving deuterium (D), an isotope of hydrogen containing one proton and one neutron, reacting with tritium (T), an isotope of hydrogen containing one proton and two neutrons, to produce helium, a neutron, and 17.6 MeV of energy has the lowest input energy requirement [1]. This reaction occurs in the following manner:

$$D + T \rightarrow {}^{4}He + n + 17.6\ MeV$$

To achieve this reaction, the required high temperatures ionize the atoms to form a plasma. This plasma must be confined at a high density such that the ionized deuterium

and tritium undergo the above mentioned reaction at a high enough rate to produce a useful energy source. Several methods of confinement exist. The most familiar form of confinement is gravitational. It is the process by which stars achieve the high temperature and density requirements for fusion, although with a different reaction. The two most promising man-made confinement methods are inertial confinement and magnetic confinement. Inertial confinement uses inertial forces to confine and compress the reacting elements to the extremely high pressures and temperatures required to achieve fusion [2]. This method utilizes high energy laser or ion beams to compress small, frozen deuterium and tritium targets. Magnetic confinement uses a magnetic field to hold the plasma together while it is heated by microwaves, neutral beam injection, and the fusion products. This method has been chosen for the ITER reactor which is scheduled to be built in Cadarache, France. It is also the method that will be used in the post-ITER reactor, DEMO. This thesis pertains to a proposed heat removal system of the divertor for the DEMO reactor.

1.1.2 Proposed Divertor

During the operation of a fusion reactor, fusion reaction ash (α-particles) and eroded particles from the reactor become present in the plasma. These products and unburned fuel reduce the quality of the plasma and hinder further fusion reactions [3]. In magnetic confinement reactors, divertors are used to remove these unwanted products from the plasma. Electromagnetic fields are used to pull these particles from the plasma and focus them onto a target called the divertor. The incident surface heat load distribution on the divertor depends on the surface topology, location, reactor type, and

plasma conditions; peak surface heat fluxes on the order of 10 MW/m^2 are expected [3]. A significant fraction (~15%) of the total fusion thermal power is removed by the divertor coolant. Helium has been proposed as the divertor coolant primarily because of its compatibility with a variety of blanket concepts due it is chemical inertness and because of its ability to operate at high temperatures, which enhances the thermal efficiency of the power conversion systems [3].

The Karlsruhe Research Center (FZK) in Karlsruhe, Germany has proposed several divertor designs which are capable of withstanding the required incident heat load of 10 MW/m^2 using helium with an inlet temperature of 600 ^{o}C and at a pressure of 10.0 MPa. The leading design relies on enhancement of the convective heat transfer coefficient through the use of multiple impinging jets. This design is called the Helium-cooled Multi-Jet (HEMJ) divertor. The plasma-facing target is a tungsten armor plate which is attached to a tungsten-alloy (WL10) cap. A cylindrical steel cartridge that has twenty-four 0.6 mm diameter holes which surround a single 1.0 mm diameter hole in the center is secured below the cap (Figure 1.1). Helium enters the cartridge and is accelerated through the twenty-five holes to create a jet impingement on the capped inner surface of the tungsten alloy. Downstream of the jet impingement location, the helium forms a turbulent wall jet along the surface of the cap (Figure 1.2). The helium then exits the divertor at approximately 700 ^{o}C by flowing through a 0.9 mm gap between the cartridge and the cap.

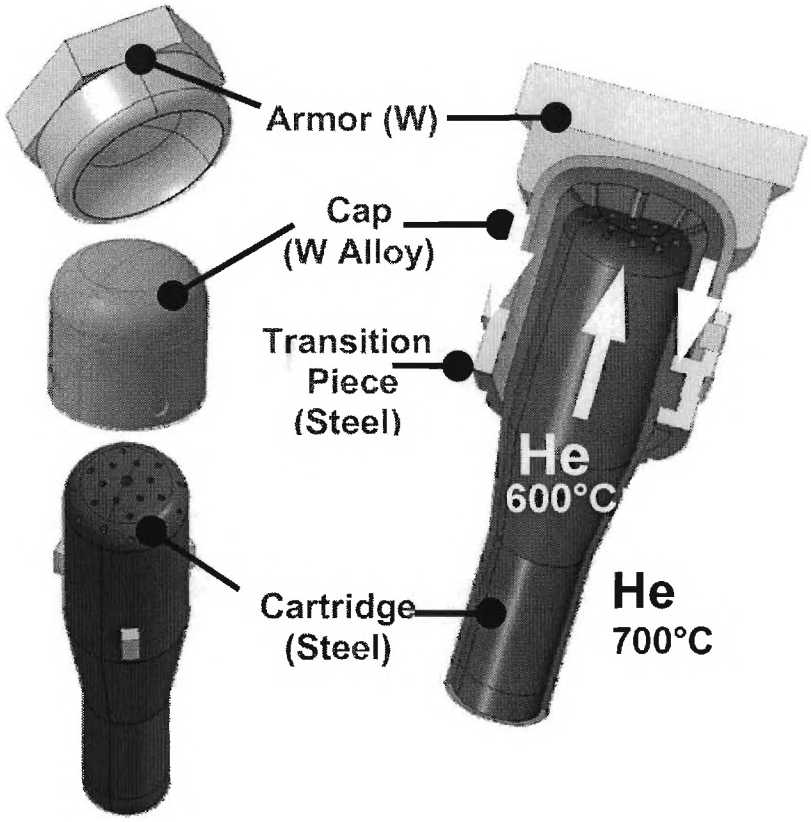

Figure 1.1: Diagram of the HEMJ divertor [4].

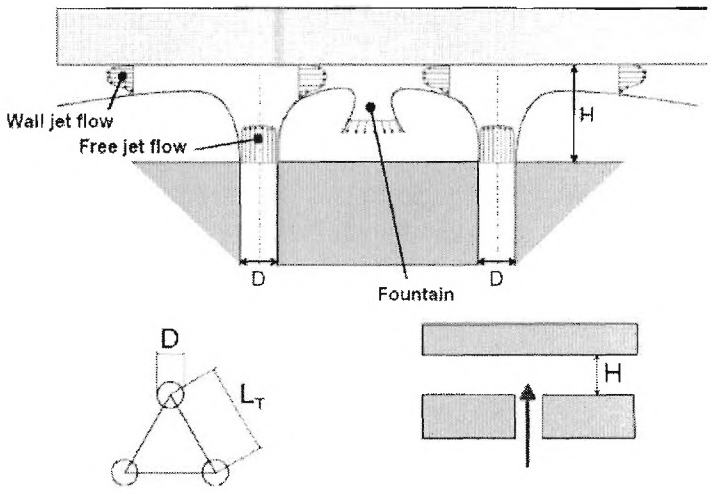

Figure 1.2: Diagram of the impinging jet cooling method [5].

Numerical and experimental analyses have been performed at FZK to characterize the divertor geometry, select appropriate materials, simulate heat removal capability, and develop high tolerance manufacturing of the proposed HEMJ divertor [5]. Parametric analyses were performed to determine the sensitivity of the design to changes in geometry and operating conditions. Further experimental tests of the HEMJ divertor are needed to validate the heat removal capability predicted by computational fluid dynamics (CFD) software packages. These experimental tests are necessary because the high convective heat transfer coefficient (~50,000 W/(m^2-K)) predicted near the impinging jets is out of the experience base of high power density gas-cooled components. To experimentally validate the HEMJ divertor design, a test module that closely simulates the thermal-hydraulic behavior of the helium-cooled HEMJ divertor was designed, constructed, and instrumented for testing in an air flow loop at the Georgia Institute of Technology. Upon successful operation in the air flow loop, the HEMJ divertor test section will undergo similar testing in the helium flow loop at FZK (HEBLO Test Facility). The operating conditions of the air flow loop have been selected to match the non-dimensional parameters expected for the HEBLO Test Facility. Since the geometry of the divertor test module exactly matches the geometry that will be used in the HEBLO Test Facility, the most important non-dimensional parameter is the Reynolds number based on the 1.0 mm diameter central jet.

$$\mathrm{Re}_{jet} = \frac{\dot{m} D_{jet}}{A_{jets} \mu_{in}}$$

$\dot{m}$ = mass flow rate $\quad A_{jets}$ = area of the jets

D_{jet} = jet diameter $\quad \mu_{in}$ = dynamic viscosity at the inlet

The Reynolds number of the central jet expected for the HEMJ test section in the HEBLO Test Facility corresponding to its nominal operating conditions is 21,400. Table 1.1 details the nominal operating conditions of the HEMJ divertor in the DEMO reactor, the HEBLO Test Facility at FZK, and the air flow loop at the Georgia Institute of Technology. The difference between the Prandtl numbers of air (0.74) and helium (0.66) is deemed to have a small effect on the measured Nusselt number and thus the convective heat transfer coefficient.

Table 1.1: Comparison of nominal operating conditions for the three scenarios.

Coolant	T_{in}	P_{in}	μ	Heat Flux	Flow Rate	Re_{jet}
	[°C]	[MPa]	[kg/m-s] x 10^{-5}	[MW/m^2]	[g/s]	[-]
He (DEMO)	634	10.0	4.16	10.0	6.80	21400
He (HEBLO)	35	8.0	2.04	2.0	3.33	21400
Air (GT)	20	0.724	1.85	1.0	3.03	21400

1.1.3 Objectives

This Master's thesis aims to experimentally validate the high convective heat transfer coefficient of the impinging jets for the HEMJ divertor design. The investigation will be performed by comparing numerical results from the computational fluid dynamics software package, FLUENT®, to experimental data obtained from the air flow loop tests. Experimental data were collected over a wide range of operating conditions that span mass flow rates from 2.0 g/s to 8.0 g/s and nominal heat fluxes of 0.8 MW/m^2 and 1.0 MW/m^2.

To simulate the thermal-hydraulic behavior of the HEMJ divertor under its anticipated operating conditions, a test section design which yields a uniform surface heat

flux on the armor top referenced in Figure 1.1 was required. This was achieved by using a 117 mm long cylindrical copper heater block which contracts from a 50 mm diameter region, containing an electric heater, to a 17 mm diameter "neck" region. In the "neck" region of the copper heater block a very uniform radial temperature distribution and thus heat flux is created. For the test section, the armor and cap pieces of the HEMJ divertor are combined into a single piece of brass, called the thimble. Brass has been selected since its thermal conductivity nearly matches that of the tungsten alloy used to construct the HEMJ divertor. The top of the thimble was brazed to the "neck" end of the copper heating block. The proposed HEMJ divertor test section (Figure 1.3) was built and instrumented to span the desired non-dimensional parameter range in the air flow loop corresponding to the conditions of the test section in the HEBLO Test Facility, which, in turn, were chosen to match the expected operating conditions of the HEMJ divertor in the DEMO reactor.

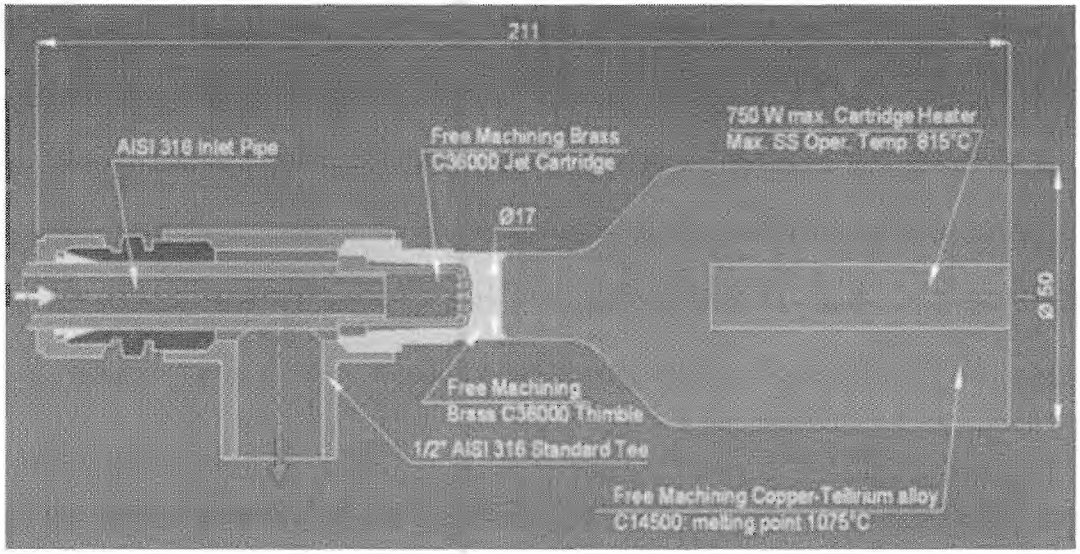

Figure 1.3: Diagram of the HEMJ divertor test section

Several parameters are of interest for successful validation of the heat transfer coefficient for the HEMJ divertor design. The azimuthal variation of the convective heat transfer coefficient is important due to the high power density anticipated during operation. The behavior of the heat transfer coefficient under varying flow rates and incident heat fluxes is also important for a robust design. Additionally, agreement between the predicted and measured pressure drop is desired.

1.2 Literature Review

1.2.1 Post-ITER Helium-cooled Divertor Designs

The fusion power plant demonstration reactor envisioned to be constructed after ITER would shift the primary focus past experimental work and towards the ultimate application of electricity generation. In power plant designs, a high thermal efficiency and thus high temperature coolant is desired. Helium appears to be the most suitable coolant due to its chemical and neutronic inertness [6]. It is compatible with materials such as beryllium, lithium, and lead that are anticipated for future fusion power plants [7]. Helium is also easily integrated into a gas turbine cycle power cycle [7]. Using a gas coolant requires significant heat transfer enhancement to withstand peak incident heat fluxes of 10 MW/m^2. Several methods of enhancing the heat transfer coefficient of helium-cooled divertors have been proposed and studied (Table 1.2).

Table 1.2: Comparison of Divertor Cooling Designs (* refers to a maximum local value)

Concept	Heat Flux [MW/m^2]	HTC [W/(m^2-K)]	Pressure [MPa]	T_{in} [°C]	T_{out} [°C]	Reference(s)
Porous Medium	5.5	20,000	8	632	800	8
Multi-channel	5.0	20,000	14	500	551	8
Eccentric Swirl	5.0	21,000	14	600	800	8
Slot	5.0	14,000	14	600	800	8
Modified Slot	10.0	56,000*	10	640	712	9,10
T-tube	10.0	40,000*	10	600	680	3
HETS	10.0	30,000	10	600	669	11
		55,000*				
HEMP	10.0	35,000	10	600	700	12
		56,000*				10
HEMS	10.0	24,000	10	634	713	13
		43,000*				
HEMJ	10.0	31,000	10	630	700	5
		57,000*				

1.2.2 Porous Medium Concept

Heat transfer enhancement through the use of a porous medium has been proposed as a method capable of withstanding an incident heat flux of up to 5.5 MW/m^2 [8,12]. The heat transfer enhancement is primarily due to two factors. First, the cooling surface area is greatly increased in a small volume by the use of a porous medium. Second, the irregular coolant flow pattern due to the porous medium enhances the turbulent mixing and thus the heat transfer capability [14]. This design utilizes helium at 8 MPa with an inlet temperature of 632 °C and an exit temperature of 800 °C [8]. The typical effective heat transfer coefficient is 20,000 W/(m^2-K) [8]. The flow configuration

forces helium through a slot at the top of the coolant inlet tube into a circular porous wick that has a void fraction of 40% [8]. The helium travels through the wick around the outer circumference of the coolant outlet tube before exiting through a slot on its bottom (Figure 1.4). The coolant in the porous medium heats up in the circumferential direction due to the local energy deposition rather than accumulating heat along the entire channel length [8]. This feature is desirable for non-uniform heating profiles [8]. To balance the flow velocities, the coolant inlet tube flow area is decreased while the coolant outlet tube flow area is increased along the length of the divertor channel (Figure 1.5). A molybdenum or tungsten alloy is the proposed material for constructing this divertor channel. Since this enhancement method relies partially on an increased surface area, it depends on the thermal conductivity of the materials used for the porous medium [6].

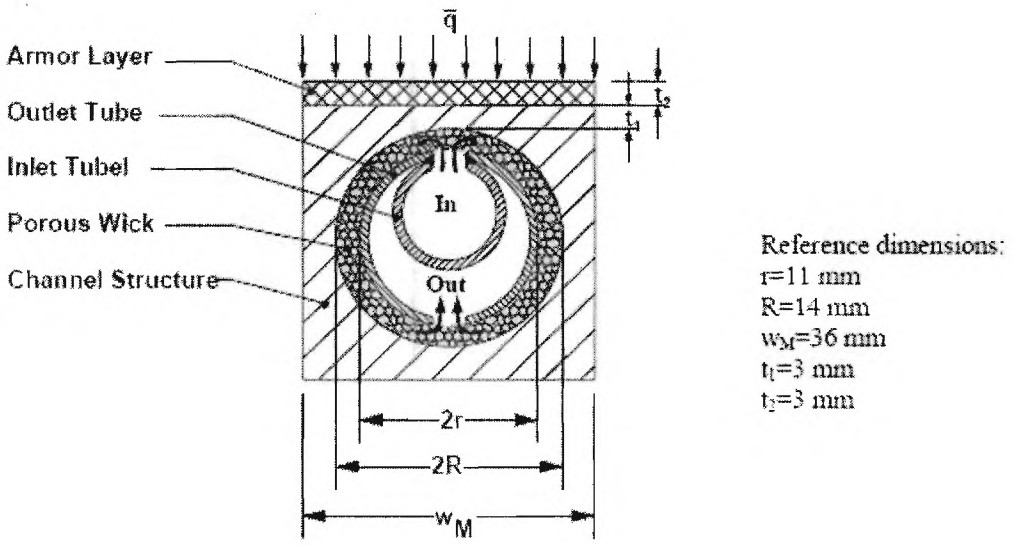

Figure 1.4: Cross-section of the porous medium concept [8]

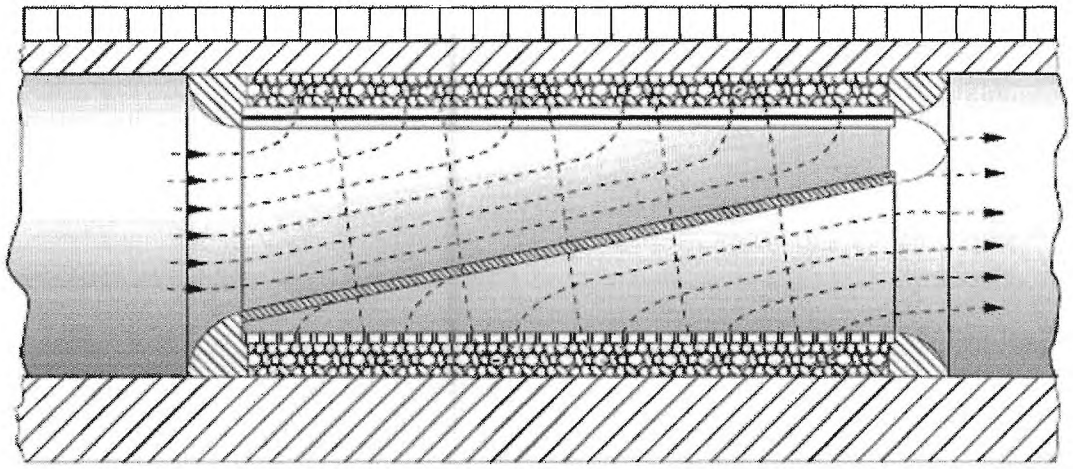

Figure 1.5: Longitudinal view of the porous medium concept [8]

1.2.3 Multi-channel Concept

The multi-channel divertor concept sought to minimize thermal stresses by reducing the temperature difference across the divertor channel [8]. This design can withstand an incident heat flux of 5 MW/m^2 when it is operated at 14 MPa with helium input at 500 °C. The typical effective heat transfer coefficient is 15,000 to 20,000 $W/(m^2-K)$ [8]. A double-wall coolant pipe is divided into halves with an insert to create a cold leg that consists of four sub-channels and a hot leg consisting of a single channel (Figure 1.6). The heat transfer coefficient is enhanced by the larger coolant velocities through the sub-channels of the cold leg. The larger relative hydraulic diameter of the hot leg section helps minimize the pressure drop across the channel [8]. However, the exit temperature of 551 °C does not offer an ideal input to the gas turbine power conversion system.

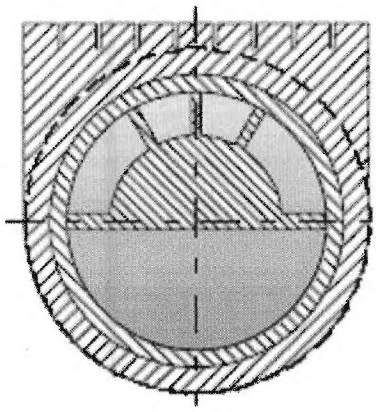

Figure 1.6: Cross-section of the multi-channel concept [8]

1.2.4 Eccentric Swirl Promoter Concept

The eccentric swirl promoter concept enhances the heat transfer coefficient by increasing the coolant velocity on the heated side of the coolant channel. A non-axisymmetric insert with helical fins that vary periodically around the spiral direction of the coolant channel is used to create the enhancement (Figure 1.7). This design is capable of withstanding an incident heat flux of 5 MW/m^2 when operated with helium at 14 MPa [8]. Helium enters the coolant channel at 600 °C and is heated to 800 °C [8]. An effective heat transfer coefficient of 21,000 $W/(m^2\text{-}K)$ can be obtained with this design [8].

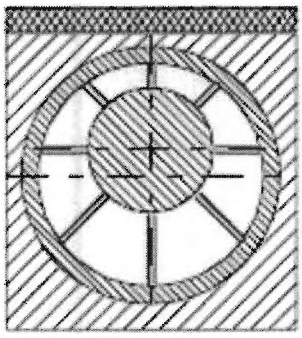

Figure 1.7: Cross-section of the eccentric swirl promoter concept [8]

1.2.5 Slot Concept

The slot concept evolved from the porous medium design. Rather than having the coolant flow circumferentially through a porous medium, a narrow gap of 0.1 to 0.2 mm is used. This improves the manufacturing of the coolant channel and eliminates bonding issues of the porous medium [8]. The coolant channel diameters are tapered longitudinally in the same manner as for the porous medium design (Figure 1.5). With helium input at 600 °C and 14 MPa, the slot concept is able to withstand an incident heat flux of 5 MW/m^2 and deliver helium at 800 °C [8]. The typical effective heat transfer coefficient is 14,000 W/(m^2-K) [8].

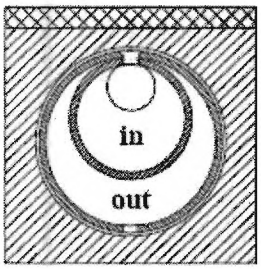

Figure 1.8: Cross-section of the slot concept [8]

An enhanced version of the slot design that increases the peak heat flux capability to 10 MW/m^2 has been proposed [9,10]. The modified design uses a narrow gap of 0.1 mm thickness to increase the coolant velocity upon exiting the inlet channel. The coolant then passes through an array of cylindrical studs and into the outlet channel. The maximum local heat transfer coefficient expected from the modified slot design is 56,000 W/(m^2-K) [10].

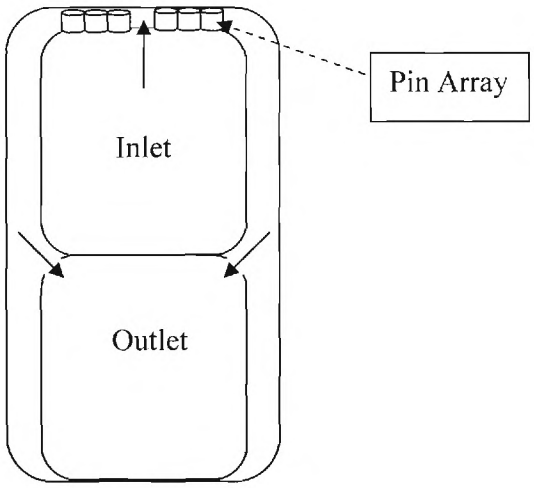

Figure 1.9: Cross-section of the modified slot concept

1.2.6 T-Tube concept

Building upon the slot concept, the T-tube divertor channel design was developed. The slot through which the coolant leaves the inlet channel was changed to 0.5 mm with the goal of creating a slot jet impingement on the heated surface. This jet impingement greatly enhances the heat transfer coefficient near the stagnation point. Maximum local heat transfer coefficients in excess of 40,000 W/(m^2-K) are predicted near the stagnation point for operation with helium at 10 MPa and an inlet temperature of 600 °C [3]. This design is capable of withstanding an incident heat flux of 10 MW/m^2 and delivering helium at 680 °C [3]. The T-tube design maintains a constant coolant inlet and outlet channel diameter. For each T-tube module, the helium enters at the center and flows to each end before impinging on the heated surface through the narrow slit. It then flows between the outer wall of the inlet coolant channel and the inner wall of the outlet coolant channel while being forced back towards the center of the module for its exit (Figure 1.10). The high heat transfer coefficient predicted for this design has been experimentally

validated with an air coolant corresponding to the non-dimensional parameters anticipated for its helium operating conditions [3]. A benefit of the T-tube design is that it can be integrated into a manifold rather easily [15].

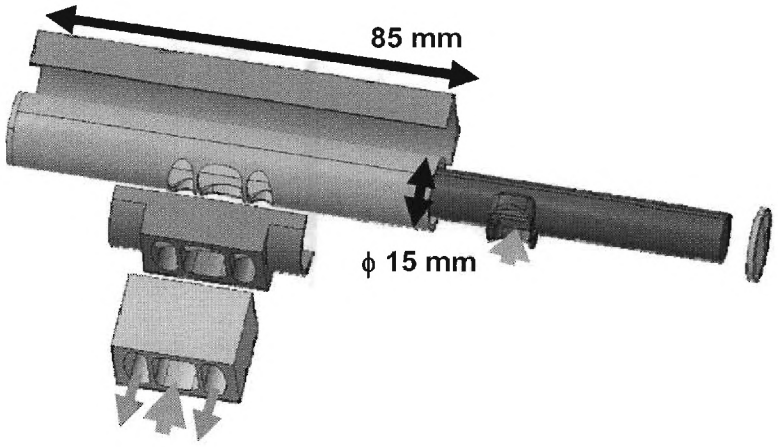

Figure 1.10: Diagram of the T-tube module [15]

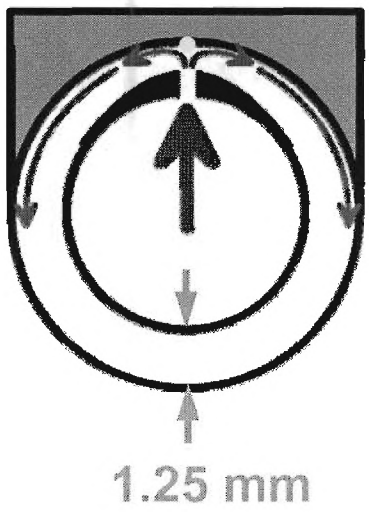

Figure 1.11: Cross-section of the T-tube module [15]

1.2.7 High Efficiency Thermal Shield Concept

The high efficiency thermal shield (HETS) concept also enhances the heat transfer coefficient by creating a jet impingement on the heated surface. This design is based on an axi-symmetric cap geometry in which a single jet impinges on a curved heated surface upon exiting a 7 mm diameter nozzle [16]. The coolant then flows down the differential area between the inner nozzle structure and the cap (Figure 1.12). The HETS design was originally developed for a water coolant, but has been adopted for using a helium coolant [16]. It is capable of sustaining an incident heat flux of 10 MW/m^2 when operating at 10 MPa with an inlet temperature of 600 °C [11]. The HETS concept achieves an exit temperature of 669 °C [11]. The maximum local heat transfer coefficient for the HETS concept is predicted to be approximately 55,000 - 60,000 $W/(m^2\text{-}K)$ [16, 17] and the typical effective value is 30,000 $W/(m^2\text{-}K)$ [11].

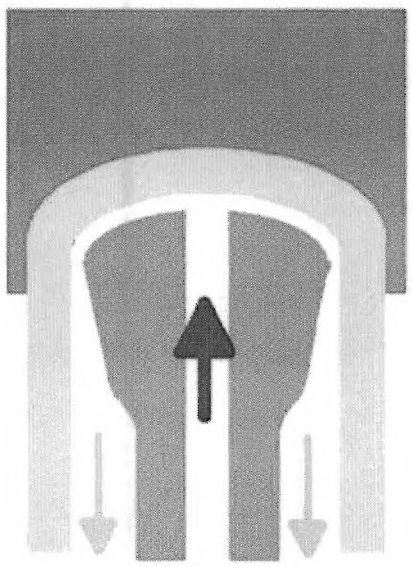

Figure 1.12: Cross-section of the HETS concept [11]

1.2.8 Helium-cooled Modular Divertor Concept with Pin Array

The helium-cooled modular divertor concept with pin array (HEMP) is a variant of the modular cap geometry that is used for the HETS concept. Rather than use the jet impingement method for heat transfer enhancement, the coolant is forced through a staggered tungsten pin array (Figure 1.13). The staggered pin array enhances the heat transfer capability by increasing the surface area and promoting turbulent mixing [18]. This method of heat transfer enhancement results in a predicted maximum local heat transfer coefficient of 56,000 W/(m^2-K) in reference to the modified slot design's use a pin array [10] or 35,000 W/(m^2-K) due to widely extrapolated data from measurements [12]. It is capable of withstanding an incident heat flux of 10 MW/m^2 for helium at 10 MPa and an inlet temperature of 600 °C. The HEMP module can deliver helium at an exit temperature of approximately 700 °C [13]. A challenge for the HEMP module is the effect of manufacturing tolerances on the pin array.

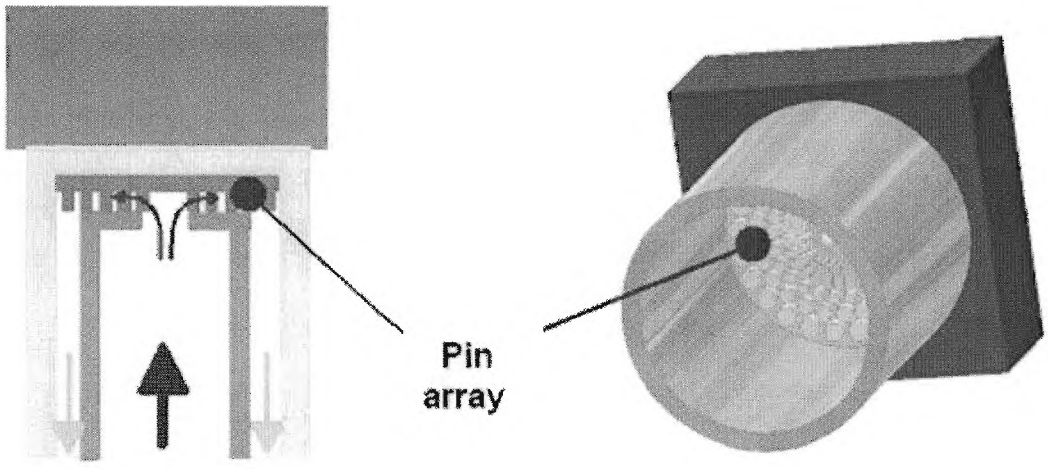

Figure 1.13: Diagram of the HEMP concept [5]

1.2.9 Helium-cooled Modular Divertor Concept with Slot Array

A proposed improvement upon the HEMP concept is the helium-cooled modular divertor with slot array (HEMS). The HEMS concept uses a tungsten flow promoter in the form of radial slots to increase the surface area and thus enhance the heat transfer capability [13]. Similar to the HEMP design, the coolant enters the slot array from the center of the module. After flowing outward in the radial direction it exits the module by flowing down the differential area between the inlet channel and outer support structure (Figure 1.14). The HEMS concept is capable of withstanding an incident heat flux of 10 MW/m^2 under operating conditions of 10 MPa and a helium inlet temperature of 634 °C. The maximum local heat transfer coefficient predicted for this design is 43,000 $W/(m^2\text{-}K)$ and the average effective value is 24,000 $W/(m^2\text{-}K)$ [13]. The HEMS design is capable of delivering helium at an outlet temperature of 713 °C [13].

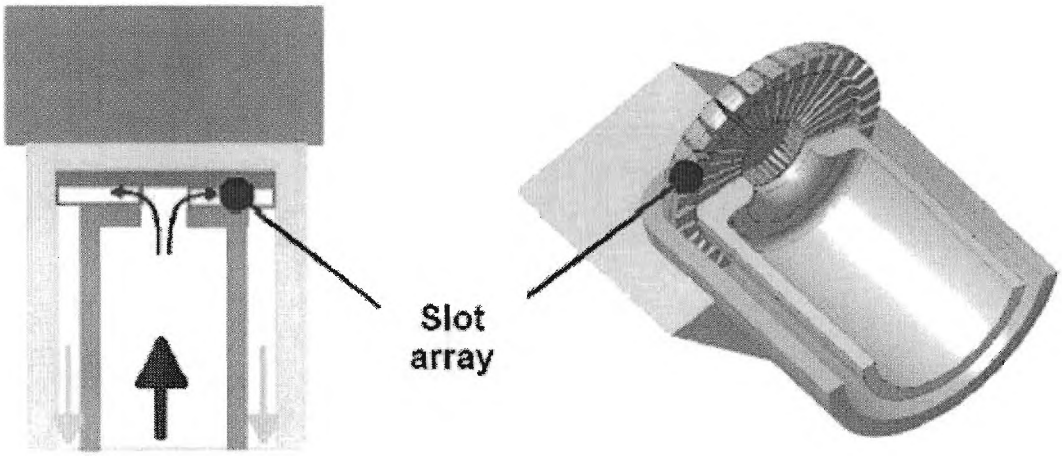

Figure 1.14: Diagram of the HEMS concept [5]

CHAPTER II

EXPERIMENTAL APPARATUS AND PROCEDURES

2.1 Experimental Test Section

The HEMJ divertor test section used to verify the numerical results mentioned in subsection 1.1.3 is described in this section. The section is organized as follows: Subsection 2.1.1 describes the details of the jet cartridge, subsection 2.1.2 describes the details of the thimble, subsection 2.1.3 describes the details of the copper heater block, subsection 2.1.4 describes the assembly of the HEMJ divertor test section, and subsection 2.1.5 describes the flow loop.

2.1.1 Jet Cartridge

The jet cartridge was constructed from free machining brass C360 to a height of 28.4 mm and an inner diameter of 9.54 mm by the Georgia Tech Research Institute (Figure 2.2). It has twenty-four holes of 0.6 mm diameter that form four concentric "bolt" circles (Table 2.1). Each "bolt" circle consists of 6 holes evenly spaced at 60° increments. Alternating "bolt" circles have their holes offset by 30° from the previous "bolt" circle. A 1.0 mm diameter hole was placed at the center of the jet cartridge. Three 2.0 mm sectors extend from the bottom of the jet cartridge and are used to secure it in the 2.0 mm thimble indention. This ensures a 0.9 mm gap between the jet cartridge and the thimble.

Each sector has an azimuthal extent of 30°. The jet cartridge is connected to the end of a 150 mm long tube made of 10.0 mm OD thin-walled SS 316 tubing using a high temperature epoxy.

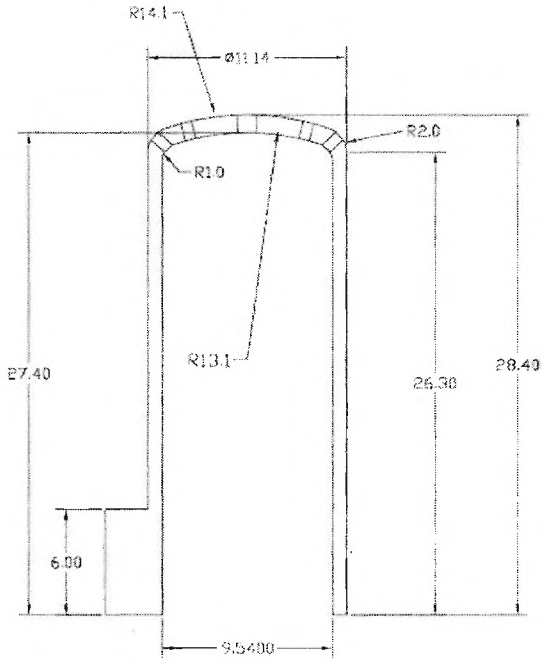

Figure 2.1: Drawing of the jet cartridge from AutoCad 2006.

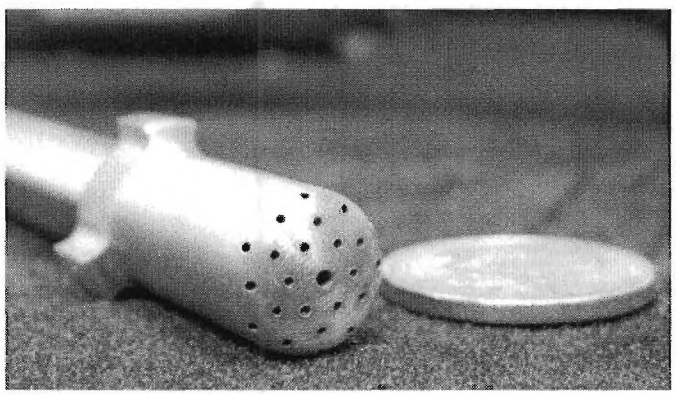

Figure 2.2: Photograph of the manufactured jet cartridge. A nickel beside the jet cartridge indicates the scale.

Table 2.1: Jet cartridge "bolt" circle radii.

"Bolt" Circle	Projected Radius [mm]
1	2.22
2	3.52
3	4.77
4	6.49

2.1.2 Thimble

The 36.3 mm long thimble with an inner-diameter of 12.94 mm is made of brass C360. It is instrumented with four 0.5 mm diameter OMEGA Type-E thermocouples. The thermocouple probes are inserted at varying depths and offset by 90° from each other (Figure 2.3) to allow measurements of the cooled surface temperature distribution. Table 2.1 provides the labeling convention of these thermocouples.

Table 2.2: Thimble Thermocouple Depths and Reference Numbers

Thermocouple Reference	Thermocouple Depth (mm)
1	2.08
2	4.20
3	6.40
4	8.50

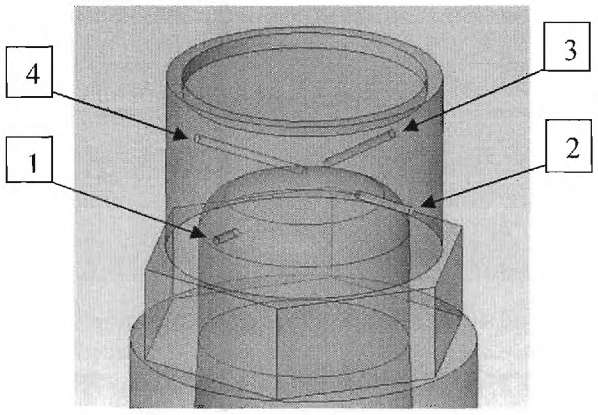

Figure 2.3: Drawing of the thermocouple locations in the brass thimble.

After inserting each thermocouple into its respective hole, it was wrapped azimuthally around the test section to reduce axial conduction and to reduce thermocouple probe movement. The thermocouple probes are secured by placing a thin layer of Rockwool insulation around the test section and tightly winding a high strength nickel wire over the insulation (Figure 2.5).

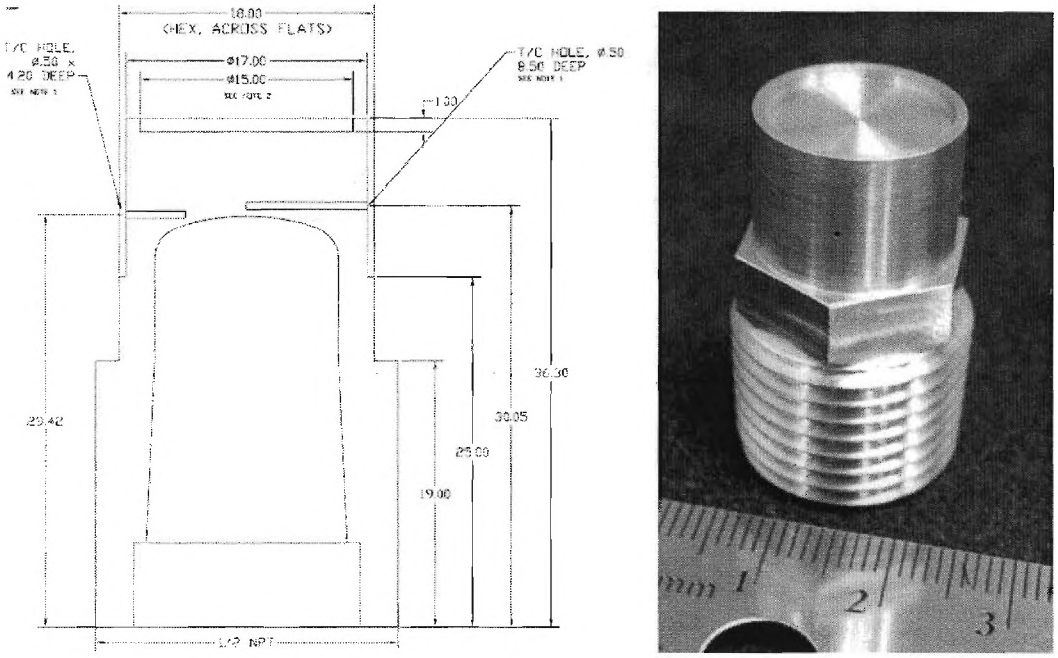

Figure 2.4: Drawing of the thimble and a photograph of the manufactured thimble.

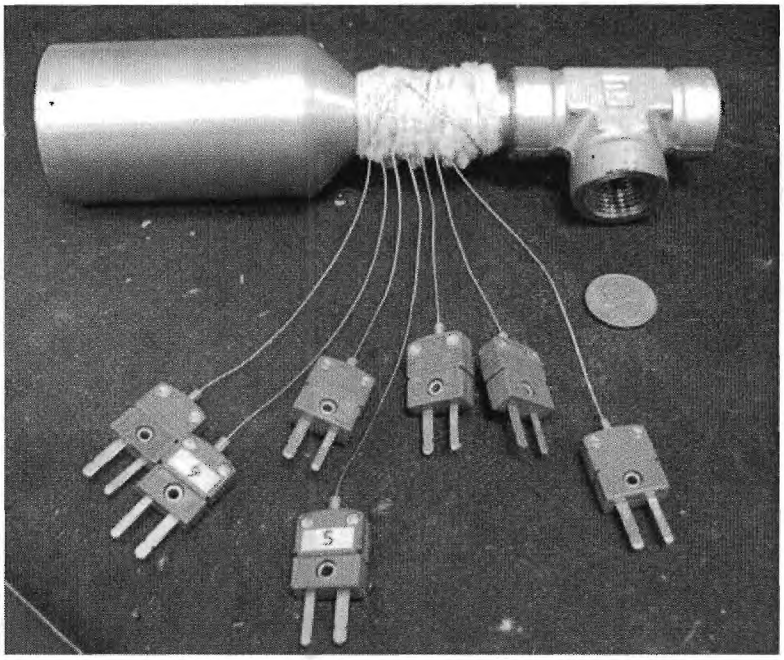

Figure 2.5: Secured thermocouples of the thimble and copper heater. A nickel in front of the tee indicates the scale.

2.1.3 Copper Heater Block

A 117 mm long cylindrical copper block is used to generate a uniform axial heat flux across the thimble (Figure 2.7). It was manufactured by the Georgia Tech Research Institute using CS 14500 (Figure 2.8). The copper heater block consists of a 50 mm diameter section which contains a Fast-Heat® Magnesium-Oxide cartridge heater in the center. The heater has a maximum output of 750 W, which exceeds the required input power needed to generate a nominal heat flux of 1.0 MW/m^2. The power input to the heater (i.e., the heat flux incident on the thimble) is controlled by controlling the voltage to the heater with a variable autotransformer (Staco Energy Products 3PN1010V). The voltage is measured with a multimeter (Hewlett Packard 34401 A) and the current is measured with an additional multimeter (Fluke 25). The copper heater block then contracts to a 17 mm diameter "neck" region which is brazed to the top of the thimble

using silver. Three 0.5 mm diameter OMEGA Type-E thermocouples are positioned at axial locations 3.0, 8.0, and 13.0 mm above the brazing surface in the "neck" region (Figure 2.6). These thermocouples are used to calculate the measured axial heat flux and are offset from each other by 90°. Additionally, two 1.59 mm diameter OMEGA Type-E thermocouples are placed 5 mm below the top of the copper heater block and at a depth of 16.0 mm to monitor the peak temperature of the test section. Table 2.3 provides the thermocouple labeling convention and positions for the copper heater block.

Table 2.3: Copper Heater Block Thermocouple Positions and Reference Numbers

Thermocouple Reference	Thermocouple height above brazing surface(mm)
5	3.0
6	8.0
7	13.0
8	112.0
9	112.0

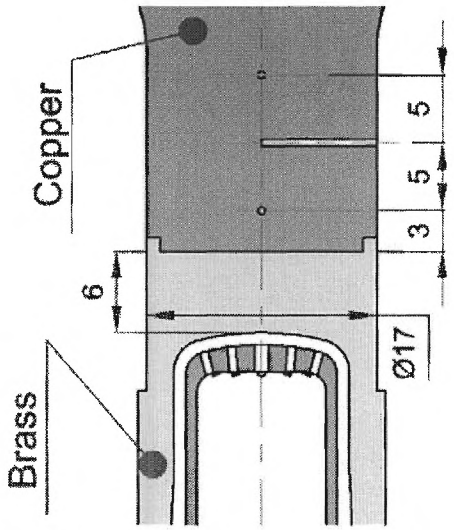

Figure 2.6: Drawing of the "neck" region of the test section.

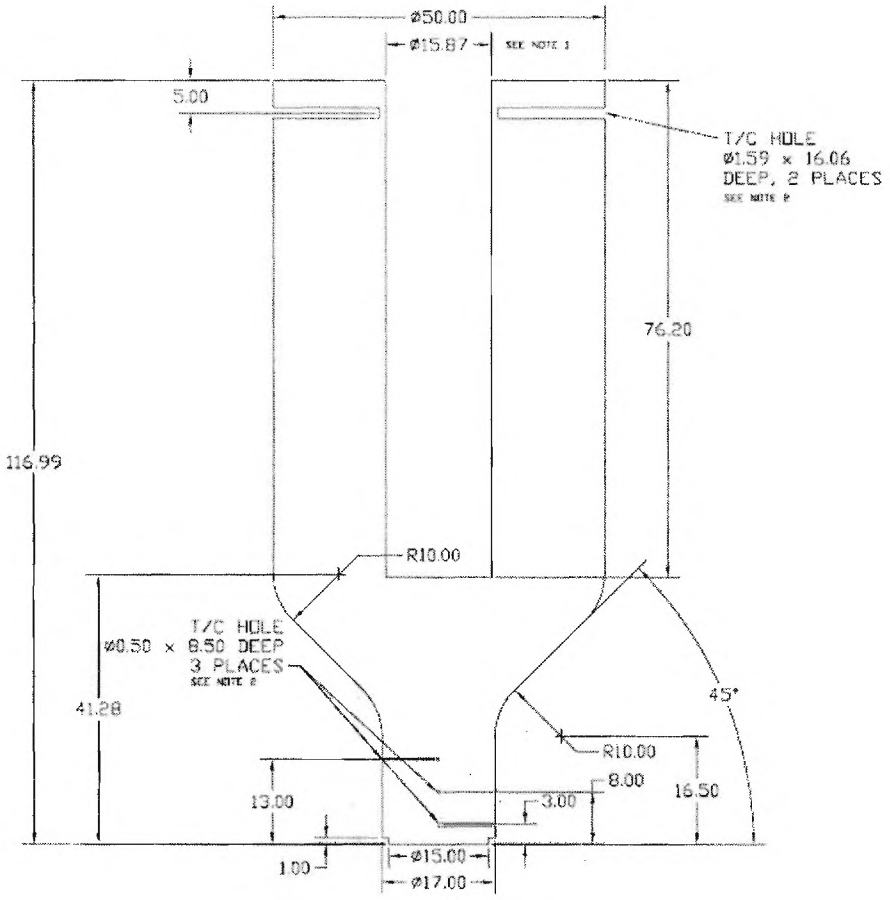

Figure 2.7: Drawing of the copper heater block from AutoCad 2006.

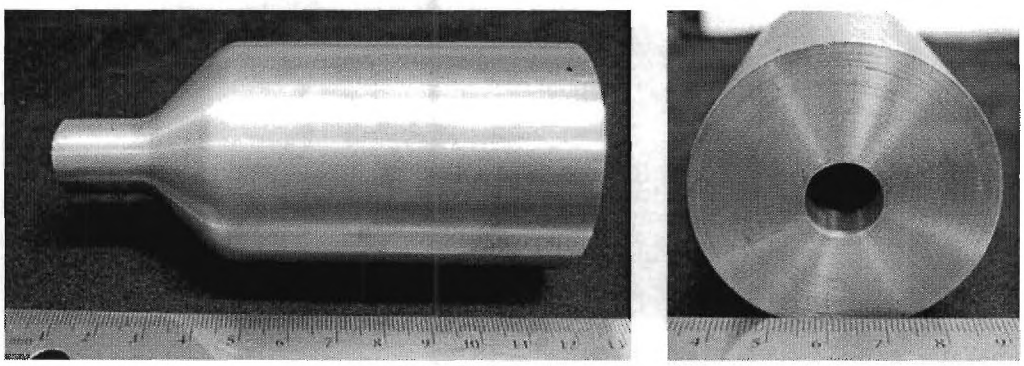

Figure 2.8: Photograph of the manufactured copper heater block

2.1.4 Assembled HEMJ Test Section

To simulate the thermal-hydraulic behavior of the HEMJ divertor, a test section that consisted of a jet cartridge, thimble, and copper heater block was constructed. The assembled test section (Figure 2.9) has the copper heater block brazed to the top of the thimble. This thimble was then screwed into a SS ½ inch diameter tee (Parker #8-8-8 FT). The jet cartridge was epoxied to a 150 mm long SS 316 tube and inserted through the tee into the thimble (Figure 2.10). The assembled HEMJ divertor test section is insulated with a 12.5 cm diameter cylinder of Rockwool that has the test section's profile carved out of its center. The insulation extents 5 cm beyond the height of the copper heater block. Figure 2.11 shows the Rockwool insulation prior to securing it to the HEMJ divertor test section.

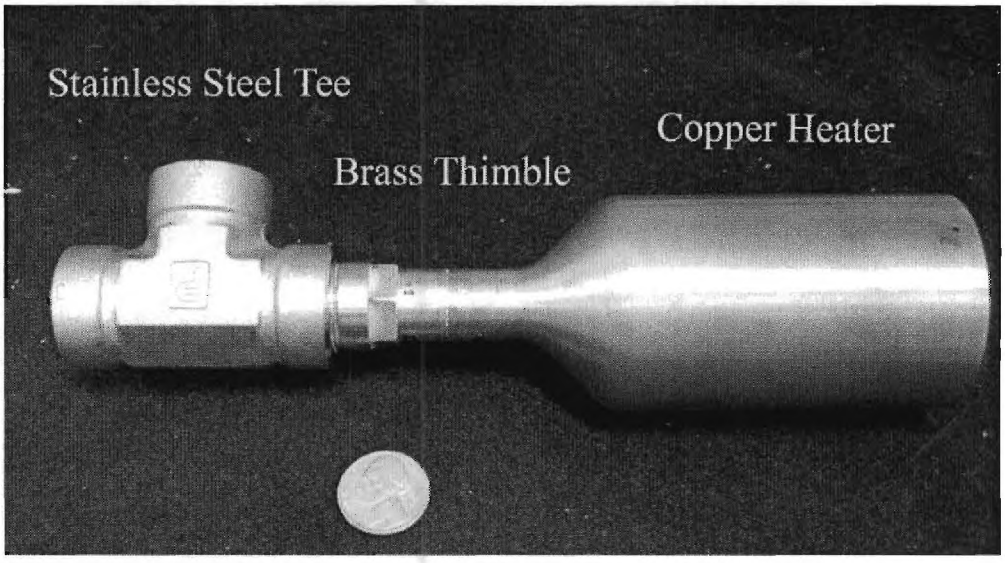

Figure 2.9: Photograph of the assembled tee, thimble, and cooper block heater. A nickel in front of the assembly indicates the scale.

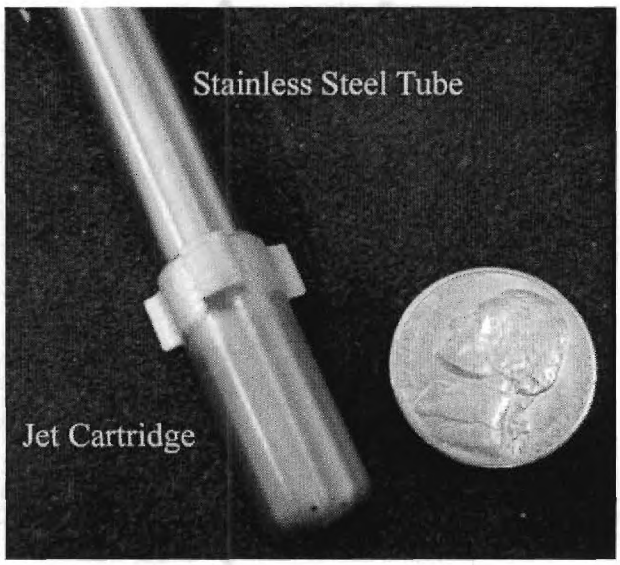

Figure 2.10: Photograph of the jet cartridge brazed to the stainless steel tube. A nickel beside the jet cartridge indicates the scale.

Figure 2.11: Photograph of the HEMJ divertor test section insulation.

2.1.5 Experimental Flow Loop

Experimental studies were performed by placing the test section in an air flow loop (Figure 2.12). Figure 2.13 provides a picture of the entire flow loop with the pertinent sections highlighted. A picture of the assembled HEMJ test section with all instrumentation attached is shown in Figure 2.14. The details of Figures 2.13 and 2.14 are provided in Table 2.4.

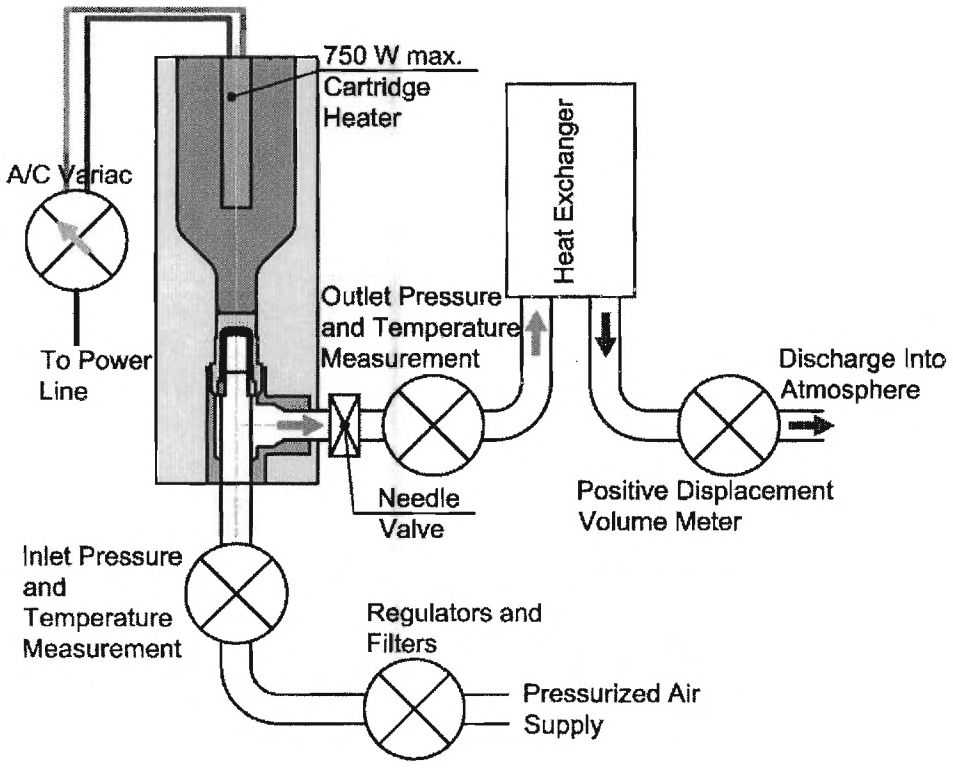

Figure 2.12: Diagram of the air flow loop.

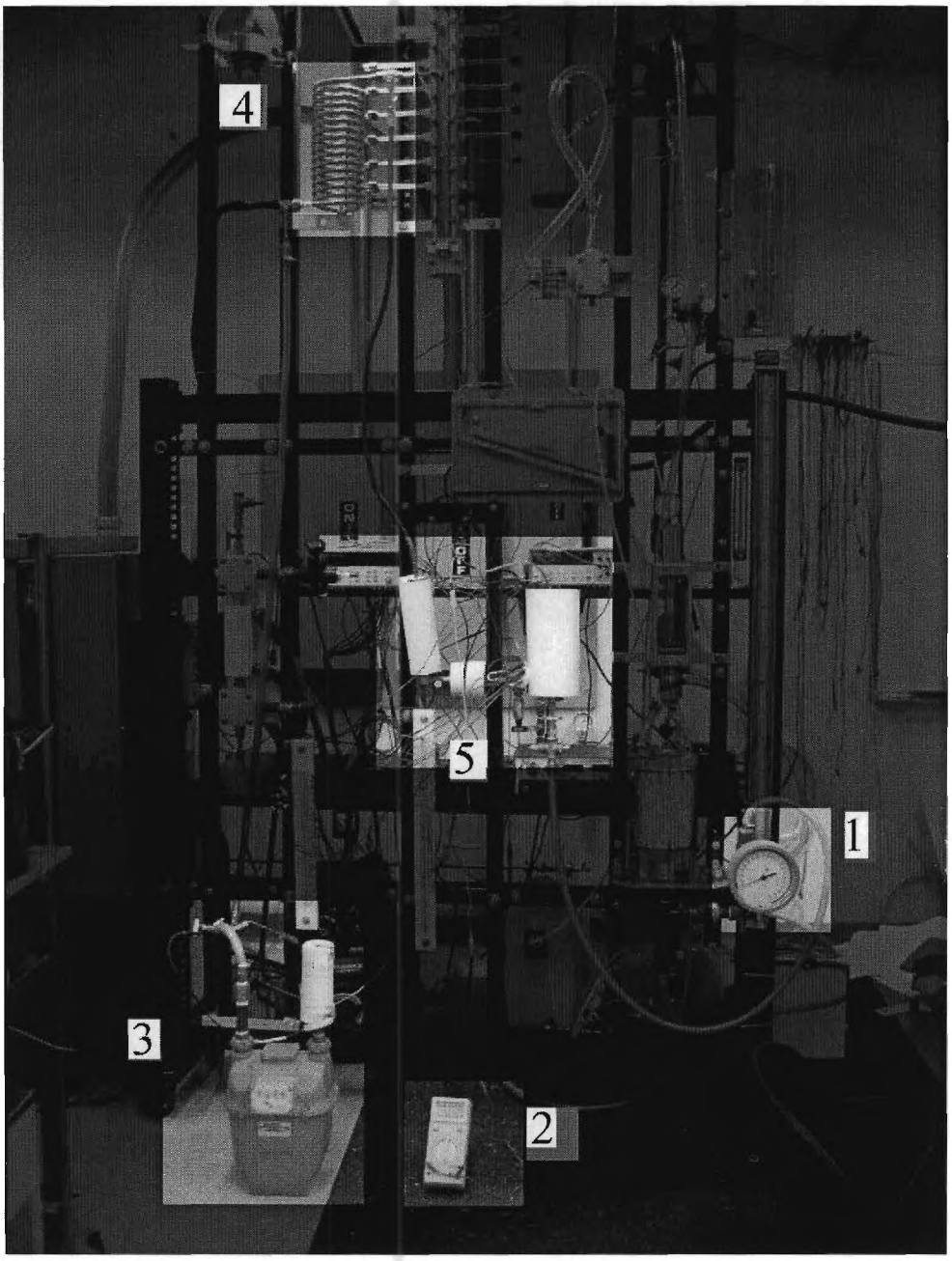

Figure 2.13: Photograph of the air flow loop.

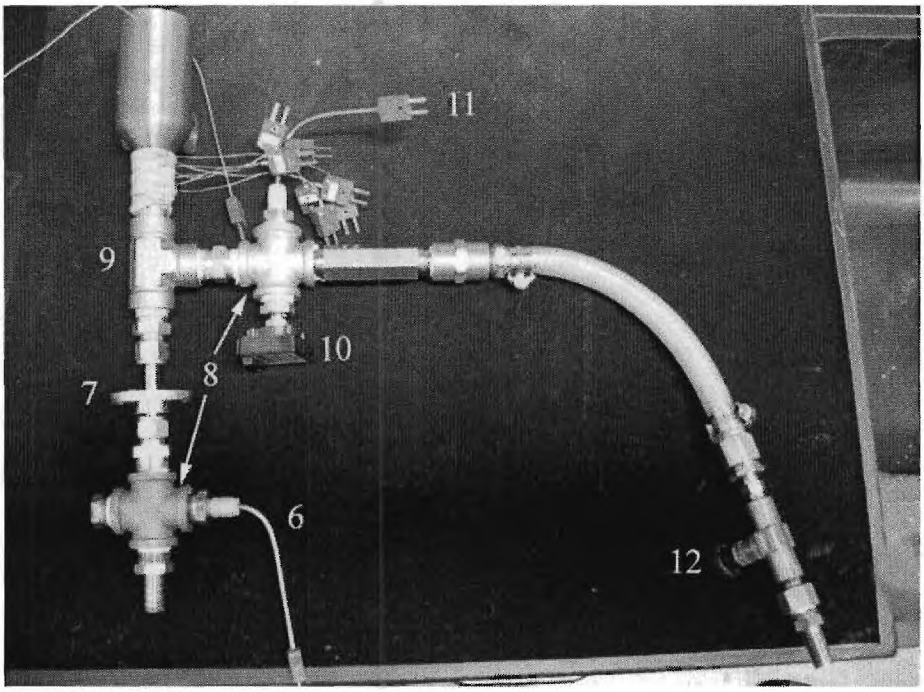

Figure 2.14: Photograph of the test section with instrument attached.

Table 2.4: Detailed list of experimental flow loop components

Label	Quantity	Description	Manufacturer	Model
1	1	Inlet Pressure Gauge 0 - 200 psig	Ashcroft	AMC-4291
2	1	Handheld Multimeter Maximum 10 Amps, 1000 V	Fluke	25
3	1	Gas Volume Flow Meter Max Pressure 5 PSIG	Rockwell International	R-315
4	1	Heat Transfer Coil	Parker Instrumentation	DYYC-55-4
5	**Experimental Test Section**			
6	1	Inlet Thermocouple	Omega	Type E EMQSS-020G-6
7	1	Angular Scale	In house	
8	2	1/2 Inch Cross	Lee USA	
9	1	1/2 Inch Tee	Parker	8-8-8 FT
10	1	Exit Pressure Transducer 0 - 600 PSIA	Omega	PX302-300AV
11	1	Exit Thermocouple	Omega	Type E EMQSS-020G-6
12	1	Needle Valve	Nupro Company	

Air from a compressed-air line enters the flow loop at a pressure of up to 724 kPa. The inlet pressure is measured with an analog test gauge (1) which has a range of 0 – 200 psig that is resolvable to 0.5 psig or 3.4 kPa. The inlet temperature is measured using an OMEGA Type-E thermocouple (6) placed in a ½ inch cross (8) which is attached to the 150 mm SS 360 tube via a bored-through SWAGELOK® heat exchanger fitting. This fitting enables the inner SS 360 tube and thus the jet cartridge to be rotated relative to the thimble. An angular scale (7) and straight steel wire are used to indicate the azimuthal position θ of the jet cartridge. The 0^{o} position corresponds to a jet on the outer "bolt" circle, reference 4, being positioned under thermocouple reference 1 (Table 2.1). Figure 2.15 shows a photograph of the angular scale and reference steel wire.

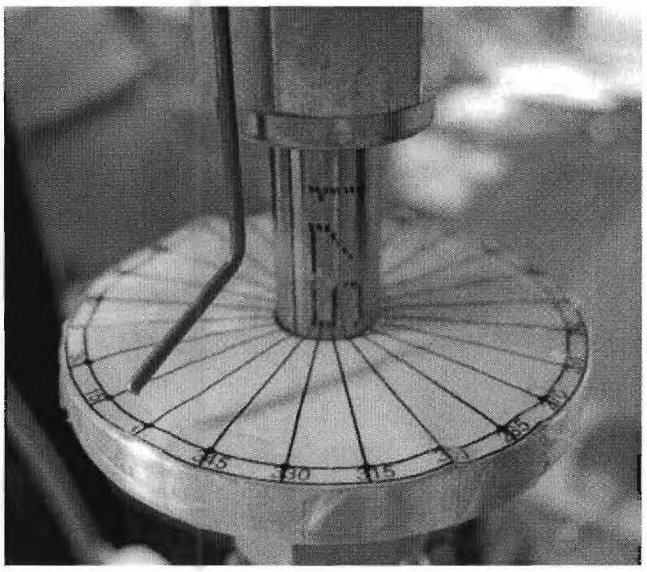

Figure 2.15: Photograph of the angular scale.

The exit pressure and temperature are measured with an OMEGA pressure transducer (10) and OMEGA Type-E thermocouple (11), respectively. They are secured in a ½ inch cross (8) that is attached to the SS tee (9) of the test section. A needle value (12) is placed after the ½ inch cross (8) to control the mass flow rate through the test section.

The air flows through a copper heat transfer coil (4) before entering a positive displacement gas flowmeter (3). The heat transfer coil was needed to reduce the temperature of the air exiting the test section prior to entering the gas flowmeter. The temperature and pressure are measured at the inlet of the gas flowmeter with a thermocouple (OMEGA Type-E) and a pressure transducer (OMEGA PX180-015GV) before being vented directly to the atmosphere.

The data acquisition system consists of a 60-channel data acquisition unit (Agilent 34970) which has three, 20-channels each, A/D cards (Agilent 34901A). It is connected to a PC through a RS-232 serial cable. The Agilent Bench Link Data Logger 3 software is used to configure the unit and monitor the data on the PC. Only steady state data is stored for each experiment.

2.2 Experimental Procedures

The experimental procedures that were used in this investigation are described in this section. The section is organized as follows: Subsection 2.2.1 describes the parameter space that experimental data was collected from, Subsection 2.2.2 describes the constant azimuthal angle experiments, and Subsection 2.2.3 describes the rotation experiments.

2.2.1 Parameter Space

The experimental test conditions were selected to cover the range of non-dimensional parameters expected in normal operation of the HEMJ divertor test section when cooled by helium. As discussed in subsection 1.1.2, the most important non-dimensional parameter is the Reynolds number based on the 1.0 mm diameter central jet.

The Reynolds number of the central jet expected for the HEMJ test section in the HEBLO Test Facility corresponding to its nominal operating conditions is 21,400. The range of Reynolds number spanned by this investigation is from 14,000 to 56,000. This range corresponds to a mass flow rate that varied from 2.0 g/s to 8.0 g/s. In this investigation, experiments were performed at power inputs corresponding to nominal heat fluxes of 0.8 MW/m^2 and 1.0 MW/m^2 in the 17 mm diameter "neck" region of the copper heater block.

2.2.2 Constant Azimuthal Angle Experiments

During the constant azimuthal angle experiments, the power input to the heater (i.e. the heat flux on the thimble surface) and the jet cartridge position remain fixed while the mass flow rate is varied. These experiments are conducted with the steel wire aligned to the 0^{o} position of the angular scale and the SWAGELOK® fitting securely tightened. The flow loop is pressurized to 710 – 730 kPa. The heater power is then set with the variable autotransformer (Staco Energy Products 3PN1010V). To generate a nominal heat flux of 0.8 MW/m^2 in the "neck" of the cooper heater block, 182 W is required. This generally resulted in a current of 2.93 Amps and a voltage of 62 Volts. The 1.0 MW/m^2 nominal heat flux required 228 W input to the heater.

The desired mass flow rate is obtained by adjusting the needle valve (12) until a measurement from the gas volume flowmeter (3) results in the desired mass flow rate. For each experiment, multiple mass flow rate measurements and adjustments of the needle valve (12) are required due to the rising exit temperature of the air as the test section heats to approach a steady state operation.

Steady state is determined by using the Agilent Bench Link Data Logger 3 software to monitor the thermocouple probes (Figure 2.16). When the thermocouple probe readings remain constant to within +/- $1^{o}C$ for multiple data scans at five second intervals, the data is collected and steady state is assumed to be reached. After steady state has been reached for the desired mass flow rate, the needle valve (12) is adjusted for the next mass flow rate and the process is repeated. The average time to reach steady state was approximately one hour and thirty minutes.

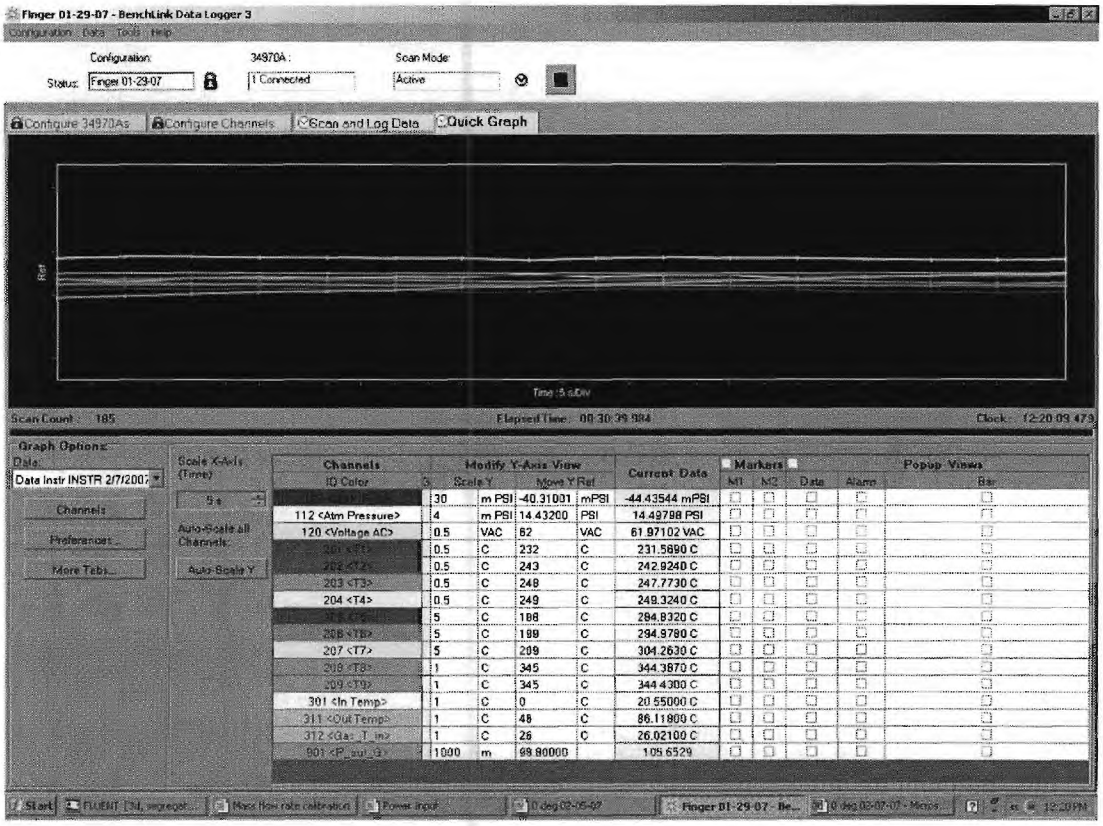

Figure 2.16: Steady state results of the Agilent Bench Link Data Logger software.

Table 2.5 details the constant azimuthal angle experiments that were performed on the air flow loop. All values provided in table 2.5 correspond to experimentally measured results. The maximum temperature refers to the temperature measured by thermocouple probe 8 (Table 2.3) which is inserted 5.0 mm below the top of the copper block. The temperature difference between thermocouple probes 8 and 9 during testing was within the manufactured uncertainty of the thermocouples (+/- 1.5°C). The constant azimuthal angle tests consist of two sets of experiments performed over the target mass flow rates of 2.0, 3.0, 4.0, 6.0 and 8.0 g/s at a power input of 182 W (tests 1 – 10). Tests 6

through 10 were performed to verify the repeatability of the experiment. Tests 11 through 15 correspond to the 1 MW/m^2 nominal heat flux case.

Table 2.5 Table of the constant azimuthal angle experiments

Test Number	Mass Flow [g/s]	Power [W]	Angle [°]	q" [MW/m^2]	ΔP [kPa]	T_{max} [°C]
1	2.08	182.3	0	0.695	11.03	342.4
2	3.11	182.3	0	0.710	17.93	303.0
3	3.99	182.2	0	0.717	35.85	282.2
4	6.01	181.5	0	0.720	73.77	252.9
5	8.39	181.2	0	0.727	176.64	234.6
6	2.01	181.4	0	0.692	9.65	344.4
7	3.16	182.2	0	0.713	22.06	305.0
8	4.20	182.8	0	0.724	41.37	280.6
9	6.10	182.9	0	0.720	77.22	251.7
10	8.06	182.8	0	0.727	152.37	235.5
11	2.07	228.4	0	0.880	11.72	417.5
12	3.10	227.0	0	0.901	24.13	363.3
13	4.05	226.6	0	0.891	35.16	333.5
14	6.20	227.6	0	0.901	84.12	299.9
15	8.18	227.9	0	0.922	166.16	284.6

2.2.3 Rotation Experiments

During the rotation experiments, the power input to the heater (i.e., the heat flux on the thimble surface) and the mass flow rate remain constant while the jet cartridge is rotated. These experiments enable the azimuthal variation of the cooled surface temperature distribution of the HEMJ divertor test section to be measured.

The flow loop is set up in the same manner as described in subsection 2.2.1. The flow loop is pressurized to 710 – 730 kPa with the power to the heater set to either 182 W for a nominal heat flux of 0.8 MW/m^2 or 228 W for a nominal heat flux of 1.0 MW/m^2.

To reach the desired mass flow rate, the needle valve (12) is adjusted until that mass flow rate is obtained for an exit temperature at steady state. Steady state is determined by the same criterion described in subsection 2.2.1. Once the steady state data has been recorded using the Agilent Bench Link Data Logger 3 software, the SWAGELOK® fitting at the inlet of the test section is loosened while maintaining an upward force on the SS tube. The SS tube and thus the jet cartridge are then rotated relative to the steel wire reference by the desired angular amount. The SWAGELOK® fitting is then securely tightened at the new rotation. A mass flow rate measurement is taken for verification that it has not changed. Once steady state has been reach for the new rotation, the data is collected and the process is repeated. All experiments were performed in 15° increments and covered sectors of 60° or 120° azimuthal extent.

Table 2.6 details the rotation experiments performed. All data in the table refers to experimentally measured results. The maximum temperature refers to the temperature measured by thermocouple probe 8 (Table 2.3) which is inserted 5.0 mm below the top of the copper heater. Tests 26 through 30 were performed for a nominal heat flux of 0.8 MW/m^2 and mass flow rate of 3.03 g/s. Tests 16 through 25, 31 through 39, and 40 through 48 were performed with the elevated nominal heat flux of 1.0 MW/m^2 at the target mass flow rates of 2.0, 3.0, and 4.0 g/s, respectively.

Table 2.6 Table of the rotation experiments

Test Number	Mass Flow [g/s]	Power [W]	Angle [°]	q" [MW/m^2]	dP [kPa]	T_{max} [°C]
16	2.07	228.4	0	0.880	11.72	417.5
17	2.06	228.2	15	0.896	12.41	417.6
18	2.07	228.5	30	0.926	11.03	416.0
19	2.08	228.5	45	0.883	13.10	415.7
20	2.07	228.5	60	0.883	13.10	415.5
21	2.07	228.4	180	0.887	13.10	415.3
22	2.07	228.8	195	0.883	11.72	415.1
23	2.07	228.7	210	0.887	11.03	415.0
24	2.07	228.9	225	0.887	11.03	414.9
25	2.07	228.9	240	0.885	11.03	414.9
26	3.03	182.8	0	0.702	17.93	303.0
27	3.03	182.7	15	0.703	14.48	304.0
28	3.03	182.3	30	0.710	17.24	304.1
29	3.03	182.7	45	0.703	20.68	305.1
30	3.03	183.0	60	0.713	17.24	305.0
31	3.03	227.0	0	0.898	17.93	366.6
32	3.03	226.9	15	0.896	40.68	366.3
33	3.03	227.0	30	0.897	39.30	366.0
34	3.03	227.0	45	0.896	16.69	365.8
35	3.03	227.1	60	0.895	16.20	365.7
36	3.03	226.7	75	0.896	14.69	365.2
37	3.03	226.9	90	0.895	14.41	365.0
38	3.03	226.8	105	0.894	16.34	364.9
39	3.03	227.1	120	0.891	19.51	364.9
40	4.05	226.6	0	0.891	35.16	333.5
41	4.05	226.6	15	0.887	33.78	334.0
42	4.05	226.1	30	0.891	33.78	334.4
43	4.05	227.3	45	0.891	32.41	334.7
44	4.05	227.3	60	0.891	31.72	335.0
45	4.05	226.0	75	0.894	31.03	335.3
46	4.05	226.3	90	0.894	30.34	335.4
47	4.05	227.0	105	0.891	33.78	335.7
48	4.05	226.3	120	0.891	33.78	335.8

CHAPTER III

NUMERICAL MODEL

3.1 Test Section Model Creation

The HEMJ divertor test section numerical model is described in this section. The section is organized as follows: Subsection 3.1.1 describes the HEMJ geometry used in the numerical model, subsection 3.1.2 describes the mesh generation, subsection 3.1.3 details the boundary conditions, subsection 3.1.4 describes the input parameters for the simulations, and subsection 3.1.5 details the convergence of the numerical model.

3.1.1 HEMJ Geometry

The HEMJ divertor test section model used for the numerical studies detailed in this chapter was prepared by Crosatti [19]. It was built using the CAD program SolidWorks® to exactly match the experimental test section's dimensions and features described in Chapter II. This model includes the electric heater, copper heater block, brass thimble, cartridge, tee, insulation, inlet tube, and outlet connector (Figure 3.1). These components are modeled in three-dimensions and include all pertinent features present on the experimental test section. The material properties used in the numerical model are provided in Table 3.1. The region labeled wrapping refers to the Rockwool

insulation which was used to secure the thermocouple probes as described in subsection 2.1.2.

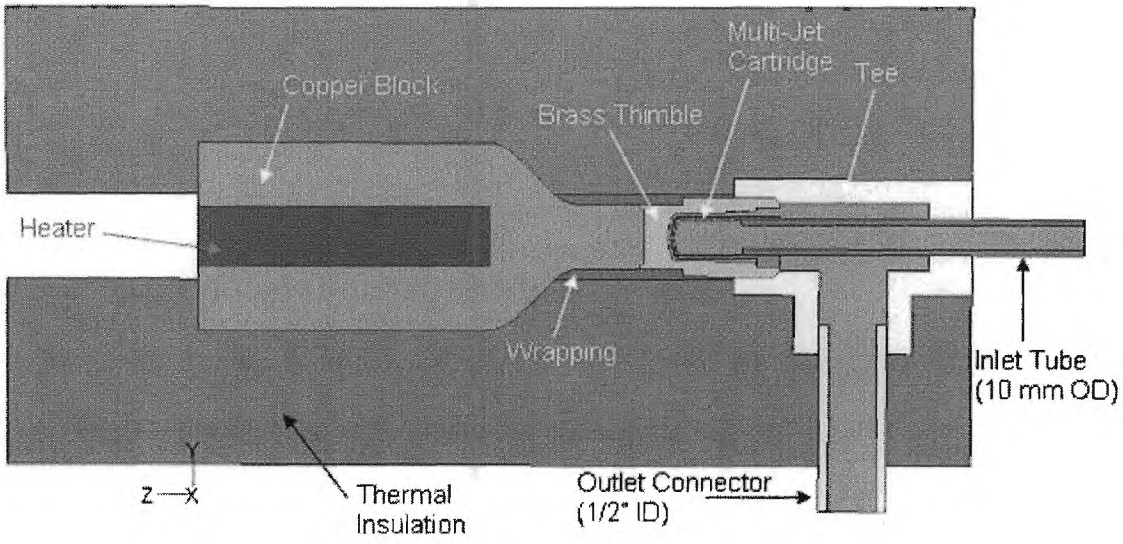

Figure 3.1: Diagram of the HEMJ divertor test section numerical model.

Table 3.1 Table of the materials used in the numerical model.

Material	Component(s)	Density [kg/m^3]	Thermal Conductivity [W/m-K]		Specific Heat [J/kg-K]
AISI 316 SS	Tee, Inlet tube	8027	16.26		502
Brass C36000	Thimble Jet Cartridge Outlet Connector	8500	116		380
Rock Wool	Insulation	130	$0.0407-10^{-4}*T+3*10^{-7}*T^2$		840
Rock Wool	Wrapping	130	$0.0407-10^{-4}*T+3*10^{-7}*T^2$		840
Copper C14500	Copper Block	8940	354.8		376.8
Magnesium Oxide	Heater	3580	**T [K]**	**k**	877
			273	42	
			400	29	
			600	20	
			800	14	
			1000	11	

3.1.2 Mesh Generation

The CAD model was imported into Gambit® version 2.2.3 in order to generate a mesh for running simulations in the computational fluid dynamics software package FLUENT® version 6.2.16. The mesh consisted of 1,456,460 cells with 695,360 nodes (Figure 3.2). This mesh was constructed by projecting face meshes along the volumes of the model. In regions of complex geometry, such as the jet cartridge head and tee, a tetragonal/hybrid mesh was used (Figure 3.3). Using the symmetry of the HEMJ test section, only half of the model was required for the simulations.

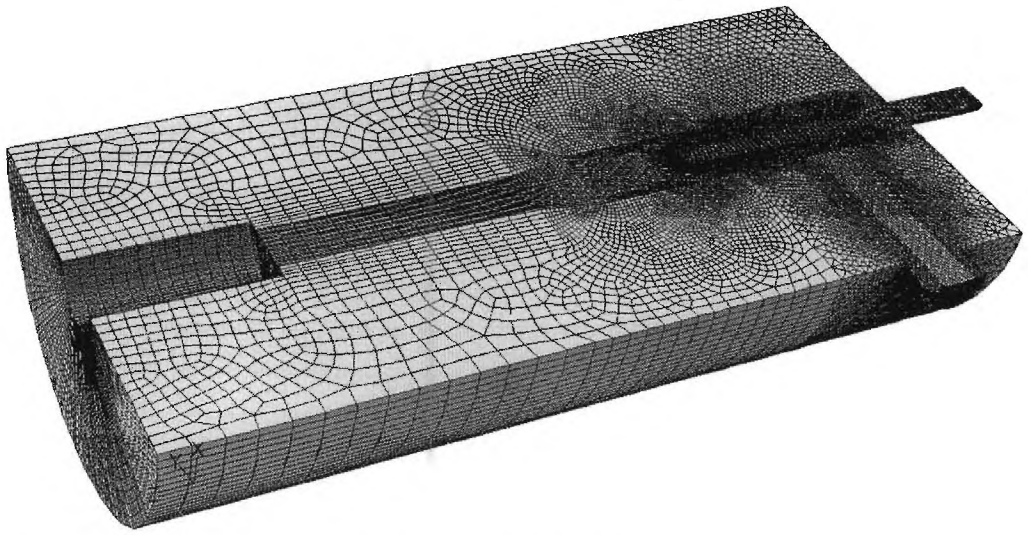

Figure 3.2: Final mesh used for the numerical model.

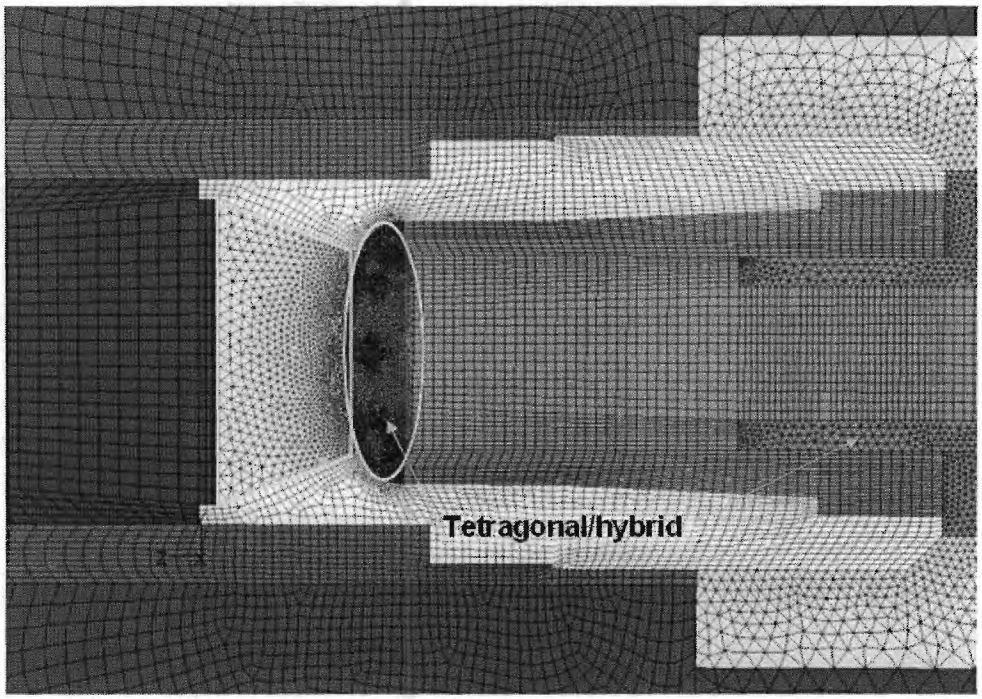

Figure 3.3: Detailed view of the mesh surrounding the jet cartridge.

3.1.3 Boundary Conditions

After the model was meshed in Gambit®, it was imported into the FLUENT® software package to simulate its thermal-hydraulic behavior. The boundary conditions applied to the test section model when used for comparison with experimental data are detailed in Figure 3.4 and Table 3.2. For each experimental test condition simulated in FLUENT®, the mass flow rate was set to the experimentally measured quantity. The outlet pressure was set to the pressure recorded with the outlet pressure transducer (Label 10 in Table 2.3). The back flow temperature of the outlet was set to the experimental outlet temperature that was measured with a thermocouple (Label 11 in Table 2.3). At steady state, the surface temperature at location C (Figure 3.4) was measured by manually inserting a thermocouple probe (OMEGA Type-E) at that location. This value

was imposed as a constant temperature boundary condition for the respective heater and copper faces at location C in FLUENT®.

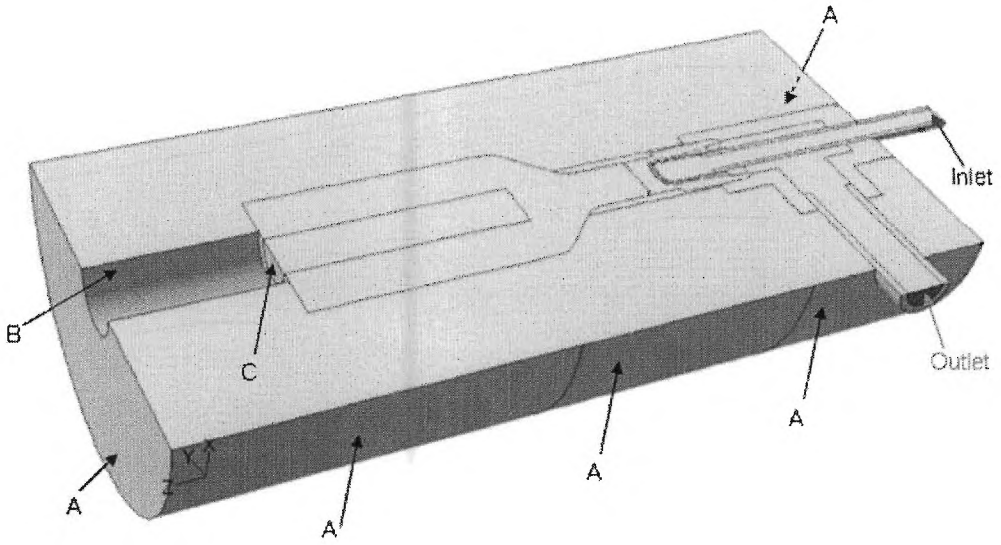

Figure 3.4: Numerical model with references for boundary conditions.

Table 3.2 Table of boundary conditions used for comparison with experimental data.

Reference	Type	Parameters
Inlet	Mass Flow Rate	experimentally measured mass flow rate
Outlet	Pressure	experimentally measured pressure
A	Convection	HTC=5 [W/(m^2-K)] and T_f = 20°C
B	Convection	HTC=15 [W/(m^2-K)] and T_f = 68°C
C	Temperature	experimentally measured temperature

3.1.4 Input Parameters

For all simulations, the k-ε closure equations were used as the turbulence model with the standard wall functions. The heat load for the heater was specified as a volumetric heat generation rate. The heater volume is 15.08×10^{-5} m^3 and required a power input of 182 W for a nominal heat flux of 0.8 MW/m^2 and 228 W for a nominal

heat flux of 1.0 MW/m^2. The turbulence intensity was calculated using the Reynolds number of the inlet tube which has an inner diameter of 0.007 m.

$$I = 0.16 * \mathrm{Re}_{inlet}^{-1/8}$$

3.1.5 Convergence

Convergence of the numerical simulation was determined by noting that the residuals had reached a nearly constant value. The standard order of magnitude for the residuals was at least 10^{-3} and decreased to 10^{-7} for the energy equation (Figure 3.5). On average it took 500 to 800 iterations for the solution to converge on a Pentium® IV 3.4 GHz workstation with 2 GB of RAM.

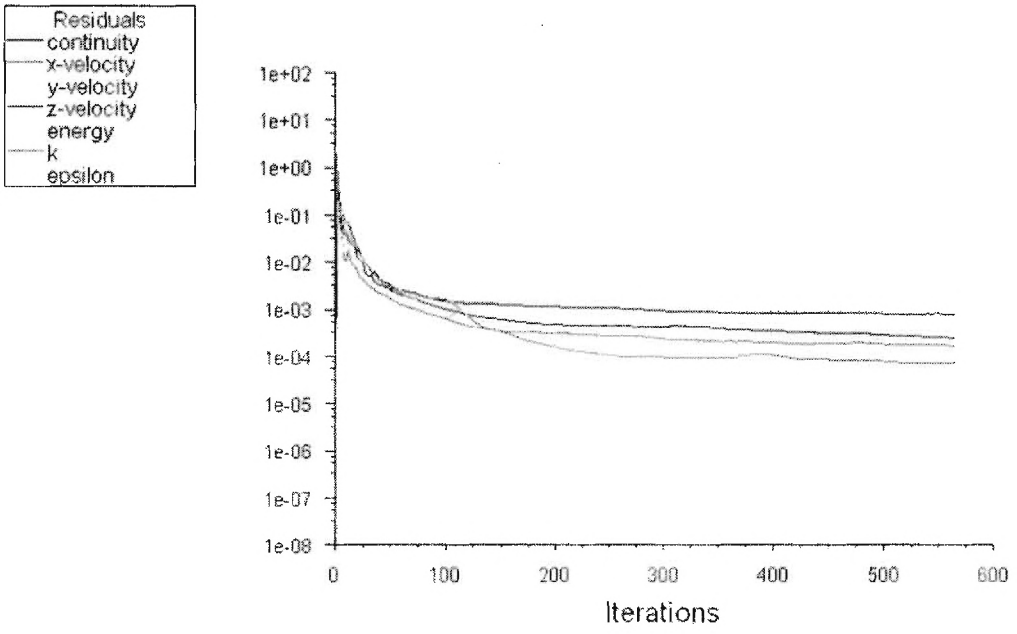

Figure 3.5: Plot of the residuals for a converged FLUENT® simulation.

3.2 Nominal Test Case Results

This subsection describes results from the numerical simulation pertaining to the nominal operating condition of the HEMJ divertor test section as detailed in subsection 1.1.2. Simulations with the model described in subsection 3.1 were performed for comparison of the air–cooled and helium-cooled test section under nominal operating conditions.

The helium-cooled simulations correspond to conditions of the FZK HEBLO Test Facility. Since the external temperature boundary condition at location C of Figure 3.2 is not known for the HEBLO Test Facility simulations, a natural convection heat transfer boundary condition was imposed at that location (Table 3.3). The remaining boundary conditions used for this investigation are provided in Table 3.3. The nominal conditions of the air-cooled and helium-cooled test section are detailed in Table 3.4. In all simulations for the nominal test case, the Reynolds number is matched for the helium and air coolants.

Table 3.3 Table of boundary conditions used for helium coolant simulation.

Reference	Type	Parameters
Inlet	Mass Flow Rate	nominal mass flow rate
Outlet	Pressure	pressure set to nominal value
A	Convection	HTC=5 [W/(m^2-K)] and T_f = 20°C
B	Convection	HTC=15 [W/(m^2-K)] and T_f = 285°C
C	Convection	HTC=35 [W/(m^2-K)] and T_f = 285°C

Table 3.4 Table of nominal operating conditions.

Medium	Helium - Demo Conditions	Air, Nominal	Helium-HEBLO Conditions
Temperature [°C]	634	20	35
Pressure [bar]	100	7.24	80
Density [kg/m^3]	5.30	8.62	12.49
Dynamic Viscosity [10^{-5} kg/(m-s)]	4.16	1.85	2.04
Reynolds Number	21400	21400	21400
Relation mass flow / viscosity	163.44	163.44	163.44
Mass Flow Rate [g/s]	6.80	3.03	3.33

The temperature distribution for the HEMJ divertor test section model (Figure 3.6) shows that in the "neck" region of the copper block, a uniform temperature distribution in the y-direction is achieved (Figure 3.7). This will create a nearly uniform heat flux in the z-direction that is incident on the brass thimble.

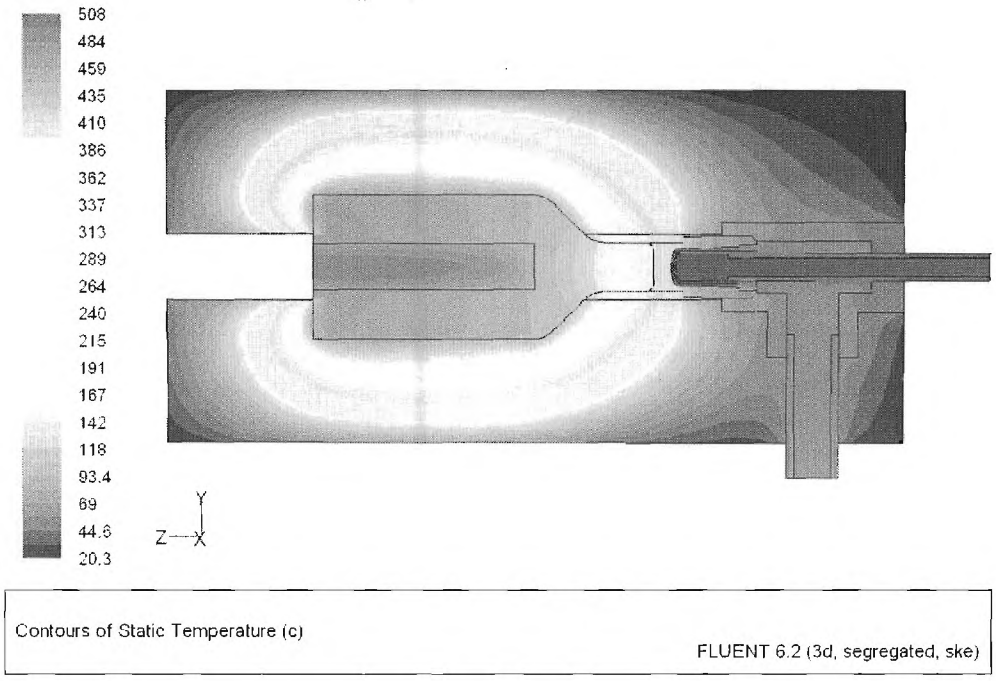

Figure 3.6: Temperature Distribution of HEMJ divertor test section.

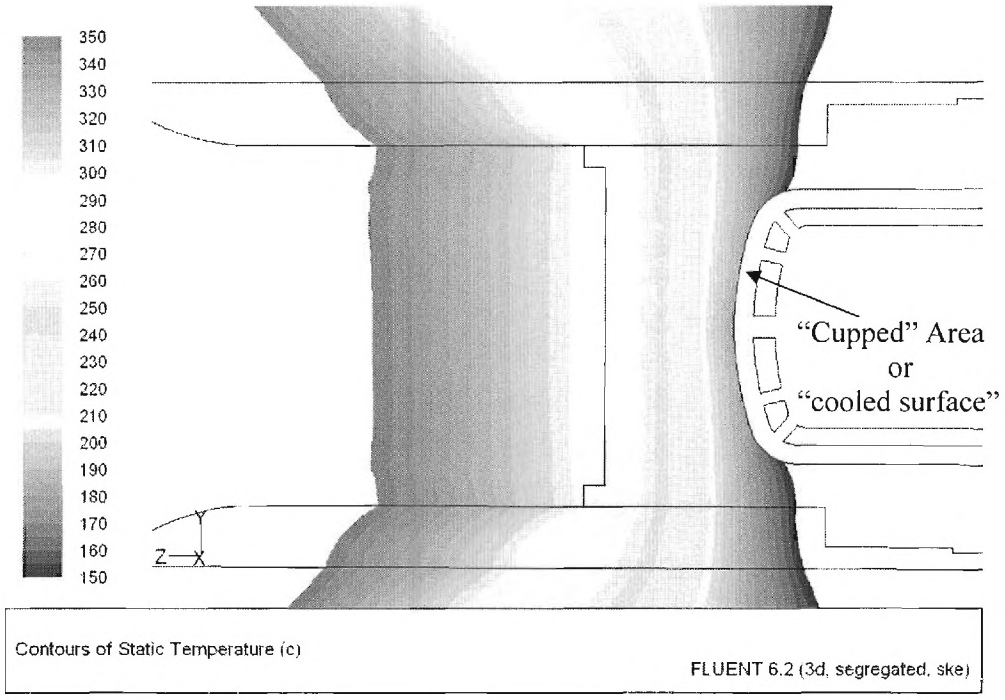

Figure 3.7: Temperature Distribution of HEMJ divertor test section "neck" region.

The heat flux and convective heat transfer coefficient on the "cupped" area above the impinging jets (i.e. the "cooled surface") are of primary interest for this investigation (Figures 3.8 and 3.9). The contours show that enhancement of the convective heat transfer coefficient is achieved near each jet with the highest value corresponding to the central jet.

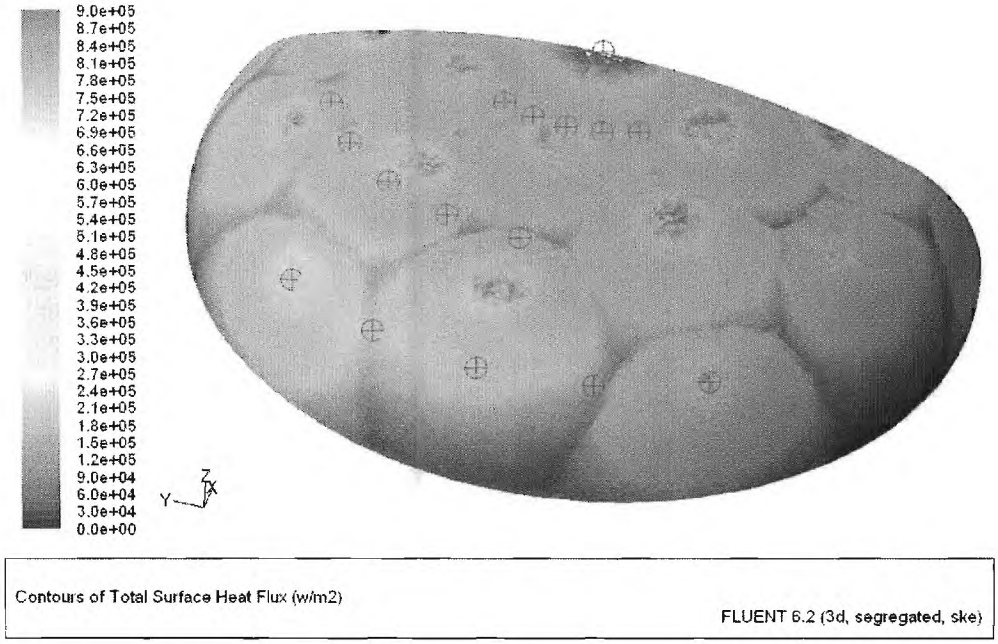

Figure 3.8: Heat flux contour plot of "cupped" region of the brass thimble for nominal operating conditions corresponding to air.

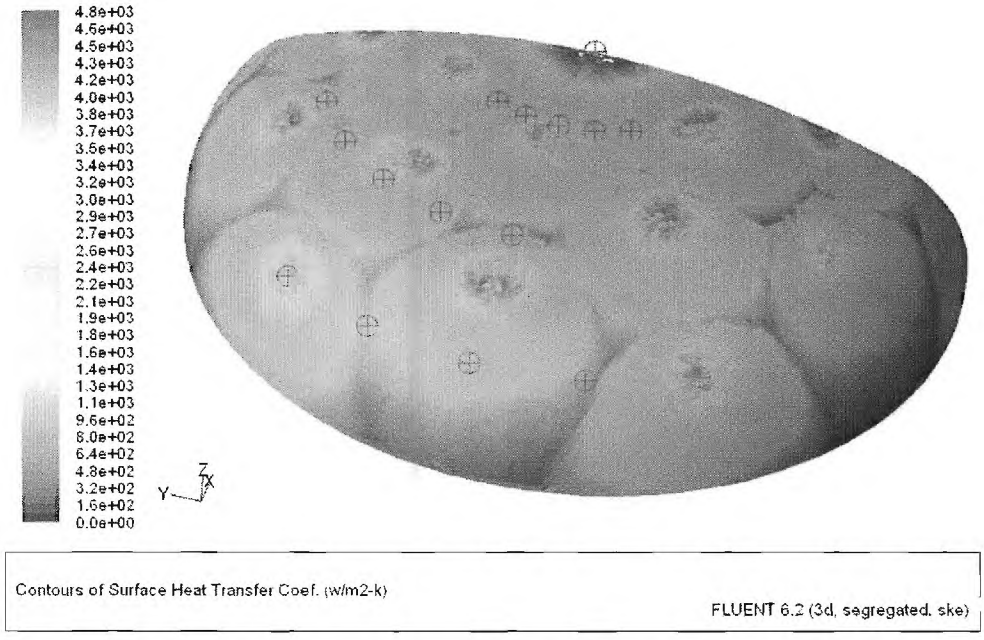

Figure 3.9: Convective heat transfer coefficient contour plot of "cupped" region of the brass thimble for nominal operating conditions corresponding to air.

A summary of the results for the nominal operating conditions of the helium-cooled and air-cooled HEMJ divertor test section is provided in Table 3.5. Based on the numerical results, the maximum temperatures in the HEMJ divertor test section will not exceed their material limits. Of particular importance, the maximum temperature of the brazing surface between the copper block and the brass thimble does not exceed 300°C.

Table 3.5: Numerical results for HEMJ divertor test section coolant comparison.

Parameter	**He (HEBLO)**	**Air (GT)**
Mass Flow Rate [g/s]	3.33	3.00
Power Input [W]	477	182
Nominal Heat Flux [MW/m^2]	2.1	0.8
Net Heat Flux [MW/m^2]	1.94	0.76
T_{max} Copper [°C]	473.6	328
T_{max} Brass (Brazing Surf.) [°C]	288.5	264
ΔT Coolant [°C]	25.6	50.4
Energy Loss Fraction	10%	16%
Inlet Temperature [°C]	35	20
Operating Pressure [bar]	80	3
Pressure Drop [kPa]	14.85	37.6
Maximum Mach Number [-]	0.049	0.344

CHAPTER IV

RESULTS AND DISCUSSION

4.1 Comparison of Experimental and Numerical Results

In this section the experimental and numerical results are analyzed for the range of parameters spanned by this investigation. This section is organized as follows: subsection 4.1.1 compares the pressure drop, subsection 4.1.2 compares the temperature profiles, subsection 4.1.3 compares the heat transfer coefficients, subsection 4.1.4 details the effect of azimuthal rotation of the test section, subsection 4.1.5 describes the effect of the incident heat flux, and subsection 4.1.6 compares the Nusselt numbers.

4.1.1 Comparison of Pressure Drop

Comparing the pressure drop that was measured experimentally with the result of the numerical simulation provides an indication of whether the numerical simulation accurately portrays the experimental test conditions. Since the experimentally measured mass flow rate is specified as the inlet boundary condition as described in Chapter III subsection 3.1.3, the inlet pressure is free to vary during the simulation. With the exit pressure fixed according to the experimentally measured value, the overall pressure drop thus gives a measure of the simulation accuracy.

A good agreement between the pressure drop measured experimentally and the value obtained from the numerical simulation was obtained (Figure 4.1). The pressure drop from the numerical simulations consistently underestimates the experimentally measured value. One factor contributing to a higher experimental pressure drop is the presence of a 1.7 m Tygon tube and valve that is between the site of the inlet pressure measurement and the HEMJ divertor test section. The numerical model does not include these objects and therefore it does not account for their contributions to the pressure drop in the flow loop. Taking this into consideration, the agreement of the numerical and experimental pressure drop suggests that the numerical model accurately represents the experimental test section.

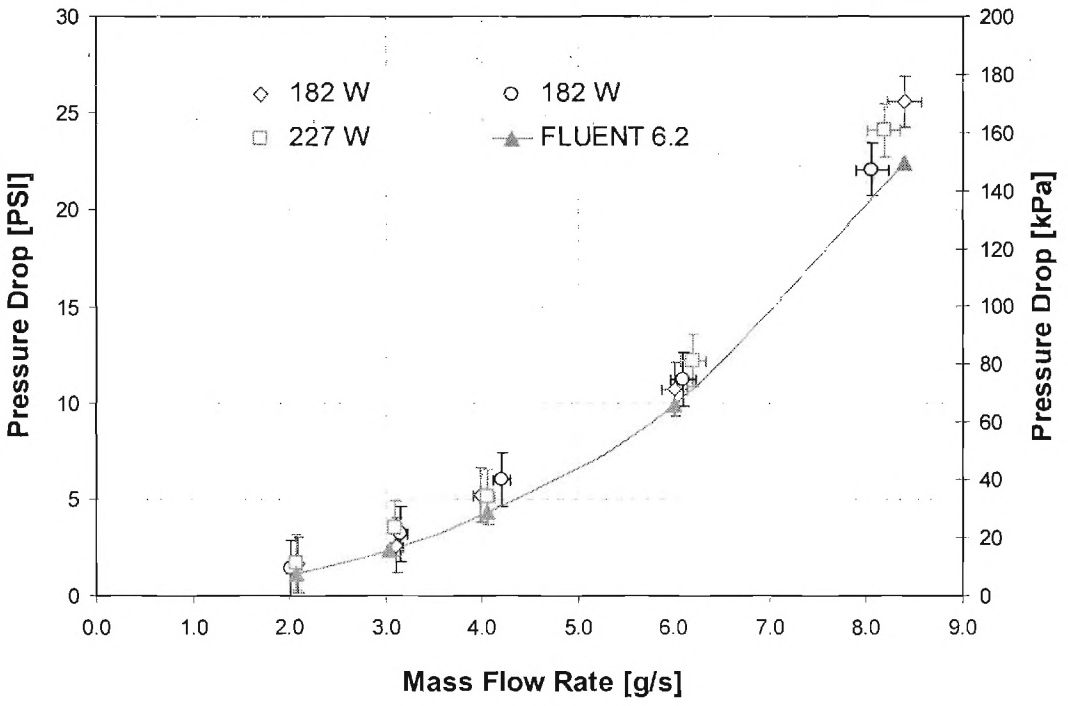

Figure 4.1: Plot of the experimental and numerical pressure drops.

4.1.2 Comparison of Temperature Profiles

The experimental temperature measurements from the thermocouple probes inserted into the brass thimble were compared to the numerical temperature field predicted by FLUENT®. The thermocouple probes are referenced by numbers 1 through 4 as described in subsection 2.1.2 and shown in Figures 4.2 and 4.3. The embedded temperature refers to the temperature reading at the thermocouple probe location. A point was created in FLUENT® at the location corresponding to the center of the end of each thermocouple hole. Numerical temperature values are referred to as FLUENT 6.2 in the result plots.

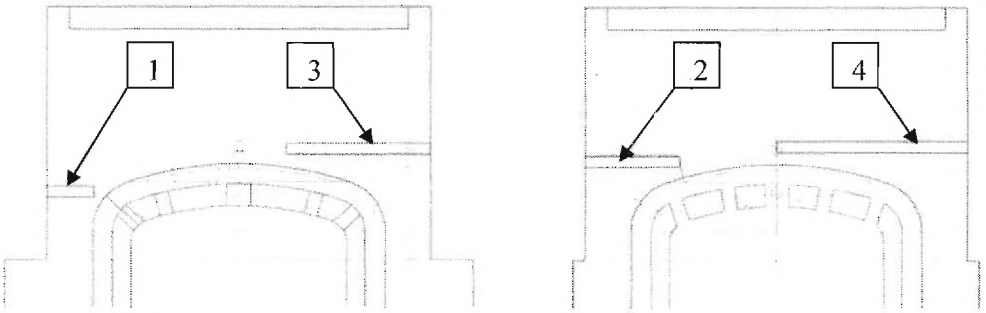

Figure 4.2: Drawing that shows the thermocouple locations in the brass thimble.

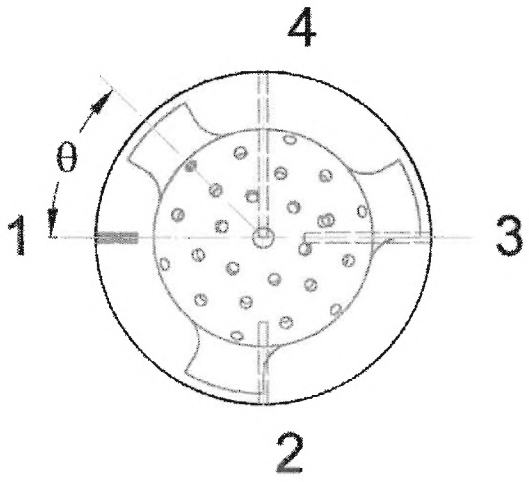

Figure 4.3: Drawing that shows the thermocouple locations in the brass thimble.

The embedded temperatures show a strong agreement between experimental and numerical values. Figure 4.4 shows embedded temperature results for an input power of 182.3 W and a mass flow rate of 3.11 g/s. This agreement between experimental and numerical embedded temperatures is consistent for the entire range of mass flow rates spanned in this investigation (Figures 4.5 through 4.8)

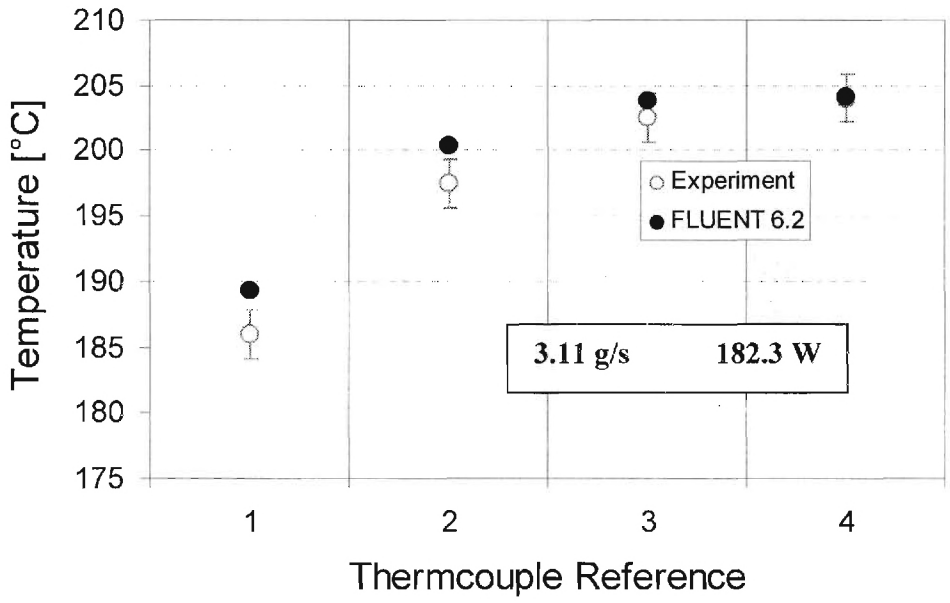

Figure 4.4: Plot of the embedded temperature results for a mass flow rate of 3.11 g/s and 182.3 W input.

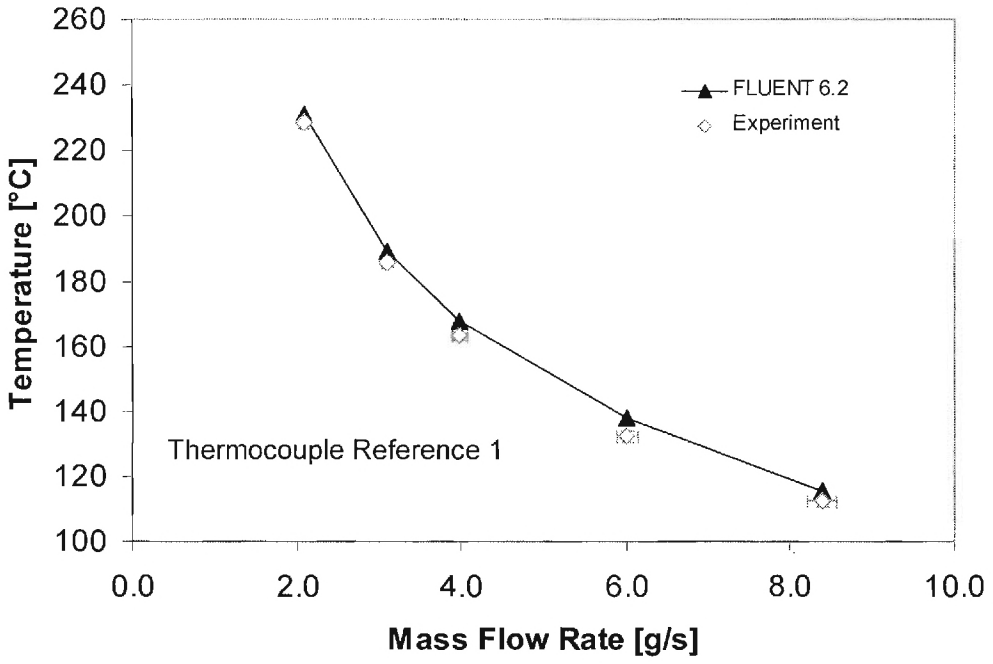

Figure 4.5: Plot of the embedded temperature results for Thermocouple Reference 1.

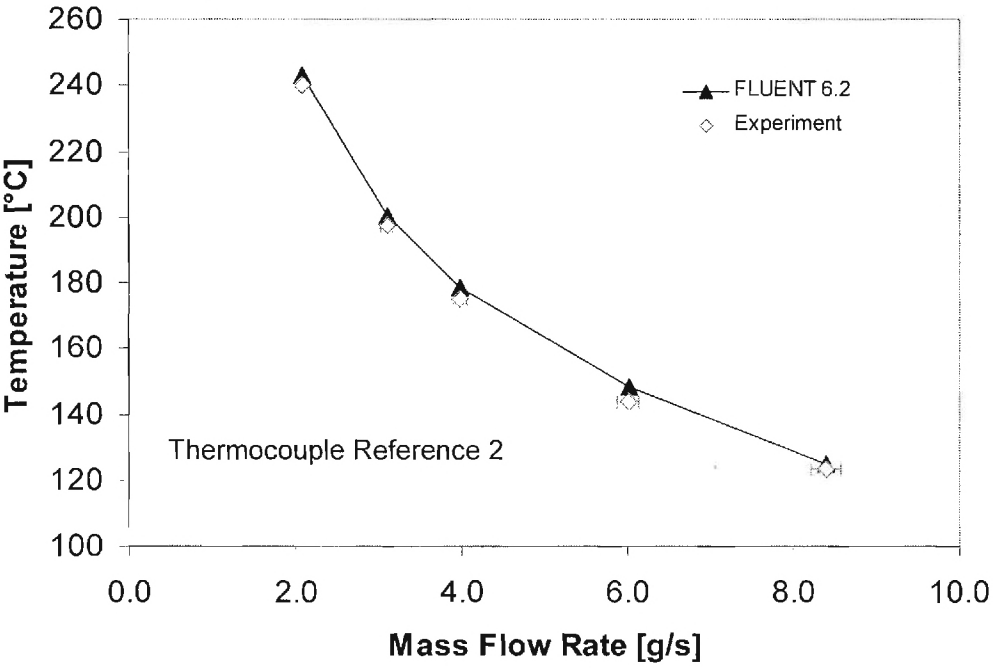

Figure 4.6: Plot of the embedded temperature results for Thermocouple Reference 2.

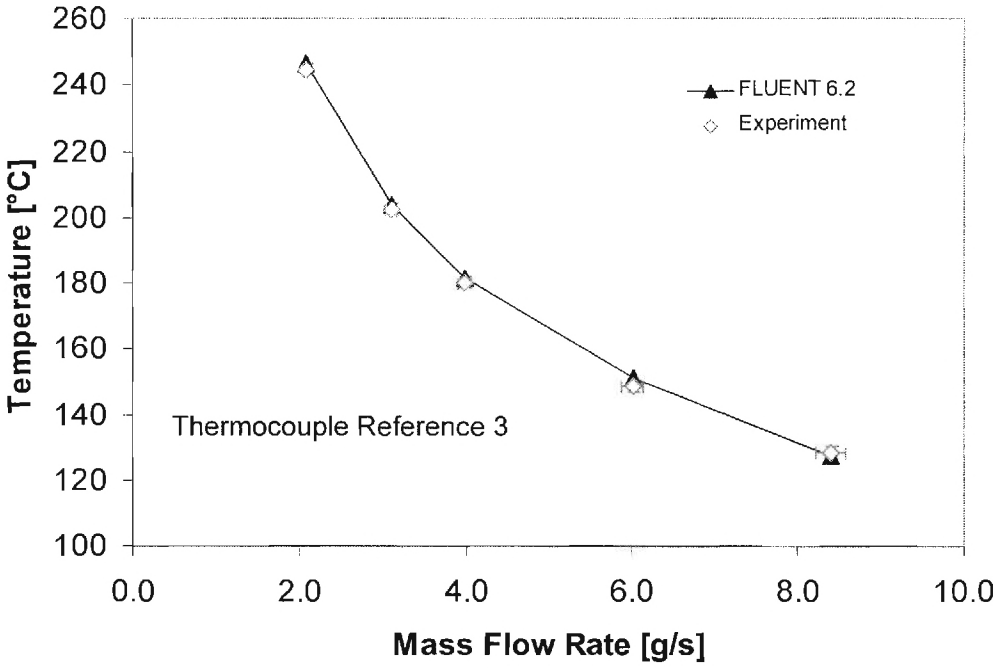

Figure 4.7: Plot of the embedded temperature results for Thermocouple Reference 3.

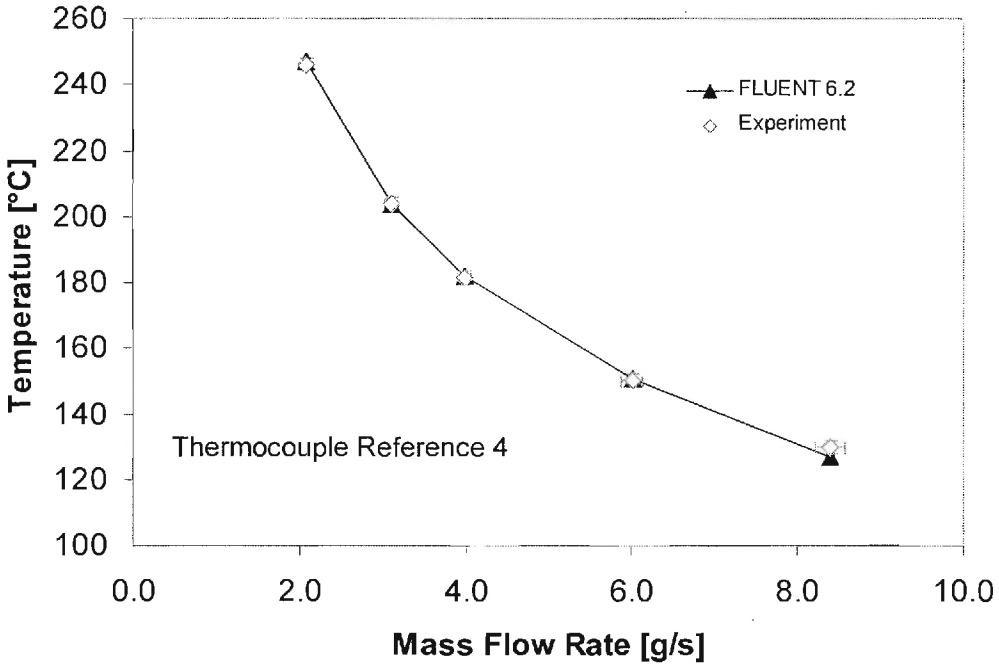

Figure 4.8: Plot of the embedded temperature results for Thermocouple Reference 4.

The surface temperature on the jet impingement surface of the brass thimble is required for determining the convective heat transfer coefficient. After verifying the FLUENT® model was accurately simulating the embedded temperatures for the brass thimble, four additional points were created in the numerical model below each embedded thermocouple location. These points were positioned on the jet impingement surface of the brass thimble such that the temperature difference between this point on the surface and the embedded point could be determined. This temperature difference was then used to correct the experimentally measured temperature for the conduction between the thermocouple embedded location and the jet impingement surface. The trend between the experimental and numerical surface temperatures followed the same trend seen previously for the embedded temperatures (Figure 4.9).

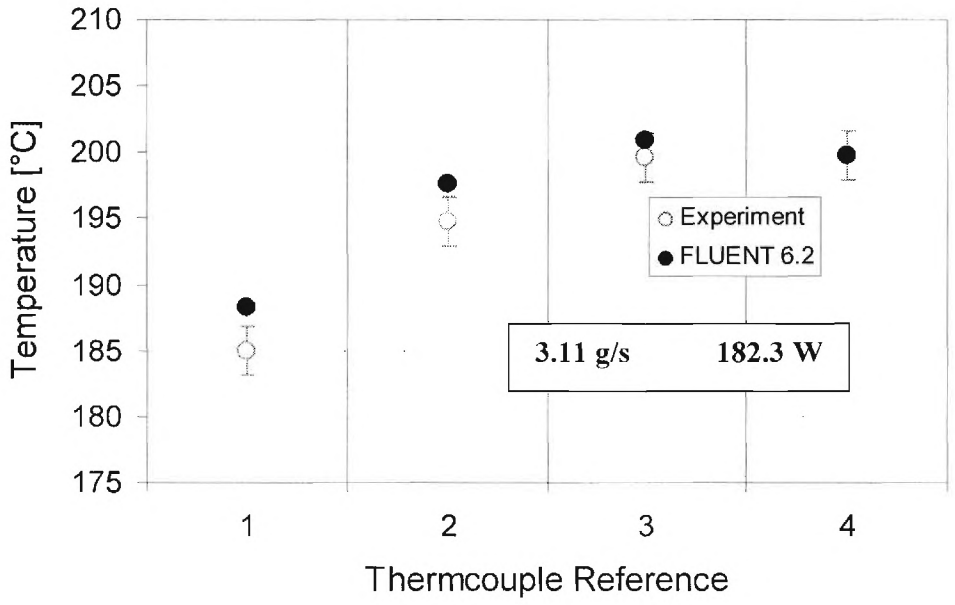

Figure 4.9: Plot of the surface temperature results for a mass flow rate of 3.11 g/s and 182.3 W input.

4.1.3 Comparison of Heat Transfer Coefficient

An experimental value for the local convective heat transfer coefficient was calculated relative to each of the thermocouple probes in the brass thimble. This calculation used a surface temperature that was determined by correcting the experimental embedded temperature for the conduction temperature difference between the embedded point and the jet impingement surface as described in subsection 4.1.4. The inlet air temperature was measured experimentally with a thermocouple (Label 6 Table 2.3). The heat flux on the jet impingement surface was determined from the numerical simulation by manually obtaining an average heat flux value in the vicinity of the desired surface point. The convective heat transfer coefficient was then calculated in the following manner:

$$h = \frac{q''_{surface}}{T_{surface} - T_{inlet}}$$

$$T_{surface} = T_{embedded} - \Delta T_{conduction}$$

Since it is impossible to experimentally measure the local heat flux at each instrumented location, the calculated values of heat flux described above were also used to evaluate the experimental heat transfer coefficient. While this argument seems somewhat "circular," the fact remains that matching between the experimental and numerical surface temperatures is, by itself, a confirmation of the matching between the local heat transfer coefficients. Comparisons of the experimental and numerical convective heat transfer coefficient showed a strong agreement. Data collected at the 0° azimuthal location illustrates this agreement (Figure 4.10). The heat transfer coefficient is

the highest near the surface under thermocouple reference four due to the central jet impinging directly upon it. In the 0° azimuthal location, a jet is also directly impinging on the surface relative to thermocouple reference one (Figure 4.3). Thermocouple reference positions two and three are not directly above a jet for the 0° azimuthal location and are thus lower relative to positions one and four. The strong agreement between the numerical and experimental values of the convective heat transfer coefficient was seen over the full range of mass flow rates spanned in this investigation (Figure 4.11).

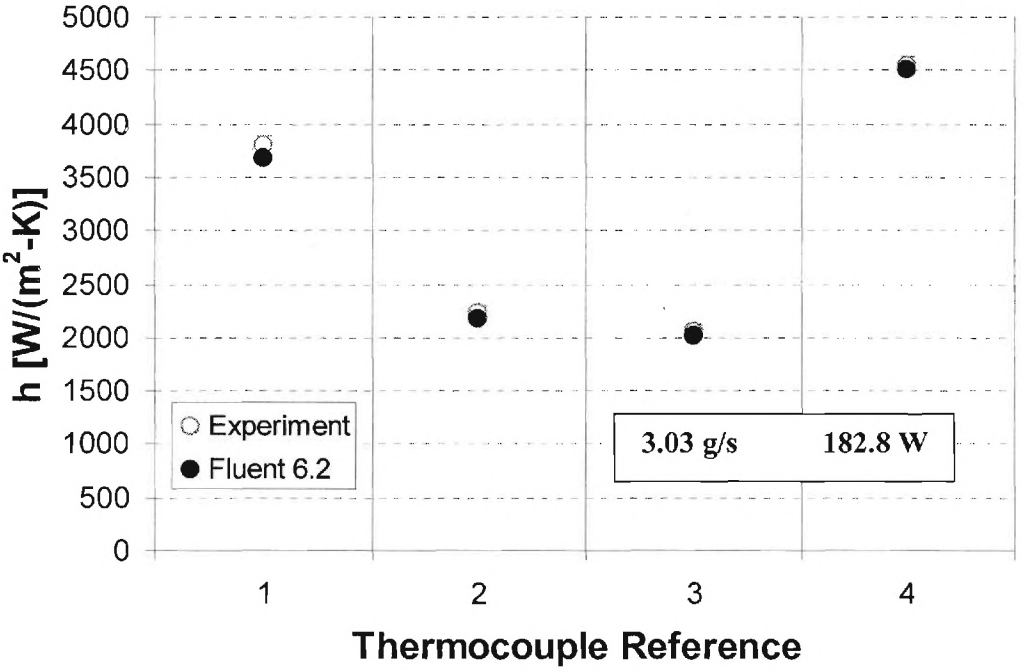

Figure 4.10: Comparison of the heat transfer coefficient for a mass flow rate of 3.03 g/s and 182.8 W input.

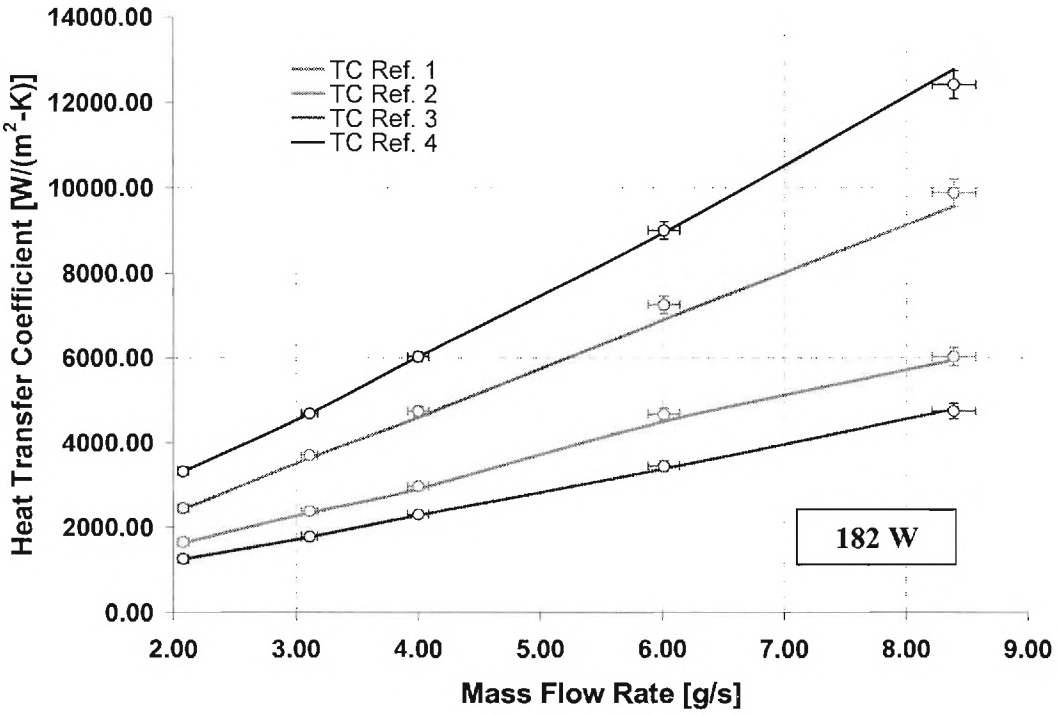

Figure 4.11: Convective heat transfer coefficients for 0° azimuthal position.

4.1.4 Effect of Azimuthal Rotation

The local heat flux values and thus the computed convective heat transfer coefficients are strongly influenced by the location of the jets. Therefore the effect of azimuthally rotating the jet cartridge relative to the brass thimble and hence the thermocouple probe locations was investigated. The layout of the jets on the jet cartridge is symmetric every 30° (Figure 4.4). To investigate the azimuthal variations of temperature and convective heat transfer coefficient, measurements were taken over 60° segments at 15° intervals.

The surface temperatures that were measured experimentally showed a symmetric pattern that matched the numerical results (Figure 4.12). The data from thermocouple reference one shows that is has the lowest temperature at the 0° location when it is next to a jet. At 60°, the thermocouple is at a location equivalent to the 0° position. The experimental values at 60° and 0° are in close agreement with each other as expected. The highest temperature should occur when the thermocouple is furthest from a direct jet impingement location. For thermocouple reference one, this corresponds to the 15° and 45° location.

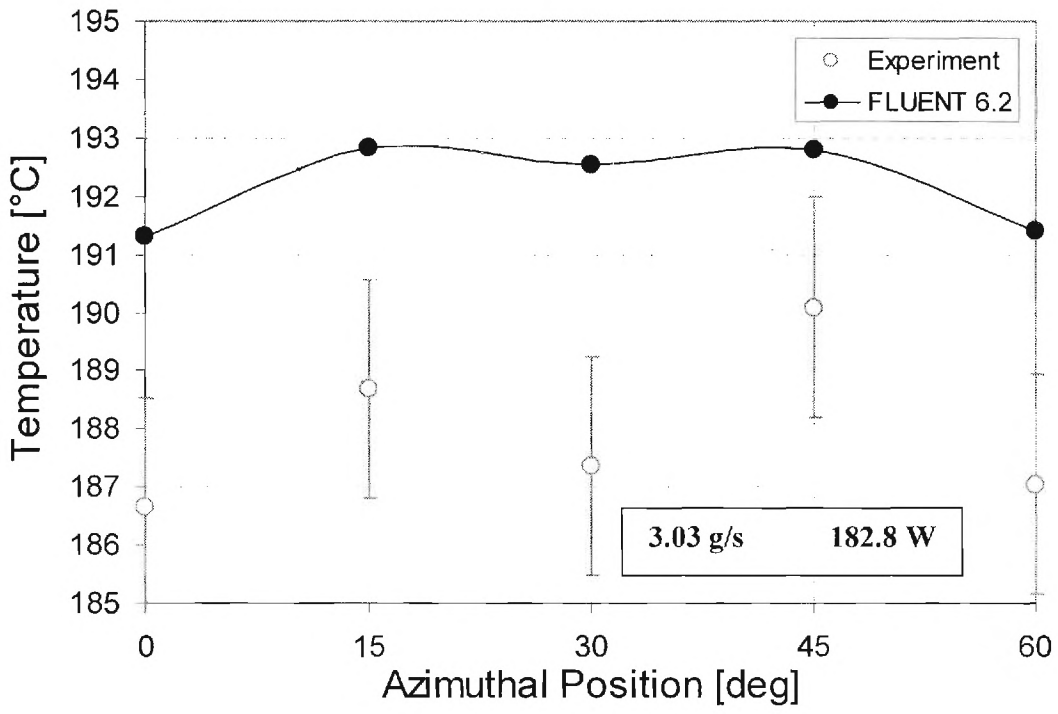

Figure 4.12: Azimuthal variation of the surface temperature of thermocouple reference position 1 for a mass flow rate of 3.03 g/s and 182.8 W input.

Thermocouple reference positions two and three also displayed 30° symmetric patterns with the highest temperature occurring when a jet impingement site was furthest away (Figure 4.13 and Figure 4.14). Since thermocouple reference positions two and three are nearer to the center of the jet cartridge, the density of the jets increases due to the decreasing radius of each jet "bolt" circle. Therefore, the azimuthal temperature variations are smaller in magnitude relative to the variation seen for thermocouple reference one (which had the largest projected radius and accordingly the most widely spaced jets).

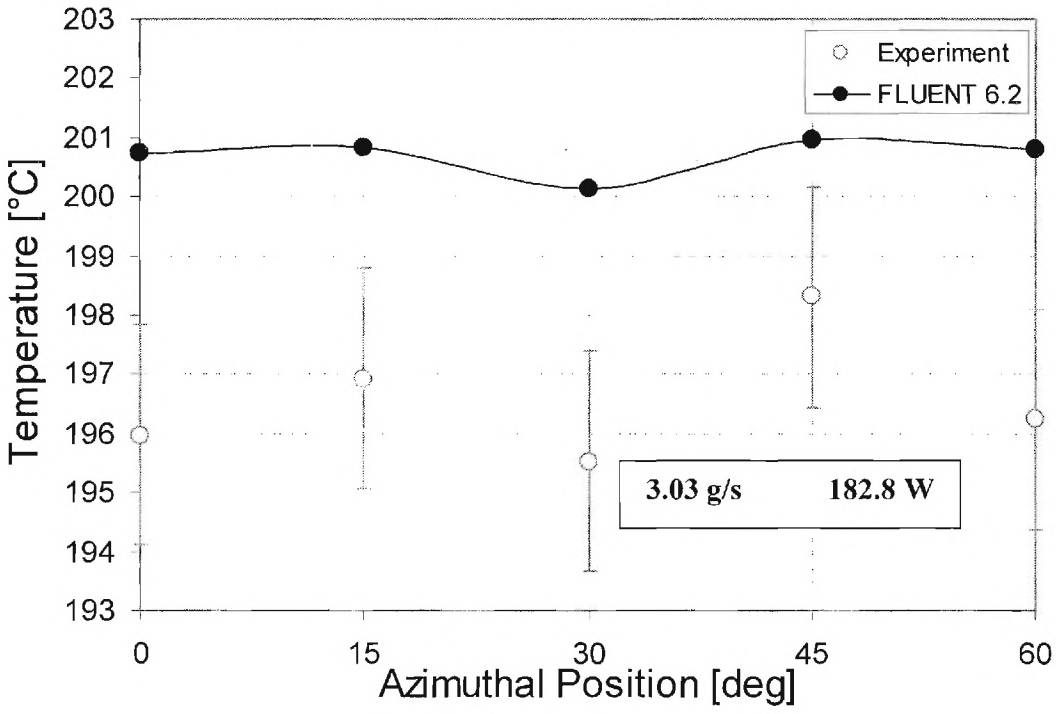

Figure 4.13: Azimuthal variation of the surface temperature of thermocouple reference position 2 for a mass flow rate of 3.03 g/s and 182.8 W input.

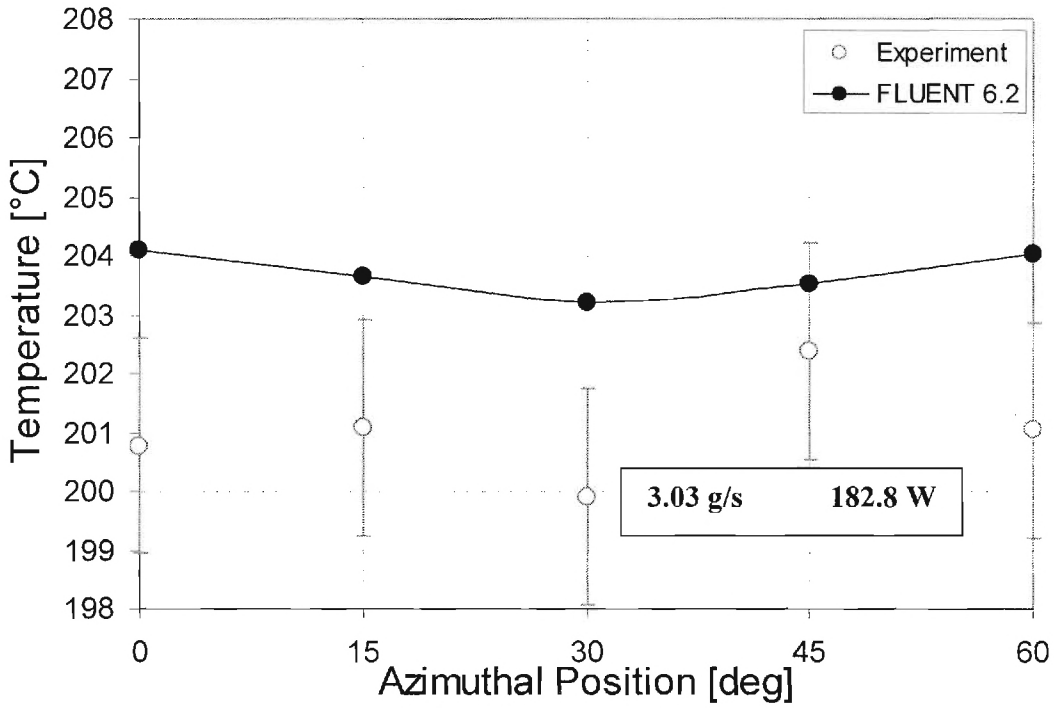

Figure 4.14: Azimuthal variation of the surface temperature of thermocouple reference position 3 for a mass flow rate of 3.03 g/s and 182.8 W input.

Thermocouple reference position four is directly above the central jet and should not be affected by azimuthal rotation. Experimental measurements confirmed that this temperature remains approximately constant relative to azimuthal rotation (Figure 4.15).

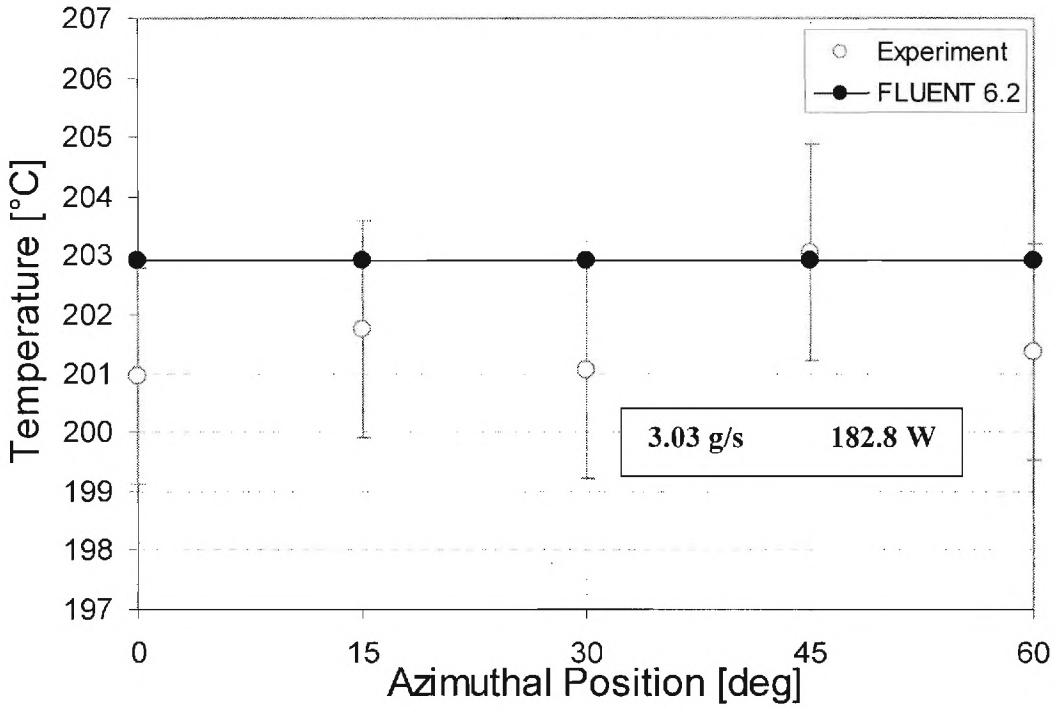

Figure 4.15: Azimuthal variation of the surface temperature of thermocouple reference position 4 for a mass flow rate of 3.03 g/s and 182.8 W input.

Due to the azimuthal variations in the heat flux and temperature field on the jet impingement surface, the convective heat transfer coefficient varied azimuthally (Figure 4.16). The convective heat transfer coefficient relative to thermocouple reference positions one, two, and three all showed higher values when they were aligned with a jet. The difference between the highest and lowest values was greatest for thermocouple reference one since it has the largest spacing between jet locations. This difference between highest and lowest values decreased as the center of the jet cartridge was approached. The convective heat transfer coefficient remained approximately constant above the central jet since this location is not affected by azimuthal rotation.

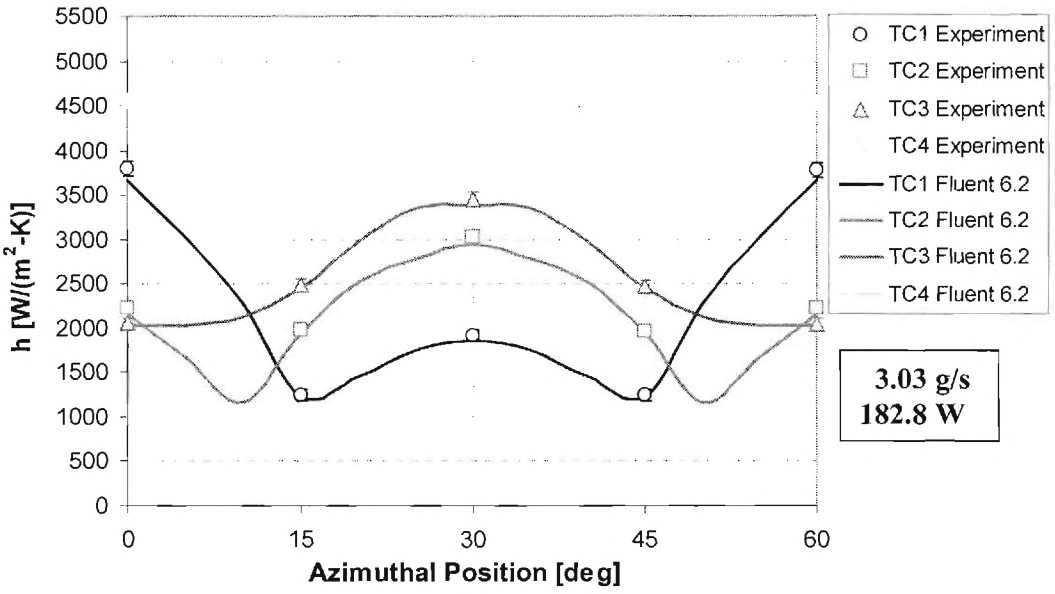

Figure 4.16: Azimuthal variation of the convective heat transfer coefficient for a mass flow rate of 3.03 g/s and 182.8 W input.

4.1.5 Effect of Incident Heat Flux

The HEMJ divertor test section was investigated under an elevated heat load of 227 W to create a nominal heat flux 1.0 MW/m^2 that is incident on the brass thimble. This heat load resulted in a measured heat flux of approximately 0.895 MW/m^2. The temperature profiles on the jet impingement surface remained similar to those for the cases with a heat input of 182 W, but with an increase in magnitude (Figure 4.17). The local convective heat transfer coefficient also exhibited a similar profile relative to the 182 W heat input case (Figure 4.18).

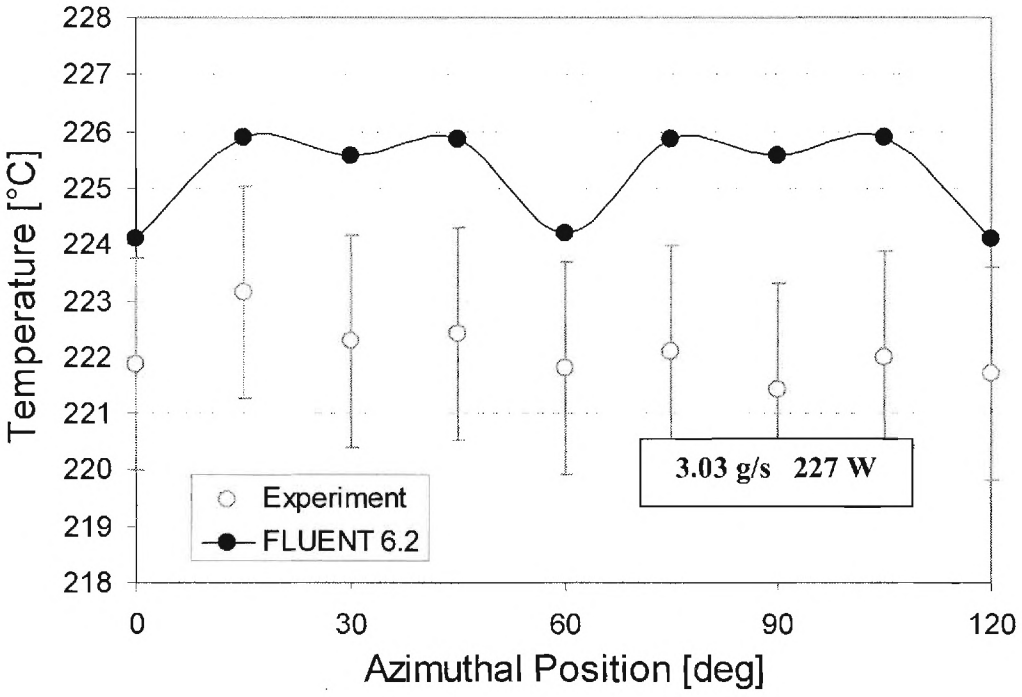

Figure 4.17: Azimuthal variation of the surface temperature of thermocouple reference position 1 for a mass flow rate of 3.03 g/s and 227 W input.

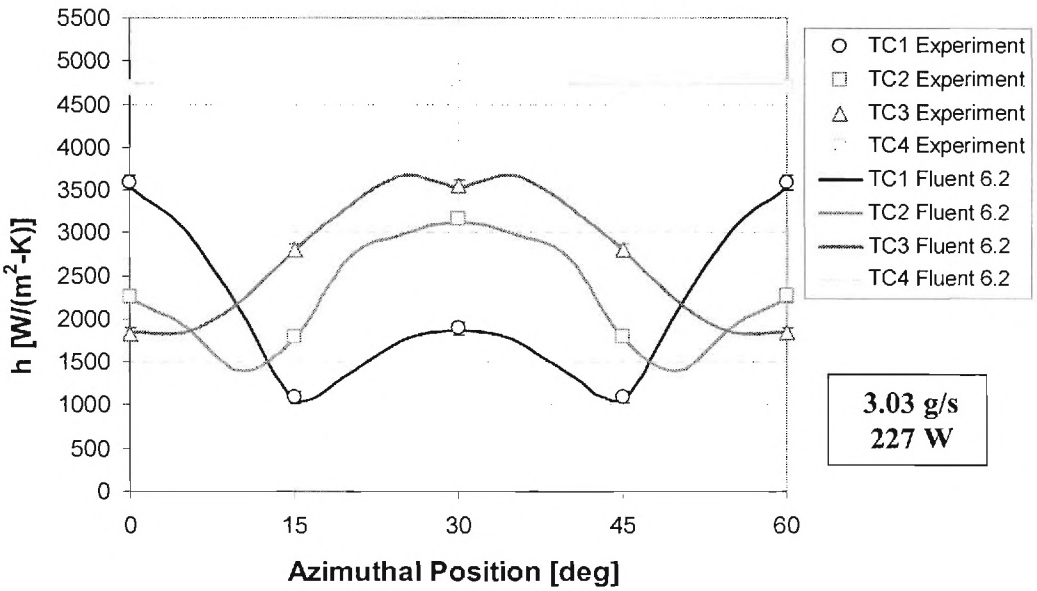

Figure 4.18: Azimuthal variation of the convective heat transfer coefficient for a mass flow rate of 3.03 g/s and 227 W input.

The experimental data collected with 227 W input to the test section was consistent with the 182 W input data over the range of mass flow rates covered by this investigation. The surface temperature above the central jet (reference position four) agreed with the numerical results and showed a similar dependence on mass flow rate as the 182 W cases.

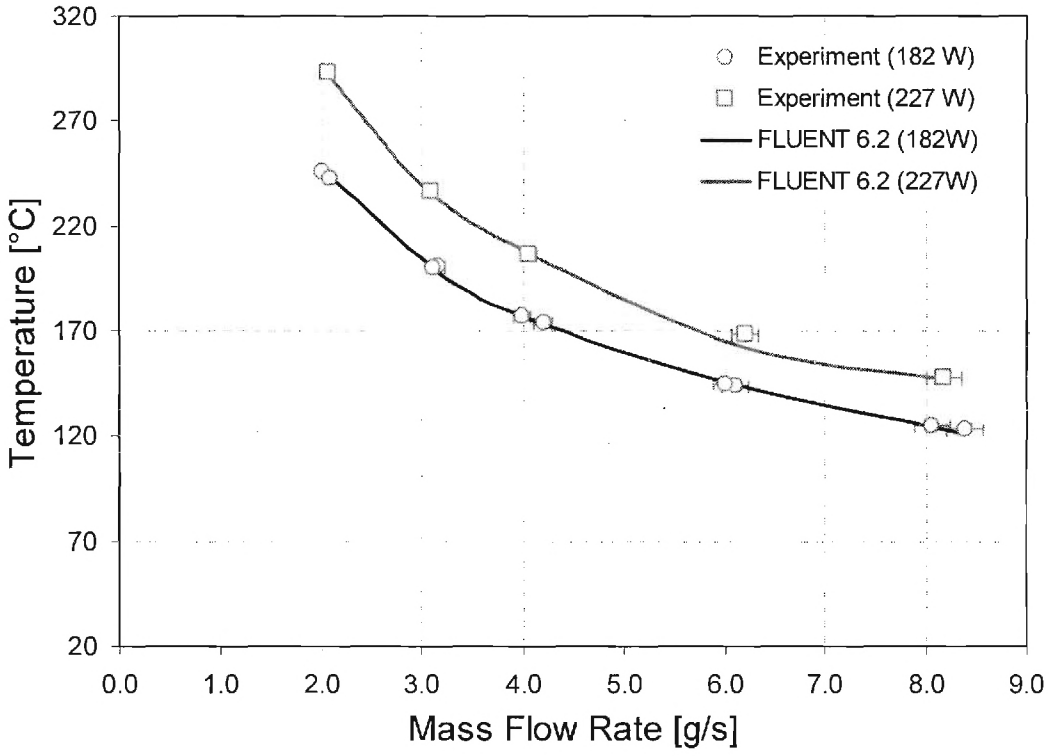

Figure 4.19: Experimental and numerical surface temperatures of thermocouple reference position four.

4.1.6 Nusselt Number Calculations

The Nusselt number was calculated with a characteristic length of 1.0 mm corresponding to the diameter of the central jet. The conductivity of air used for all calculations was 0.02521 W/(m-K). A constant conductivity was used because the FLUENT® model used a constant conductivity. Therefore, since the Nusselt number is simply the heat transfer coefficient multiplied by a constant for this analysis, it displays the same form as the heat transfer coefficient. The two power inputs used in this investigation did not affect the Nusselt number over the range of mass flow rates studied here (Figure 4.20).

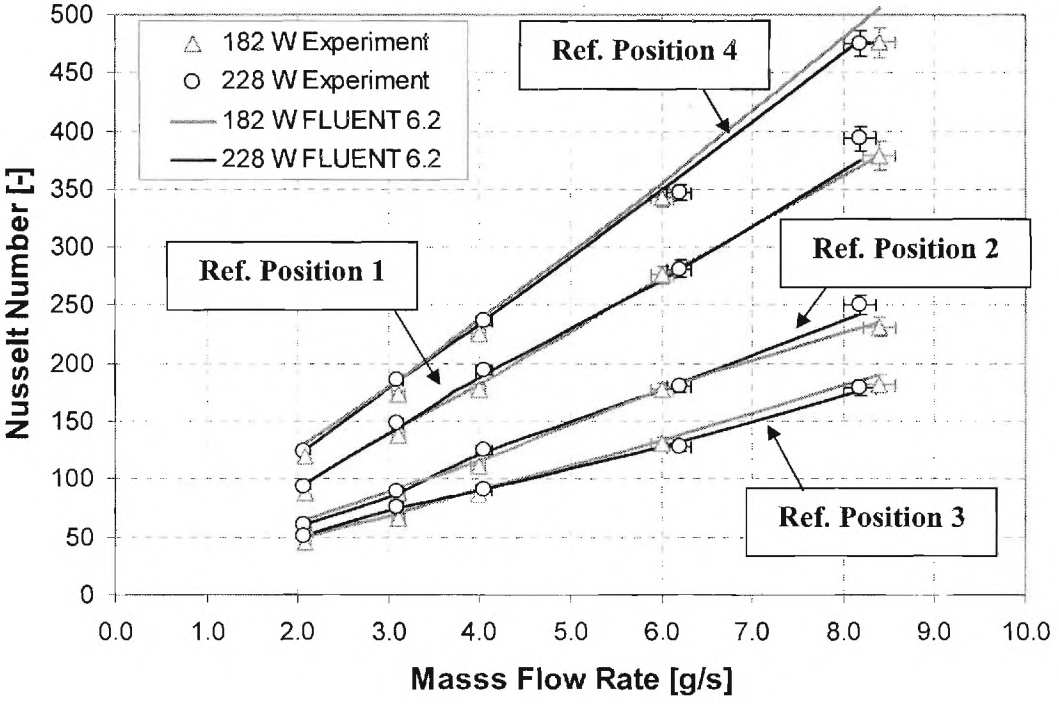

Figure 4.20: Nusselt number relative to the four thermocouple reference locations at the 0^{o} azimuthal position.

CHAPTER V

CONCLUSIONS AND RECOMMENDATIONS

5.1 Conclusions

The heat transfer performance of the HEMJ divertor design was experimentally investigated in an air flow loop under non-dimensional operating conditions corresponding to its end-use application of cooling the divertor in the DEMO reactor. A test section was designed to create a heat flux equivalent to the anticipated form of loading that the HEMJ divertor will be subject to in the DEMO reactor. This test section was instrumented in a manner that enabled boundary conditions and thermal-hydraulic data to be collected and then used for performing numerical simulations of the experiments. Validating the numerical model was accomplished by comparing the experimental and numerical temperature field in the uniform heat flux area of the test section ("neck" region of the copper heater block). Comparing the experimental and numerical pressure drop provided an additional metric of whether the two cases were in agreement. After establishing that the thermal (judged by the agreement in temperatures) and fluid dynamics (judged by the agreement in pressure drop) aspects of the experimental test section and numerical model conformed to one another, derived quantities were compared. The numerical model was used to obtain experimental temperatures on the jet impingement surface. Then using the experimental surface

temperatures and heat fluxes on the jet impingement surface attained from the numerical model, experimental heat transfer coefficients were computed. The numerical and experimental heat transfer coefficients were then compared for varying azimuthal locations on the jet impingement surface and nominal incident heat fluxes of 0.8 MW/m^2 and 1.0 MW/m^2. The experimental and numerical quantities typically fell within the calculated uncertainty of the experimental methods used in this investigation.

5.1.1 Pressure Drop

Comparison between the experimental and numerical pressure drop values showed a strong agreement over the range of Reynolds number spanned by this investigation. This gave added confidence that the numerical model was accurate for the test section. The measured pressure drop was always greater than the numerical value. The most probable cause of this is the presence of a 1.7 m long Tygon tube and valve between the air supply and the test section, which were not included in the model. Improved accuracy of the experimental pressure drop could be obtained by using a pressure transducer rather than an analog test gauge and by measuring the inlet pressure after the Tygon tube and valve.

5.1.2 Heat Transfer Coefficient

There was strong agreement between the embedded thermocouple temperatures of the test section and the numerical temperatures at those locations. This gave reassurance to the proposed method of calculating the experimental heat transfer coefficient by using surface temperature corrections and local heat flux values from the numerical model. The

experimental heat transfer coefficient agreed well with the numerical results for all mass flow rates and heat loads. The experimental and numerical results showed that the enhancement of the heat transfer coefficient is very sensitive to the location of the jets. As expected *a priori*, the highest heat transfer coefficient was above the central jet. The magnitude of the difference between the maximum and minimum heat transfer coefficients for a given "bolt" circle was greatest for the outermost "bolt" circle four. This is most likely due to increased spacing between the jets.

5.2 Recommendations

Further studies of the HEMJ divertor design should focus on decreasing the uncertainty in the measurements and expansion of the experimental test space. The uncertainty could be improved by performing an additional calibration of the thermocouples and replacing the analog test gauge with a pressure transducer. In future designs of a test section, a longer "neck" region could also improve the accuracy of the experimental heat flux measurement by increasing the distance between thermocouple holes.

The experimental test space should be expanded to include higher heat fluxes under the condition that the temperature of the brazing surface between the copper heater block and the brass thimble remains below its limit. Higher heat fluxes can also be accommodated by using helium since it has a larger thermal conductivity. After the HEMJ divertor test section has been tested in the HEBLO Test Facility, comparisons between the two coolants should be made. If the helium experiments behave as expected,

a larger test section which would accommodate multiple HEMJ modules should be investigated.

APPENDIX A

ERROR ANALYSIS

Appendix A details the sources of error that occurred in the investigation. The total uncertainty was calculated as the root-mean-square of the uncertainty due to statistical fluctuations, U_A, and the uncertainty due to the instrumentation, U_B. An error propagation formula (A.3) was used to determine the uncertainty for derived quantities. The multiplier, k_C, of the sample standard deviation was determined from an appropriate distribution such that 95% of the data should fall within the statistical fluctuations. The error propagation contribution to the total uncertainty did not include covariance terms.

$$U_A = k_c \sigma_{Sample} \qquad \textbf{A.1}$$

$$\sigma_{Sample} = \sqrt{\frac{1}{N-1}\sum (x_i - \bar{x})^2} \qquad \textbf{A.2}$$

$$U_X(i, j.., k) = \sqrt{U_i^2\left(\frac{\partial U_i}{\partial i}\right)^2 + U_j^2\left(\frac{\partial U_j}{\partial j}\right)^2 + ... + U_k^2\left(\frac{\partial U_k}{\partial k}\right)^2} \qquad \textbf{A.3}$$

$$U_{Total} = \sqrt{U_A^2 + U_B^2} \qquad \textbf{A.4}$$

A.1 Uncertainty in Mass Flow Rate

For the uncertainty of the mass flow rate measurement, only the uncertainty due to statistical fluctuations was considered. To calculate the sample standard deviation (A.2) a set of four measurements made during a steady state experiment was used. The calculated sample standard deviation for this data is 0.0205 g/s. The Student's t-distribution for 3 degrees of freedom was used to determine that k_C should be 3.2 for 95% of the measurements to fall within the total uncertainty. The total uncertainty for this sample set was found to be 0.0656 g/s. The relative uncertainty was then calculated based on the mean value of the sample set. Thus the relative error in the mass flow rate measurement was found to be 2.14%. This relative uncertainty was assumed to be constant over the range of mass flow rates for this investigation.

Table A.1 Sample set of mass flow rate measurements.

Flow Rate [g/s]
3.08
3.08
3.04
3.08

A.2 Uncertainty in Thermocouple Measurements

The total uncertainty in the thermocouple reading was found by considering the manufacturer stated instrumental uncertainty of +/- 1.5 ^{o}C and the statistical fluctuations during an experiment. U_A was found by analyzing the temperature fluctuations during the experiment at steady state for 75 data points. This represents data collected for 12.5 minutes. A Gaussian distribution with k_C equal to 2.0 was used to encompass 95% of the measurements.

Table A.2. Thermocouple uncertainty data.

	Mean [°C]	σ_{Sample}	U_A	U_B	U_{total}
T1	185.8	0.571	1.142	1.50	1.89
T2	196.8	0.547	1.094	1.50	1.86
T3	201.7	0.530	1.060	1.50	1.84
T4	203.3	0.528	1.057	1.50	1.83
T5	241.4	0.382	0.764	1.50	1.68
T6	251.8	0.353	0.705	1.50	1.66
T7	261.4	0.330	0.661	1.50	1.64
T8	302.3	0.278	0.556	1.50	1.60
T9	302.3	0.279	0.558	1.50	1.60
T_{in}	20.4	0.121	0.241	1.50	1.52
T_{out}	66.8	0.287	0.574	1.50	1.61

A.3 Uncertainty in Heat Transfer Coefficient

The total uncertainty in the heat transfer coefficient was found by using an error propagation formula (A.5). The heat transfer coefficient has an influence coefficient and standard uncertainty for the surface temperature, inlet temperature, and heat flux. The temperature standard uncertainties were computed in subsection A.1. The heat flux standard uncertainty is due to the manner in which it was obtained from FLUENT ®. By manually picking the heat flux at the desired location on the jet impingement surface, a heat flux range is returned for each element. This is a result of the number of intervals that the full range of values is divided into. The full range in FLUENT® was divided into 40 intervals which results in a +/- 1.25% relative uncertainty of the heat flux. The total uncertainty of the heat flux, $U_{q''}^2$, was determined by multiplying the recorded heat flux

value by the relative uncertainty. The total uncertainty in the heat transfer coefficient varied from 1.8% to 5.5% depending on experiment conditions and azimuthal location.

$$U_{HTC} = \sqrt{\left(U_{q''}^2 \frac{1}{(T_s - T_{in})^2} + U_{T_s}^2 \frac{q''^2}{(T_s - T_{in})^4} + U_{T_{in}}^2 \frac{q''^2}{(T_{in} - T_s)^4} \right)} \quad \textbf{A.5}$$

A.4 Uncertainty in Nusselt Number

With the total uncertainty of the heat transfer coefficient know, the total uncertainty for the Nusselt number can be easily calculated based on the jet diameter and thermal conductivity of the coolant. The relative uncertainty of the Nusselt number was 2.38% for the 0.6 mm diameter jets and 3.97% for the 1.0 mm diameter central jet.

$$U_{Nu} = \sqrt{\left(\frac{d}{k} \right)^2 U_{HTC}^2} \quad \textbf{A.6}$$

Table A.3. Heat transfer coefficient and Nusselt number uncertainty data.

Probe	m [g/s]	HTC W/(m^2-K)	U_{HTC} W/(m^2-K)	Relative Uncertainty		Nu [-]	U_{Nu} [-]	Relative Uncertainty
TC1	2.08	2454.57	52.91	2.16%		97.36	2.10	2.16%
	3.11	3709.81	84.03	2.27%		147.16	3.33	2.27%
	4.00	4742.12	116.27	2.45%		188.10	4.61	2.45%
	6.01	7244.41	203.22	2.81%		287.36	8.06	2.81%
	8.39	9874.66	322.03	3.26%		391.70	12.77	3.26%
TC2	2.08	1655.94	46.31	2.80%		65.69	1.84	2.80%
	3.11	2381.43	68.60	2.88%		94.46	2.72	2.88%
	4.00	2978.75	91.03	3.06%		118.16	3.61	3.06%
	6.01	4662.20	149.19	3.20%		184.93	5.92	3.20%
	8.39	6030.08	217.67	3.61%		239.19	8.63	3.61%
TC3	2.08	1259.73	43.75	3.47%		49.97	1.74	3.47%
	3.11	1786.06	63.24	3.54%		70.85	2.51	3.54%
	4.00	2307.35	83.15	3.60%		91.53	3.30	3.60%
	6.01	3442.81	129.93	3.77%		136.57	5.15	3.77%
	8.39	4744.43	188.72	3.98%		188.20	7.49	3.98%
TC4	2.08	3326.14	54.75	1.65%		131.94	2.17	1.65%
	3.11	4686.92	85.52	1.82%		185.92	3.39	1.82%
	4.00	6029.08	119.02	1.97%		239.15	4.72	1.97%
	6.01	9001.33	205.82	2.29%		357.05	8.16	2.29%
	8.39	12404.89	327.66	2.64%		492.06	13.00	2.64%

A.5 Uncertainty in Experimental Incident Heat Flux Measurement

The uncertainty of the experimental incident heat flux measurement in the "neck" region of the HEMJ divertor test section was calculated by determining the error propagation formula for the heat flux (A.8). The total uncertainty is computed for the average of the three heat flux measurements made by using three combinations of thermocouples five, six, and seven (A.7). The total uncertainty in the heat flux measurement is 0.083 MW/m^2. This corresponds to a relative error of approximately 10 - 12% for this investigation.

$$q''_{measured} = \left(\frac{k}{3}\right)\left[\frac{T_7 - T_6}{.005} + \frac{T_6 - T_5}{.005} + \frac{T_7 - T_5}{.01}\right] \quad \textbf{A.7}$$

$$U_{q''_{measured}} = \sqrt{\left(\sigma_{T_i}^2 (100k)^2 + \sigma_{T_j}^2 (100k)^2\right)} \quad \textbf{A.8}$$

A.6 Uncertainty in Power Measurement

The uncertainty in the power input was determined by considering the statistical uncertainty due to fluctuations during the experiment and the manufacturer stated tolerances for the voltage and current measurement instruments. The statistical uncertainty was found by first calculating a sample standard deviation for the voltage and current recorded during steady state using formula A.2. A Gaussian distribution and k_C of 2.0 was used for a 95% confidence level. These statistical uncertainties were then used in the error propagation formula for the power input (A.9).

The manufacturers' stated tolerance of the Agilent Data Acquisition unit is 0.01% and the Fluke 25 multimeter is 0.75%. These tolerances were used to determine the uncertainty of the voltage and current due to the instruments. Next these uncertainties were used in the error propagation formula for the power input (A.9). Finally the total uncertainty was found by taking the root-mean-square of the two sources of error computed for the power input. The relative uncertainty found for the power measurement was approximately 1.0%.

$$U_{Power} = \sqrt{P^2\left(\frac{U_I^2}{I^2} + \frac{U_v^2}{V^2}\right)} \qquad \text{A.9}$$

Table A.4. Power measurement uncertainty data.

	Power	Voltage	Current		Power	Voltage	Current
	182.8	62.09	2.94		227.0	69.3	3.28
$U_{Statistical}$	1.256	0.064	0.020		1.402	0.064	0.020
$U_{Instrumentation}$	1.371	0.006	0.022		1.703	0.007	0.025
U_{Power}	1.859				2.205		
Relative Uncertainty	1.02%				0.97%		

A.7 Uncertainty in Pressure Drop

The uncertainty in the pressure drop was determined by considering statistical fluctuations in the inlet pressure during operation of the test section as well as manufacturing uncertainties. The uncertainty for the statistical component was found by using a Gaussian distribution with k_C equal to 2.0. Then the total statistical uncertainty was determined by using the error propagation formula for the pressure drop (A.10). The Omega pressure transducer has a manufacturer stated tolerance of 0.75% and the Ashcroft test gauge was distinguishable to 0.5 psi. The instrumentation uncertainties were computed for the experimental pressure readings. Then the total instrumentation uncertainty was computed with the error propagation formula for the pressure drop (A.10). Finally the total uncertainty in the pressure drop was calculated by taking the root-mean-squared value of the total instrumental and statistical uncertainties. The relative uncertainty in the pressure drop measurement was high for the low mass flow rate experiments due to the magnitude of the pressure drop being small.

$$U_{dP} = \sqrt{\sigma_{Pin}^2 + \sigma_{Pout}^2} \qquad \text{A.10}$$

Table A.5. Pressure drop uncertainty data.

m	P_{in}	P_{out}	σ_{Pout}^2	σ_{Pin}^2	$U_{Statistical}$	$U_{Instrumentation}$	U_{total}	Relative
2.08	107.0	105.40	0.79	0.50	1.08	0.94	1.43	89.5%
3.11	106.0	103.40	0.78	0.50	1.08	0.92	1.42	54.8%
4.00	106.0	100.80	0.76	0.50	1.08	0.91	1.41	27.2%
6.01	103.5	92.80	0.70	0.50	1.08	0.86	1.38	12.9%
8.39	101.5	75.88	0.57	0.50	1.08	0.76	1.32	5.2%

APPENDIX B

PARAMETRIC STUDY FOR HEBLO TEST CONDITIONS

Appendix B details a parametric study of the HEMJ divertor test section's predicted thermal performance in the HEBLO Test Facility. The purpose of this analysis is to provide guidance in selecting the operating conditions of the HEBLO Test Facility. Recommended maximum copper (500°C) and brass thimble (300°C) temperatures were used as the limit of safe operation. The parametric study spanned heater power inputs corresponding to nominal heat fluxes of 1.0 to 5.0 MW/m^2 for mass flow rates of 1.5 to 8.0 g/s. Figure B.1 and Table B.1 detail the boundary conditions used for the simulations. In all cases, the pressure is 8.0 MPa and the helium inlet temperature is 35 °C. The standard k-epsilon turbulence model with the standard wall functions was used for all simulations. The simulations generally converged after 350 to 500 iterations (Figure B.2).

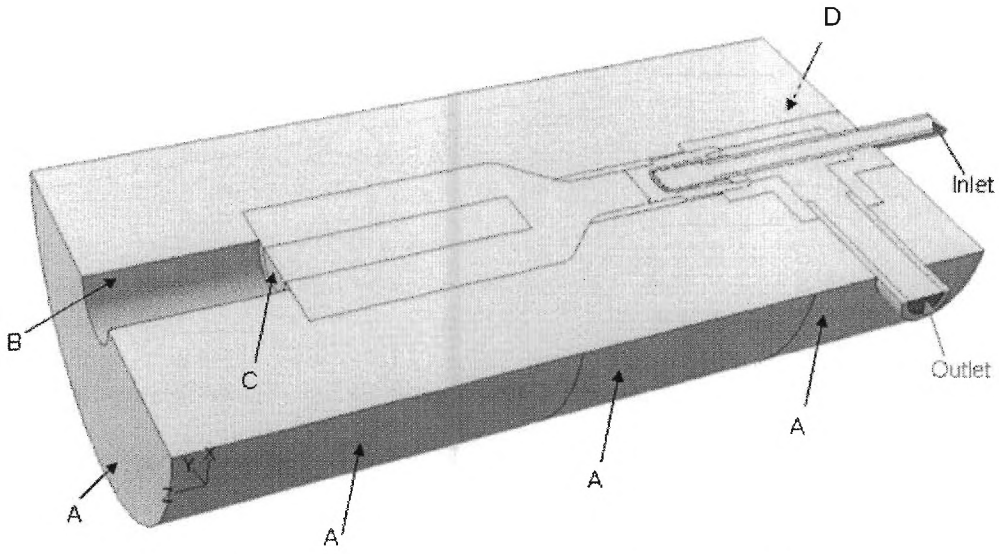

Figure B.1 Boundary condition locations for the FLUENT® model.

Table B.1. Details of the boundary conditions used in the FLUENT® model.

Reference	Type	Parameters
Inlet	Mass Flow Rate	1.5 to 8.0 g/s at 35°C
Outlet	Pressure	8.0 MPa
A	Convection	HTC=5 [W/(m^2-K)] and T_f = 20°C
B	Convection	HTC=15 [W/(m^2-K)] and T_f = 68°C
C	Convection	HTC=35 [W/(m^2-K)] and T_f = 260°C
D	Convection	HTC=10 [W/(m^2-K)] and T_f = 20°C
Q	Volumetric Heat Generation Rate	[W/m^3] Corresponding to nominal heat fluxes of 1.0 to 5.0 [MW/m^2]

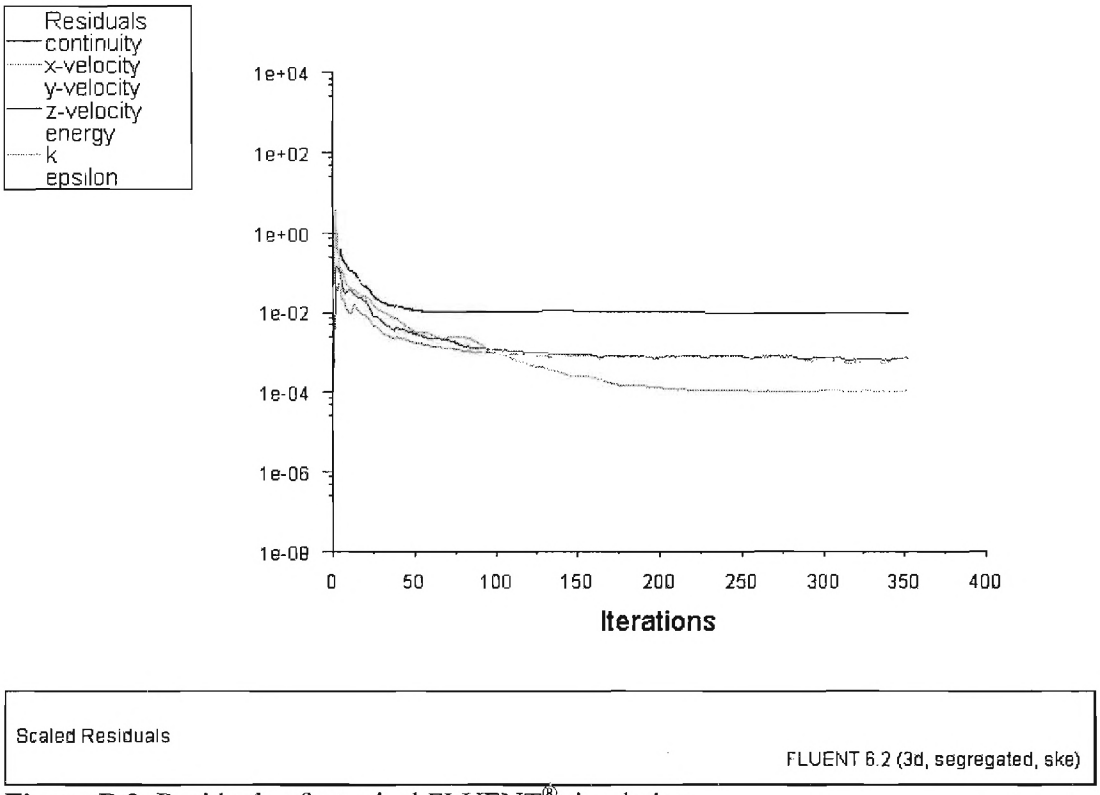

Figure B.2. Residuals of a typical FLUENT® simulation.

B.1 Maximum Brass Thimble Temperature

The analysis of the maximum brass thimble temperature for the range of mass flow rates and heat fluxes (Figure B.3) was performed using a recommended limit of 300°C as well as a more conservative (200 °C) and less conservative (400 °C) limit. The Reynolds number of the 3.33 g/s mass flow rate case matches the HEMJ nominal Reynolds number. The brass thimble temperature distribution for the standard case of 3.33 g/s and 2.0 MW/m^2 is shown in Figure B.4. For this case the volumetric average temperature of the brass thimble is 126.5°C and the maximum temperature is 280.1°C.

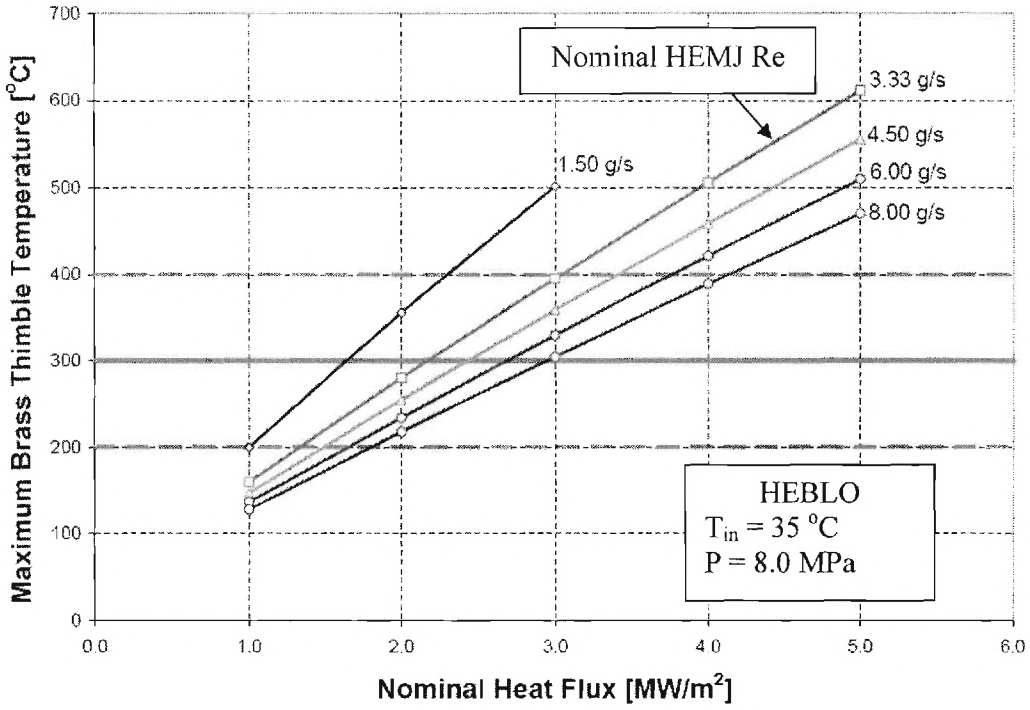

Figure B.3. Maximum Brass Thimble Temperature for the parametric simulations.

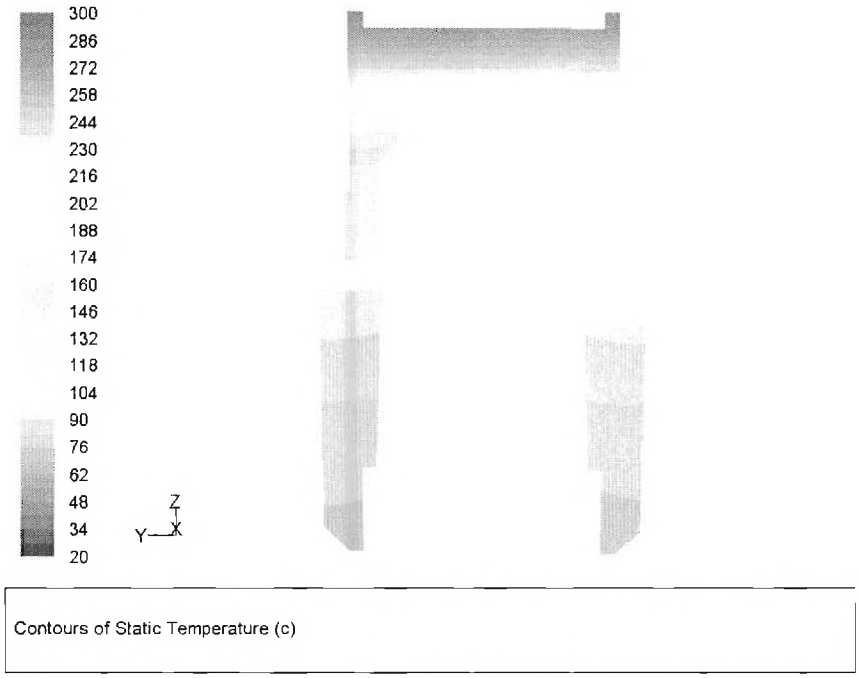

Figure B.4. Temperature distribution of the brass thimble.

By performing a linear interpolation between the FLUENT® cases, the operating conditions of the HEMJ test section relative to a maximum brass thimble temperature limit was obtained (Figure B.5).

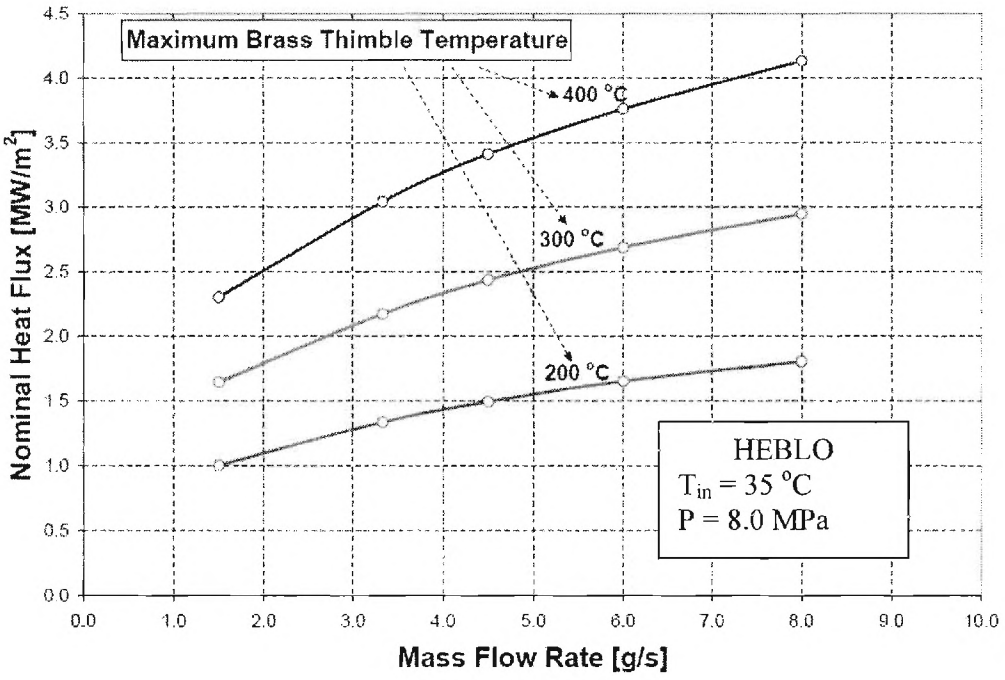

Figure B.5. HEMJ Test section predicted operation relative to a maximum brass thimble temperature.

Additionally, the pressure drop versus the nominal heat flux was determined relative to the maximum brass thimble temperature limits (Figure B.6). The results suggest that the pressure drop for each temperature limit is approximately equal.

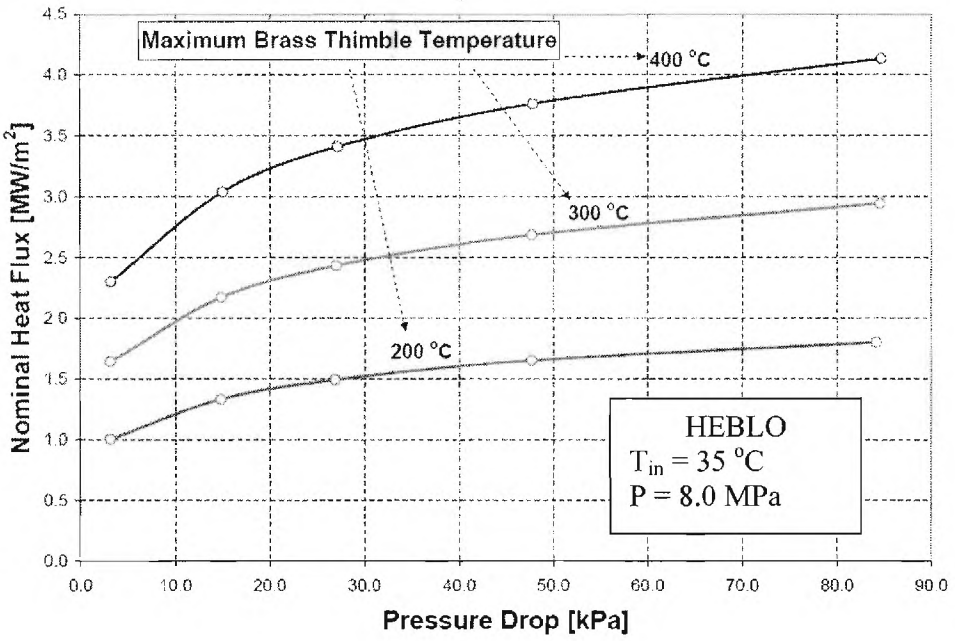

Figure B.6. HEMJ Test Section predicted nominal heat flux versus pressure drop relative to a maximum brass thimble temperature.

B.2 Maximum Copper Temperature

A similar analysis of the HEMJ test section was performed relative to the maximum copper temperature (Figure B.7). The results of a recommended maximum temperature of 500°C and a more conservative (400°C) and less conservative (600°C) temperature indicates that the maximum copper temperature is a "tighter" limit than the maximum brass thimble temperature. This is seen by noting that for the recommended limit of the brass thimble (300°C), a heat flux ranging from approximately 1.6 to 3.0 MW/m^2 can be accommodated. For the suggested temperature limit of the copper (500°C), a heat flux range of approximately 1.9 to 2.6 MW/m^2 can be accommodated. Therefore by using the suggested copper limit, the operating range is effectively reduced by half compared to the brass thimble limit range. The "tight" nature of the copper

temperature limit relative to the brass thimble temperature limit is most likely due to the higher thermal conductivity of copper.

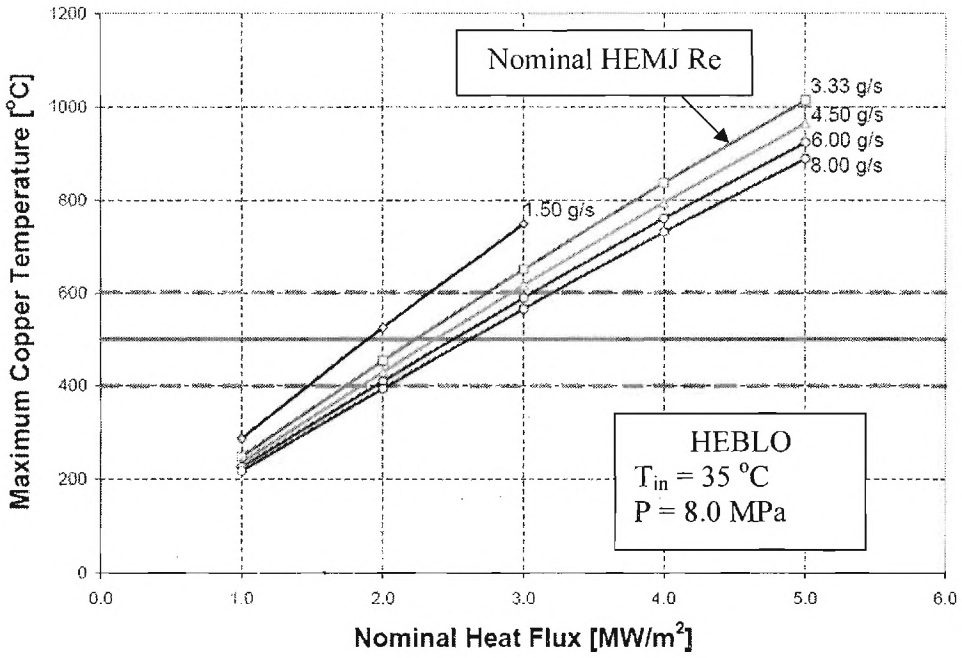

Figure B.7. Maximum Copper Temperature for the parametric simulations.

Similar to subsection B.1, linear interpolation was used to determine the operating conditions of the HEMJ test section (Figure B.8) and the predicted pressure drop (B.9) for each copper temperature limit. The slope of each copper operating limit line is less than the corresponding brass operating limit line; reflecting the stiffness of the copper limit.

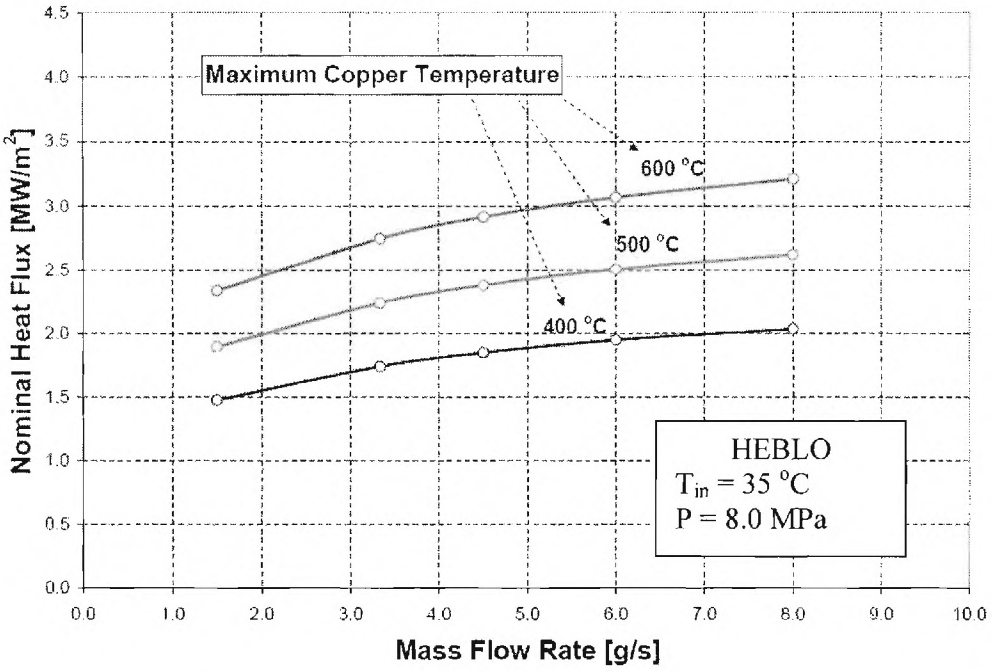

Figure B.8. HEMJ Test Section predicted operation relative to a maximum copper temperature.

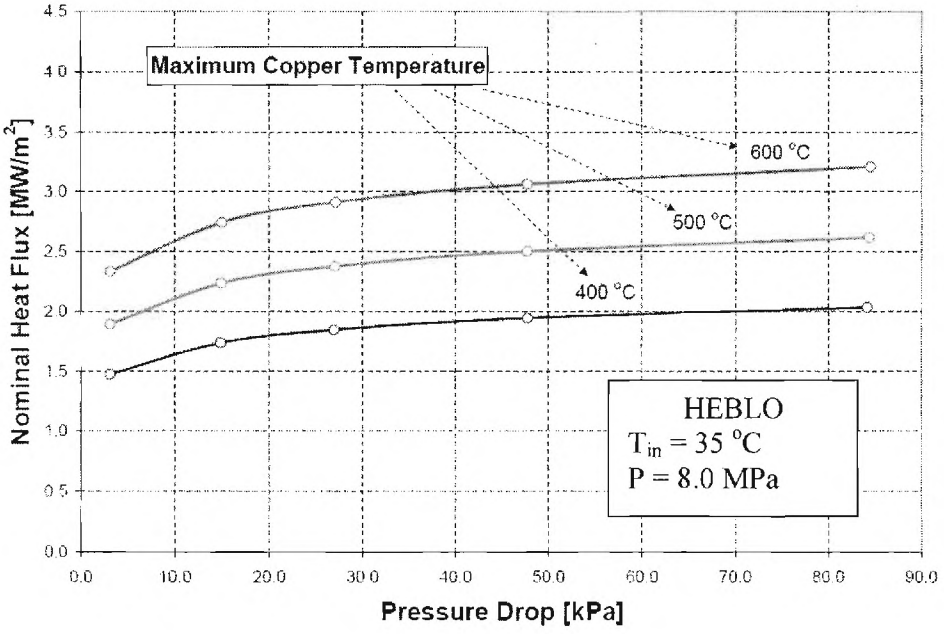

Figure B.9. HEMJ Test Section predicted nominal heat flux versus pressure drop relative to a maximum copper temperature.

Note that tests 6 through 10 were used to verify the repeatability of the experiment. The agreement between the temperature measurements in tests 1 through 10 provided confidence in the repeatability of the results. Therefore FLUENT® simulations were not performed for the experimental data of tests 6 through 10.

Table C. 2 Summary table of the rotation experiments

Test Number	Mass Flow [g/s]	Power [W]	Angle [°]	q" [MW/m^2]	dP [kPa]	T_{max} [°C]
16	2.07	228.4	0	0.880	11.72	417.5
17	2.06	228.2	15	0.896	12.41	417.6
18	2.07	228.5	30	0.926	11.03	416.0
19	2.08	228.5	45	0.883	13.10	415.7
20	2.07	228.5	60	0.883	13.10	415.5
21	2.07	228.4	180	0.887	13.10	415.3
22	2.07	228.8	195	0.883	11.72	415.1
23	2.07	228.7	210	0.887	11.03	415.0
24	2.07	228.9	225	0.887	11.03	414.9
25	2.07	228.9	240	0.885	11.03	414.9
26	3.03	182.8	0	0.702	17.93	303.0
27	3.03	182.7	15	0.703	14.48	304.0
28	3.03	182.3	30	0.710	17.24	304.1
29	3.03	182.7	45	0.703	20.68	305.1
30	3.03	183.0	60	0.713	17.24	305.0
31	3.03	227.0	0	0.898	17.93	366.6
32	3.03	226.9	15	0.896	40.68	366.3
33	3.03	227.0	30	0.897	39.30	366.0
34	3.03	227.0	45	0.896	16.69	365.8
35	3.03	227.1	60	0.895	16.20	365.7
36	3.03	226.7	75	0.896	14.69	365.2
37	3.03	226.9	90	0.895	14.41	365.0
38	3.03	226.8	105	0.894	16.34	364.9
39	3.03	227.1	120	0.891	19.51	364.9
40	4.05	226.6	0	0.891	35.16	333.5
41	4.05	226.6	15	0.887	33.78	334.0
42	4.05	226.1	30	0.891	33.78	334.4
43	4.05	227.3	45	0.891	32.41	334.7
44	4.05	227.3	60	0.891	31.72	335.0
45	4.05	226.0	75	0.894	31.03	335.3
46	4.05	226.3	90	0.894	30.34	335.4
47	4.05	227.0	105	0.891	33.78	335.7
48	4.05	226.3	120	0.891	33.78	335.8

Table C.3 Experimentally measured data for Test 1

	Value	Units	Description
Q_{Heater}	182.3	[W]	Heater Input Power
MFR	2.08	[g/s]	Measured Mass Flow Rate
Θ	0.00	[°]	Azimuthal Position
T1	228.40	[°C]	Embedded TC Ref. 1 in brass
T2	239.90	[°C]	Embedded TC Ref. 2 in brass
T3	244.80	[°C]	Embedded TC Ref. 3 in brass
T4	246.20	[°C]	Embedded TC Ref. 4 in brass
T5	282.30	[°C]	TC Ref. 5 in copper "neck"
T6	292.50	[°C]	TC Ref. 6 in copper "neck"
T7	301.90	[°C]	TC Ref. 7 in copper "neck"
T8	342.40	[°C]	TC Ref. 8 in copper (maximum)
T9	342.50	[°C]	TC Ref. 9 in copper (maximum)
T_{in}	20.00	[°C]	Inlet Temperature
T_{out}	84.50	[°C]	Outlet Temperature
P_{in}	737.74	[kPa]	Inlet Pressure
P_{out}	726.71	[kPa]	Outlet Pressure

Table C.4 Calculated quantities for Test 1

	Value	Units	Description
$T1_{Surface}$	227.78	[°C]	Surface TC Ref. 1 in brass
$T2_{Surface}$	237.40	[°C]	Surface TC Ref. 2 in brass
$T3_{Surface}$	242.27	[°C]	Surface TC Ref. 3 in brass
$T4_{Surface}$	242.48	[°C]	Surface TC Ref. 4 in brass
$T_{Brazing}$	276.42	[°C]	Brazing Surface Temperature
dP	11.03	[kPa]	Pressure Drop
$Q_{Balance}$	135.37	[W]	Energy Balance
% Losses	25.74%	[-]	Energy Loss
$q''_{nominal}$	0.80	[MW/m^2]	Nominal Heat Flux
$q''_{experiment}$	0.70	[MW/m^2]	Measured Heat Flux
$q''_{FLUENT\ 1}$	0.51	[MW/m^2]	FLUENT Heat Flux at Ref. 1
$q''_{FLUENT\ 2}$	0.36	[MW/m^2]	FLUENT Heat Flux at Ref. 2
$q''_{FLUENT\ 3}$	0.28	[MW/m^2]	FLUENT Heat Flux at Ref. 3
$q''_{FLUENT\ 4}$	0.74	[MW/m^2]	FLUENT Heat Flux at Ref. 4
HTC 1	2454.57	[W/m^2-K]	Heat Transfer Coefficient at Ref. 1
HTC 2	1655.94	[W/m^2-K]	Heat Transfer Coefficient at Ref. 2
HTC 3	1259.73	[W/m^2-K]	Heat Transfer Coefficient at Ref. 3
HTC 4	3326.14	[W/m^2-K]	Heat Transfer Coefficient at Ref. 4
Nu 1	97.36	[-]	Nusselt Number at Ref. 1
Nu 2	65.69	[-]	Nusselt Number at Ref. 2
Nu 3	49.97	[-]	Nusselt Number at Ref. 3
Nu 4	131.94	[-]	Nusselt Number at Ref. 4

Table C.5 Experimentally measured data for Test 2

	Value	Units	Description
Q_{Heater}	182.3	[W]	Heater Input Power
MFR	3.11	[g/s]	Measured Mass Flow Rate
Θ	0.00	[°]	Azimuthal Position
T1	185.90	[°C]	Embedded TC Ref. 1 in brass
T2	197.50	[°C]	Embedded TC Ref. 2 in brass
T3	202.50	[°C]	Embedded TC Ref. 3 in brass
T4	204.00	[°C]	Embedded TC Ref. 4 in brass
T5	242.10	[°C]	TC Ref. 5 in copper "neck"
T6	252.60	[°C]	TC Ref. 6 in copper "neck"
T7	262.10	[°C]	TC Ref. 7 in copper "neck"
T8	303.00	[°C]	TC Ref. 8 in copper (maximum)
T9	303.00	[°C]	TC Ref. 9 in copper (maximum)
T_{in}	20.50	[°C]	Inlet Temperature
T_{out}	66.20	[°C]	Outlet Temperature
P_{in}	730.84	[kPa]	Inlet Pressure
P_{out}	712.92	[kPa]	Outlet Pressure

Table C.6 Calculated quantities for Test 2

	Value	Units	Description
$T1_{Surface}$	184.93	[°C]	Surface TC Ref. 1 in brass
$T2_{Surface}$	194.77	[°C]	Surface TC Ref. 2 in brass
$T3_{Surface}$	199.67	[°C]	Surface TC Ref. 3 in brass
$T4_{Surface}$	199.72	[°C]	Surface TC Ref. 4 in brass
$T_{Brazing}$	236.10	[°C]	Brazing Surface Temperature
dP	17.93	[kPa]	Pressure Drop
$Q_{Balance}$	143.41	[W]	Energy Balance
% Losses	21.34%	[-]	Energy Loss
$q''_{nominal}$	0.80	[MW/m^2]	Nominal Heat Flux
$q''_{experiment}$	0.71	[MW/m^2]	Measured Heat Flux
$q''_{FLUENT\ 1}$	0.61	[MW/m^2]	FLUENT Heat Flux at Ref. 1
$q''_{FLUENT\ 2}$	0.42	[MW/m^2]	FLUENT Heat Flux at Ref. 2
$q''_{FLUENT\ 3}$	0.32	[MW/m^2]	FLUENT Heat Flux at Ref. 3
$q''_{FLUENT\ 4}$	0.84	[MW/m^2]	FLUENT Heat Flux at Ref. 4
HTC 1	3709.81	[W/m^2-K]	Heat Transfer Coefficient at Ref. 1
HTC 2	2381.43	[W/m^2-K]	Heat Transfer Coefficient at Ref. 2
HTC 3	1786.06	[W/m^2-K]	Heat Transfer Coefficient at Ref. 3
HTC 4	4686.92	[W/m^2-K]	Heat Transfer Coefficient at Ref. 4
Nu 1	147.16	[-]	Nusselt Number at Ref. 1
Nu 2	94.46	[-]	Nusselt Number at Ref. 2
Nu 3	70.85	[-]	Nusselt Number at Ref. 3
Nu 4	185.92	[-]	Nusselt Number at Ref. 4

Table C.7 Experimentally measured data for Test 3

	Value	Units	Description
Q_{Heater}	182.2	[W]	Heater Input Power
MFR	3.99	[g/s]	Measured Mass Flow Rate
Θ	0.00	[°]	Azimuthal Position
T1	163.50	[°C]	Embedded TC Ref. 1 in brass
T2	175.00	[°C]	Embedded TC Ref. 2 in brass
T3	180.10	[°C]	Embedded TC Ref. 3 in brass
T4	181.60	[°C]	Embedded TC Ref. 4 in brass
T5	220.90	[°C]	TC Ref. 5 in copper "neck"
T6	231.50	[°C]	TC Ref. 6 in copper "neck"
T7	241.10	[°C]	TC Ref. 7 in copper "neck"
T8	282.20	[°C]	TC Ref. 8 in copper (maximum)
T9	282.20	[°C]	TC Ref. 9 in copper (maximum)
T_{in}	21.00	[°C]	Inlet Temperature
T_{out}	57.70	[°C]	Outlet Temperature
P_{in}	730.84	[kPa]	Inlet Pressure
P_{out}	694.99	[kPa]	Outlet Pressure

Table C.8 Calculated quantities for Test 3

	Value	Units	Description
$T1_{Surface}$	162.29	[°C]	Surface TC Ref. 1 in brass
$T2_{Surface}$	172.07	[°C]	Surface TC Ref. 2 in brass
$T3_{Surface}$	177.02	[°C]	Surface TC Ref. 3 in brass
$T4_{Surface}$	176.91	[°C]	Surface TC Ref. 4 in brass
$T_{Brazing}$	214.84	[°C]	Brazing Surface Temperature
dP	35.85	[kPa]	Pressure Drop
$Q_{Balance}$	147.60	[W]	Energy Balance
% Losses	18.99%	[-]	Energy Loss
$q''_{nominal}$	0.80	[MW/m^2]	Nominal Heat Flux
$q''_{experiment}$	0.72	[MW/m^2]	Measured Heat Flux
$q''_{FLUENT\ 1}$	0.67	[MW/m^2]	FLUENT Heat Flux at Ref. 1
$q''_{FLUENT\ 2}$	0.45	[MW/m^2]	FLUENT Heat Flux at Ref. 2
$q''_{FLUENT\ 3}$	0.36	[MW/m^2]	FLUENT Heat Flux at Ref. 3
$q''_{FLUENT\ 4}$	0.94	[MW/m^2]	FLUENT Heat Flux at Ref. 4
HTC 1	4742.12	[W/m^2-K]	Heat Transfer Coefficient at Ref. 1
HTC 2	2978.75	[W/m^2-K]	Heat Transfer Coefficient at Ref. 2
HTC 3	2307.35	[W/m^2-K]	Heat Transfer Coefficient at Ref. 3
HTC 4	6029.08	[W/m^2-K]	Heat Transfer Coefficient at Ref. 4
Nu 1	188.10	[-]	Nusselt Number at Ref. 1
Nu 2	118.16	[-]	Nusselt Number at Ref. 2
Nu 3	91.53	[-]	Nusselt Number at Ref. 3
Nu 4	239.15	[-]	Nusselt Number at Ref. 4

Table C.9 Experimentally measured data for Test 4

	Value	Units	Description
Q_{Heater}	181.5	[W]	Heater Input Power
MFR	6.01	[g/s]	Measured Mass Flow Rate
Θ	0.00	[°]	Azimuthal Position
T1	132.20	[°C]	Embedded TC Ref. 1 in brass
T2	143.60	[°C]	Embedded TC Ref. 2 in brass
T3	148.60	[°C]	Embedded TC Ref. 3 in brass
T4	150.10	[°C]	Embedded TC Ref. 4 in brass
T5	191.30	[°C]	TC Ref. 5 in copper "neck"
T6	202.00	[°C]	TC Ref. 6 in copper "neck"
T7	211.60	[°C]	TC Ref. 7 in copper "neck"
T8	252.90	[°C]	TC Ref. 8 in copper (maximum)
T9	252.80	[°C]	TC Ref. 9 in copper (maximum)
T_{in}	20.10	[°C]	Inlet Temperature
T_{out}	45.30	[°C]	Outlet Temperature
P_{in}	713.61	[kPa]	Inlet Pressure
P_{out}	639.83	[kPa]	Outlet Pressure

Table C.10 Calculated quantities for Test 4

	Value	Units	Description
$T1_{Surface}$	130.53	[°C]	Surface TC Ref. 1 in brass
$T2_{Surface}$	140.22	[°C]	Surface TC Ref. 2 in brass
$T3_{Surface}$	145.00	[°C]	Surface TC Ref. 3 in brass
$T4_{Surface}$	144.53	[°C]	Surface TC Ref. 4 in brass
$T_{Brazing}$	185.21	[°C]	Brazing Surface Temperature
dP	73.77	[kPa]	Pressure Drop
$Q_{Balance}$	152.82	[W]	Energy Balance
% Losses	15.80%	[-]	Energy Loss
$q''_{nominal}$	0.80	[MW/m^2]	Nominal Heat Flux
$q''_{experiment}$	0.72	[MW/m^2]	Measured Heat Flux
$q''_{FLUENT\ 1}$	0.80	[MW/m^2]	FLUENT Heat Flux at Ref. 1
$q''_{FLUENT\ 2}$	0.56	[MW/m^2]	FLUENT Heat Flux at Ref. 2
$q''_{FLUENT\ 3}$	0.43	[MW/m^2]	FLUENT Heat Flux at Ref. 3
$q''_{FLUENT\ 4}$	1.12	[MW/m^2]	FLUENT Heat Flux at Ref. 4
HTC 1	7244.41	[W/m^2-K]	Heat Transfer Coefficient at Ref. 1
HTC 2	4662.20	[W/m^2-K]	Heat Transfer Coefficient at Ref. 2
HTC 3	3442.81	[W/m^2-K]	Heat Transfer Coefficient at Ref. 3
HTC 4	9001.33	[W/m^2-K]	Heat Transfer Coefficient at Ref. 4
Nu 1	287.36	[-]	Nusselt Number at Ref. 1
Nu 2	184.93	[-]	Nusselt Number at Ref. 2
Nu 3	136.57	[-]	Nusselt Number at Ref. 3
Nu 4	357.05	[-]	Nusselt Number at Ref. 4

Table C.11 Experimentally measured data for Test 5

	Value	Units	Description
Q_{Heater}	181.2	[W]	Heater Input Power
MFR	8.39	[g/s]	Measured Mass Flow Rate
Θ	0.00	[°]	Azimuthal Position
T1	112.30	[°C]	Embedded TC Ref. 1 in brass
T2	123.50	[°C]	Embedded TC Ref. 2 in brass
T3	128.40	[°C]	Embedded TC Ref. 3 in brass
T4	129.80	[°C]	Embedded TC Ref. 4 in brass
T5	172.60	[°C]	TC Ref. 5 in copper "neck"
T6	183.40	[°C]	TC Ref. 6 in copper "neck"
T7	193.10	[°C]	TC Ref. 7 in copper "neck"
T8	234.60	[°C]	TC Ref. 8 in copper (maximum)
T9	234.50	[°C]	TC Ref. 9 in copper (maximum)
T_{in}	21.20	[°C]	Inlet Temperature
T_{out}	39.20	[°C]	Outlet Temperature
P_{in}	699.82	[kPa]	Inlet Pressure
P_{out}	523.17	[kPa]	Outlet Pressure

Table C.12 Calculated quantities for Test 5

	Value	Units	Description
$T1_{Surface}$	110.32	[°C]	Surface TC Ref. 1 in brass
$T2_{Surface}$	119.87	[°C]	Surface TC Ref. 2 in brass
$T3_{Surface}$	124.48	[°C]	Surface TC Ref. 3 in brass
$T4_{Surface}$	123.58	[°C]	Surface TC Ref. 4 in brass
$T_{Brazing}$	166.45	[°C]	Brazing Surface Temperature
dP	176.64	[kPa]	Pressure Drop
$Q_{Balance}$	152.34	[W]	Energy Balance
% Losses	15.91%	[-]	Energy Loss
$q''_{nominal}$	0.80	[MW/m^2]	Nominal Heat Flux
$q''_{experiment}$	0.73	[MW/m^2]	Measured Heat Flux
$q''_{FLUENT\ 1}$	0.88	[MW/m^2]	FLUENT Heat Flux at Ref. 1
$q''_{FLUENT\ 2}$	0.60	[MW/m^2]	FLUENT Heat Flux at Ref. 2
$q''_{FLUENT\ 3}$	0.49	[MW/m^2]	FLUENT Heat Flux at Ref. 3
$q''_{FLUENT\ 4}$	1.27	[MW/m^2]	FLUENT Heat Flux at Ref. 4
HTC 1	9874.66	[W/m^2-K]	Heat Transfer Coefficient at Ref. 1
HTC 2	6030.08	[W/m^2-K]	Heat Transfer Coefficient at Ref. 2
HTC 3	4744.43	[W/m^2-K]	Heat Transfer Coefficient at Ref. 3
HTC 4	12404.89	[W/m^2-K]	Heat Transfer Coefficient at Ref. 4
Nu 1	391.70	[-]	Nusselt Number at Ref. 1
Nu 2	239.19	[-]	Nusselt Number at Ref. 2
Nu 3	188.20	[-]	Nusselt Number at Ref. 3
Nu 4	492.06	[-]	Nusselt Number at Ref. 4

Table C.13 Experimentally measured data for Test 6

	Value	Units	Description
Q_{Heater}	181.4	[W]	Heater Input Power
MFR	2.01	[g/s]	Measured Mass Flow Rate
Θ	0.00	[°]	Azimuthal Position
T1	231.60	[°C]	Embedded TC Ref. 1 in brass
T2	242.90	[°C]	Embedded TC Ref. 2 in brass
T3	247.80	[°C]	Embedded TC Ref. 3 in brass
T4	249.30	[°C]	Embedded TC Ref. 4 in brass
T5	284.80	[°C]	TC Ref. 5 in copper "neck"
T6	295.00	[°C]	TC Ref. 6 in copper "neck"
T7	304.30	[°C]	TC Ref. 7 in copper "neck"
T8	344.40	[°C]	TC Ref. 8 in copper (maximum)
T9	344.40	[°C]	TC Ref. 9 in copper (maximum)
T_{in}	20.55	[°C]	Inlet Temperature
T_{out}	86.10	[°C]	Outlet Temperature
P_{in}	737.74	[kPa]	Inlet Pressure
P_{out}	728.09	[kPa]	Outlet Pressure

Table C.14 Calculated quantities for Test 6

	Value	Units	Description
$T1_{Surface}$		[°C]	Surface TC Ref. 1 in brass
$T2_{Surface}$		[°C]	Surface TC Ref. 2 in brass
$T3_{Surface}$		[°C]	Surface TC Ref. 3 in brass
$T4_{Surface}$		[°C]	Surface TC Ref. 4 in brass
$T_{Brazing}$	278.95	[°C]	Brazing Surface Temperature
dP	9.65	[kPa]	Pressure Drop
$Q_{Balance}$	132.94	[W]	Energy Balance
% Losses	26.71%	[-]	Energy Loss
$q''_{nominal}$	0.80	[MW/m^2]	Nominal Heat Flux
$q''_{experiment}$	0.69	[MW/m^2]	Measured Heat Flux
$q''_{FLUENT\ 1}$		[MW/m^2]	FLUENT Heat Flux at Ref. 1
$q''_{FLUENT\ 2}$		[MW/m^2]	FLUENT Heat Flux at Ref. 2
$q''_{FLUENT\ 3}$		[MW/m^2]	FLUENT Heat Flux at Ref. 3
$q''_{FLUENT\ 4}$		[MW/m^2]	FLUENT Heat Flux at Ref. 4
HTC 1		[W/m^2-K]	Heat Transfer Coefficient at Ref. 1
HTC 2		[W/m^2-K]	Heat Transfer Coefficient at Ref. 2
HTC 3		[W/m^2-K]	Heat Transfer Coefficient at Ref. 3
HTC 4		[W/m^2-K]	Heat Transfer Coefficient at Ref. 4
Nu 1		[-]	Nusselt Number at Ref. 1
Nu 2		[-]	Nusselt Number at Ref. 2
Nu 3		[-]	Nusselt Number at Ref. 3
Nu 4		[-]	Nusselt Number at Ref. 4

Table C.15 Experimentally measured data for Test 7

	Value	Units	Description
Q_{Heater}	182.2	[W]	Heater Input Power
MFR	3.16	[g/s]	Measured Mass Flow Rate
Θ	0.00	[°]	Azimuthal Position
T1	187.10	[°C]	Embedded TC Ref. 1 in brass
T2	198.70	[°C]	Embedded TC Ref. 2 in brass
T3	203.70	[°C]	Embedded TC Ref. 3 in brass
T4	205.20	[°C]	Embedded TC Ref. 4 in brass
T5	243.60	[°C]	TC Ref. 5 in copper "neck"
T6	254.20	[°C]	TC Ref. 6 in copper "neck"
T7	263.70	[°C]	TC Ref. 7 in copper "neck"
T8	305.00	[°C]	TC Ref. 8 in copper (maximum)
T9	305.00	[°C]	TC Ref. 9 in copper (maximum)
T_{in}	21.00	[°C]	Inlet Temperature
T_{out}	67.50	[°C]	Outlet Temperature
P_{in}	730.84	[kPa]	Inlet Pressure
P_{out}	708.78	[kPa]	Outlet Pressure

Table C.16 Calculated quantities for Test 7

	Value	Units	Description
$T1_{Surface}$		[°C]	Surface TC Ref. 1 in brass
$T2_{Surface}$		[°C]	Surface TC Ref. 2 in brass
$T3_{Surface}$		[°C]	Surface TC Ref. 3 in brass
$T4_{Surface}$		[°C]	Surface TC Ref. 4 in brass
$T_{Brazing}$		[°C]	Brazing Surface Temperature
dP	22.06	[kPa]	Pressure Drop
$Q_{Balance}$	148.26	[W]	Energy Balance
% Losses	18.63%	[-]	Energy Loss
$q''_{nominal}$	0.80	[MW/m^2]	Nominal Heat Flux
$q''_{experiment}$	0.71	[MW/m^2]	Measured Heat Flux
$q''_{FLUENT\ 1}$		[MW/m^2]	FLUENT Heat Flux at Ref. 1
$q''_{FLUENT\ 2}$		[MW/m^2]	FLUENT Heat Flux at Ref. 2
$q''_{FLUENT\ 3}$		[MW/m^2]	FLUENT Heat Flux at Ref. 3
$q''_{FLUENT\ 4}$		[MW/m^2]	FLUENT Heat Flux at Ref. 4
HTC 1		[W/m^2-K]	Heat Transfer Coefficient at Ref. 1
HTC 2		[W/m^2-K]	Heat Transfer Coefficient at Ref. 2
HTC 3		[W/m^2-K]	Heat Transfer Coefficient at Ref. 3
HTC 4		[W/m^2-K]	Heat Transfer Coefficient at Ref. 4
Nu 1		[-]	Nusselt Number at Ref. 1
Nu 2		[-]	Nusselt Number at Ref. 2
Nu 3		[-]	Nusselt Number at Ref. 3
Nu 4		[-]	Nusselt Number at Ref. 4

Table C.17 Experimentally measured data for Test 8

	Value	Units	Description
Q_{Heater}	182.8	[W]	Heater Input Power
MFR	4.20	[g/s]	Measured Mass Flow Rate
Θ	0.00	[°]	Azimuthal Position
T1	160.60	[°C]	Embedded TC Ref. 1 in brass
T2	172.30	[°C]	Embedded TC Ref. 2 in brass
T3	177.30	[°C]	Embedded TC Ref. 3 in brass
T4	178.90	[°C]	Embedded TC Ref. 4 in brass
T5	218.60	[°C]	TC Ref. 5 in copper "neck"
T6	229.40	[°C]	TC Ref. 6 in copper "neck"
T7	239.00	[°C]	TC Ref. 7 in copper "neck"
T8	280.60	[°C]	TC Ref. 8 in copper (maximum)
T9	280.60	[°C]	TC Ref. 9 in copper (maximum)
T_{in}	20.30	[°C]	Inlet Temperature
T_{out}	56.10	[°C]	Outlet Temperature
P_{in}	730.84	[kPa]	Inlet Pressure
P_{out}	689.48	[kPa]	Outlet Pressure

Table C.18 Calculated quantities for Test 8

	Value	Units	Description
$T1_{Surface}$		[°C]	Surface TC Ref. 1 in brass
$T2_{Surface}$		[°C]	Surface TC Ref. 2 in brass
$T3_{Surface}$		[°C]	Surface TC Ref. 3 in brass
$T4_{Surface}$		[°C]	Surface TC Ref. 4 in brass
$T_{Brazing}$	212.48	[°C]	Brazing Surface Temperature
dP	41.37	[kPa]	Pressure Drop
$Q_{Balance}$	151.71	[W]	Energy Balance
% Losses	17.01%	[-]	Energy Loss
$q''_{nominal}$	0.80	[MW/m^2]	Nominal Heat Flux
$q''_{experiment}$	0.72	[MW/m^2]	Measured Heat Flux
$q''_{FLUENT\ 1}$		[MW/m^2]	FLUENT Heat Flux at Ref. 1
$q''_{FLUENT\ 2}$		[MW/m^2]	FLUENT Heat Flux at Ref. 2
$q''_{FLUENT\ 3}$		[MW/m^2]	FLUENT Heat Flux at Ref. 3
$q''_{FLUENT\ 4}$		[MW/m^2]	FLUENT Heat Flux at Ref. 4
HTC 1		[W/m^2-K]	Heat Transfer Coefficient at Ref. 1
HTC 2		[W/m^2-K]	Heat Transfer Coefficient at Ref. 2
HTC 3		[W/m^2-K]	Heat Transfer Coefficient at Ref. 3
HTC 4		[W/m^2-K]	Heat Transfer Coefficient at Ref. 4
Nu 1		[-]	Nusselt Number at Ref. 1
Nu 2		[-]	Nusselt Number at Ref. 2
Nu 3		[-]	Nusselt Number at Ref. 3
Nu 4		[-]	Nusselt Number at Ref. 4

Table C.19 Experimentally measured data for Test 9

	Value	Units	Description
Q_{Heater}	182.9	[W]	Heater Input Power
MFR	6.10	[g/s]	Measured Mass Flow Rate
Θ	0.00	[°]	Azimuthal Position
T1	131.90	[°C]	Embedded TC Ref. 1 in brass
T2	143.30	[°C]	Embedded TC Ref. 2 in brass
T3	148.10	[°C]	Embedded TC Ref. 3 in brass
T4	149.60	[°C]	Embedded TC Ref. 4 in brass
T5	190.40	[°C]	TC Ref. 5 in copper "neck"
T6	201.10	[°C]	TC Ref. 6 in copper "neck"
T7	210.70	[°C]	TC Ref. 7 in copper "neck"
T8	251.70	[°C]	TC Ref. 8 in copper (maximum)
T9	251.60	[°C]	TC Ref. 9 in copper (maximum)
T_{in}	21.00	[°C]	Inlet Temperature
T_{out}	46.00	[°C]	Outlet Temperature
P_{in}	717.05	[kPa]	Inlet Pressure
P_{out}	639.83	[kPa]	Outlet Pressure

Table C.20 Calculated quantities for Test 9

	Value	Units	Description
$T1_{Surface}$		[°C]	Surface TC Ref. 1 in brass
$T2_{Surface}$		[°C]	Surface TC Ref. 2 in brass
$T3_{Surface}$		[°C]	Surface TC Ref. 3 in brass
$T4_{Surface}$		[°C]	Surface TC Ref. 4 in brass
$T_{Brazing}$	184.31	[°C]	Brazing Surface Temperature
dP	77.22	[kPa]	Pressure Drop
$Q_{Balance}$	153.87	[W]	Energy Balance
% Losses	15.85%	[-]	Energy Loss
$q''_{nominal}$	0.80	[MW/m^2]	Nominal Heat Flux
$q''_{experiment}$	0.72	[MW/m^2]	Measured Heat Flux
$q''_{FLUENT\ 1}$		[MW/m^2]	FLUENT Heat Flux at Ref. 1
$q''_{FLUENT\ 2}$		[MW/m^2]	FLUENT Heat Flux at Ref. 2
$q''_{FLUENT\ 3}$		[MW/m^2]	FLUENT Heat Flux at Ref. 3
$q''_{FLUENT\ 4}$		[MW/m^2]	FLUENT Heat Flux at Ref. 4
HTC 1		[W/m^2-K]	Heat Transfer Coefficient at Ref. 1
HTC 2		[W/m^2-K]	Heat Transfer Coefficient at Ref. 2
HTC 3		[W/m^2-K]	Heat Transfer Coefficient at Ref. 3
HTC 4		[W/m^2-K]	Heat Transfer Coefficient at Ref. 4
Nu 1		[-]	Nusselt Number at Ref. 1
Nu 2		[-]	Nusselt Number at Ref. 2
Nu 3		[-]	Nusselt Number at Ref. 3
Nu 4		[-]	Nusselt Number at Ref. 4

Table C.21 Experimentally measured data for Test 10

	Value	Units	Description
Q_{Heater}	182.8	[W]	Heater Input Power
MFR	8.06	[g/s]	Measured Mass Flow Rate
Θ	0.00	[°]	Azimuthal Position
T1	113.70	[°C]	Embedded TC Ref. 1 in brass
T2	124.90	[°C]	Embedded TC Ref. 2 in brass
T3	129.80	[°C]	Embedded TC Ref. 3 in brass
T4	131.10	[°C]	Embedded TC Ref. 4 in brass
T5	173.50	[°C]	TC Ref. 5 in copper "neck"
T6	184.40	[°C]	TC Ref. 6 in copper "neck"
T7	194.00	[°C]	TC Ref. 7 in copper "neck"
T8	235.50	[°C]	TC Ref. 8 in copper (maximum)
T9	235.40	[°C]	TC Ref. 9 in copper (maximum)
T_{in}	20.44	[°C]	Inlet Temperature
T_{out}	39.10	[°C]	Outlet Temperature
P_{in}	717.05	[kPa]	Inlet Pressure
P_{out}	564.68	[kPa]	Outlet Pressure

Table C.22 Calculated quantities for Test 10

	Value	Units	Description
$T1_{Surface}$		[°C]	Surface TC Ref. 1 in brass
$T2_{Surface}$		[°C]	Surface TC Ref. 2 in brass
$T3_{Surface}$		[°C]	Surface TC Ref. 3 in brass
$T4_{Surface}$		[°C]	Surface TC Ref. 4 in brass
$T_{Brazing}$	167.35	[°C]	Brazing Surface Temperature
dP	152.37	[kPa]	Pressure Drop
$Q_{Balance}$	151.75	[W]	Energy Balance
% Losses	16.98%	[-]	Energy Loss
$q''_{nominal}$	0.80	[MW/m^2]	Nominal Heat Flux
$q''_{experiment}$	0.73	[MW/m^2]	Measured Heat Flux
$q''_{FLUENT\ 1}$		[MW/m^2]	FLUENT Heat Flux at Ref. 1
$q''_{FLUENT\ 2}$		[MW/m^2]	FLUENT Heat Flux at Ref. 2
$q''_{FLUENT\ 3}$		[MW/m^2]	FLUENT Heat Flux at Ref. 3
$q''_{FLUENT\ 4}$		[MW/m^2]	FLUENT Heat Flux at Ref. 4
HTC 1		[W/m^2-K]	Heat Transfer Coefficient at Ref. 1
HTC 2		[W/m^2-K]	Heat Transfer Coefficient at Ref. 2
HTC 3		[W/m^2-K]	Heat Transfer Coefficient at Ref. 3
HTC 4		[W/m^2-K]	Heat Transfer Coefficient at Ref. 4
Nu 1		[-]	Nusselt Number at Ref. 1
Nu 2		[-]	Nusselt Number at Ref. 2
Nu 3		[-]	Nusselt Number at Ref. 3
Nu 4		[-]	Nusselt Number at Ref. 4

Table C.23 Experimentally measured data for Test 11

	Value	Units	Description
Q_{Heater}	228.4	[W]	Heater Input Power
MFR	2.07	[g/s]	Measured Mass Flow Rate
Θ	0.00	[°]	Azimuthal Position
T1	277.40	[°C]	Embedded TC Ref. 1 in brass
T2	291.00	[°C]	Embedded TC Ref. 2 in brass
T3	296.60	[°C]	Embedded TC Ref. 3 in brass
T4	298.50	[°C]	Embedded TC Ref. 4 in brass
T5	342.00	[°C]	TC Ref. 5 in copper "neck"
T6	354.90	[°C]	TC Ref. 6 in copper "neck"
T7	366.80	[°C]	TC Ref. 7 in copper "neck"
T8	417.50	[°C]	TC Ref. 8 in copper (maximum)
T9	417.50	[°C]	TC Ref. 9 in copper (maximum)
T_{in}	21.10	[°C]	Inlet Temperature
T_{out}	101.30	[°C]	Outlet Temperature
P_{in}	737.74	[kPa]	Inlet Pressure
P_{out}	726.02	[kPa]	Outlet Pressure

Table C.24 Calculated quantities for Test 11

	Value	Units	Description
$T1_{Surface}$	277.56	[°C]	Surface TC Ref. 1 in brass
$T2_{Surface}$	288.57	[°C]	Surface TC Ref. 2 in brass
$T3_{Surface}$	294.33	[°C]	Surface TC Ref. 3 in brass
$T4_{Surface}$	294.32	[°C]	Surface TC Ref. 4 in brass
$T_{Brazing}$	334.56	[°C]	Brazing Surface Temperature
dP	11.72	[kPa]	Pressure Drop
$Q_{Balance}$	167.51	[W]	Energy Balance
% Losses	26.66%	[-]	Energy Loss
$q''_{nominal}$	1.00	[MW/m^2]	Nominal Heat Flux
$q''_{experiment}$	0.88	[MW/m^2]	Measured Heat Flux
$q''_{FLUENT\ 1}$	0.61	[MW/m^2]	FLUENT Heat Flux at Ref. 1
$q''_{FLUENT\ 2}$	0.41	[MW/m^2]	FLUENT Heat Flux at Ref. 2
$q''_{FLUENT\ 3}$	0.35	[MW/m^2]	FLUENT Heat Flux at Ref. 3
$q''_{FLUENT\ 4}$	0.85	[MW/m^2]	FLUENT Heat Flux at Ref. 4
HTC 1	2378.58	[W/m^2-K]	Heat Transfer Coefficient at Ref. 1
HTC 2	1532.88	[W/m^2-K]	Heat Transfer Coefficient at Ref. 2
HTC 3	1280.96	[W/m^2-K]	Heat Transfer Coefficient at Ref. 3
HTC 4	3111.10	[W/m^2-K]	Heat Transfer Coefficient at Ref. 4
Nu 1	94.35	[-]	Nusselt Number at Ref. 1
Nu 2	60.80	[-]	Nusselt Number at Ref. 2
Nu 3	50.81	[-]	Nusselt Number at Ref. 3
Nu 4	123.41	[-]	Nusselt Number at Ref. 4

Table C.25 Experimentally measured data for Test 12

	Value	Units	Description
Q_{Heater}	227.0	[W]	Heater Input Power
MFR	3.10	[g/s]	Measured Mass Flow Rate
Θ	0.00	[°]	Azimuthal Position
T1	219.20	[°C]	Embedded TC Ref. 1 in brass
T2	233.10	[°C]	Embedded TC Ref. 2 in brass
T3	238.90	[°C]	Embedded TC Ref. 3 in brass
T4	241.00	[°C]	Embedded TC Ref. 4 in brass
T5	286.50	[°C]	TC Ref. 5 in copper "neck"
T6	299.80	[°C]	TC Ref. 6 in copper "neck"
T7	311.90	[°C]	TC Ref. 7 in copper "neck"
T8	363.30	[°C]	TC Ref. 8 in copper (maximum)
T9	363.30	[°C]	TC Ref. 9 in copper (maximum)
T_{in}	20.10	[°C]	Inlet Temperature
T_{out}	76.90	[°C]	Outlet Temperature
P_{in}	730.84	[kPa]	Inlet Pressure
P_{out}	706.71	[kPa]	Outlet Pressure

Table C.26 Calculated quantities for Test 12

	Value	Units	Description
$T1_{Surface}$	218.08	[°C]	Surface TC Ref. 1 in brass
$T2_{Surface}$	229.87	[°C]	Surface TC Ref. 2 in brass
$T3_{Surface}$	235.56	[°C]	Surface TC Ref. 3 in brass
$T4_{Surface}$	236.10	[°C]	Surface TC Ref. 4 in brass
$T_{Brazing}$	278.88	[°C]	Brazing Surface Temperature
dP	24.13	[kPa]	Pressure Drop
$Q_{Balance}$	177.66	[W]	Energy Balance
% Losses	21.73%	[-]	Energy Loss
$q''_{nominal}$	1.00	[MW/m^2]	Nominal Heat Flux
$q''_{experiment}$	0.90	[MW/m^2]	Measured Heat Flux
$q''_{FLUENT\ 1}$	0.74	[MW/m^2]	FLUENT Heat Flux at Ref. 1
$q''_{FLUENT\ 2}$	0.47	[MW/m^2]	FLUENT Heat Flux at Ref. 2
$q''_{FLUENT\ 3}$	0.41	[MW/m^2]	FLUENT Heat Flux at Ref. 3
$q''_{FLUENT\ 4}$	1.01	[MW/m^2]	FLUENT Heat Flux at Ref. 4
HTC 1	3737.73	[W/m^2-K]	Heat Transfer Coefficient at Ref. 1
HTC 2	2240.52	[W/m^2-K]	Heat Transfer Coefficient at Ref. 2
HTC 3	1902.95	[W/m^2-K]	Heat Transfer Coefficient at Ref. 3
HTC 4	4675.97	[W/m^2-K]	Heat Transfer Coefficient at Ref. 4
Nu 1	148.26	[-]	Nusselt Number at Ref. 1
Nu 2	88.87	[-]	Nusselt Number at Ref. 2
Nu 3	75.48	[-]	Nusselt Number at Ref. 3
Nu 4	185.48	[-]	Nusselt Number at Ref. 4

Table C.27 Experimentally measured data for Test 13

	Value	Units	Description
Q_{Heater}	226.6	[W]	Heater Input Power
MFR	4.05	[g/s]	Measured Mass Flow Rate
Θ	0.00	[°]	Azimuthal Position
T1	190.50	[°C]	Embedded TC Ref. 1 in brass
T2	204.10	[°C]	Embedded TC Ref. 2 in brass
T3	209.90	[°C]	Embedded TC Ref. 3 in brass
T4	211.90	[°C]	Embedded TC Ref. 4 in brass
T5	257.90	[°C]	TC Ref. 5 in copper "neck"
T6	271.10	[°C]	TC Ref. 6 in copper "neck"
T7	283.00	[°C]	TC Ref. 7 in copper "neck"
T8	333.50	[°C]	TC Ref. 8 in copper (maximum)
T9	333.50	[°C]	TC Ref. 9 in copper (maximum)
T_{in}	20.60	[°C]	Inlet Temperature
T_{out}	65.40	[°C]	Outlet Temperature
P_{in}	723.95	[kPa]	Inlet Pressure
P_{out}	688.79	[kPa]	Outlet Pressure

Table C.28 Calculated quantities for Test 13

	Value	Units	Description
$T1_{Surface}$	189.93	[°C]	Surface TC Ref. 1 in brass
$T2_{Surface}$	201.24	[°C]	Surface TC Ref. 2 in brass
$T3_{Surface}$	207.12	[°C]	Surface TC Ref. 3 in brass
$T4_{Surface}$	206.71	[°C]	Surface TC Ref. 4 in brass
$T_{Brazing}$	250.37	[°C]	Brazing Surface Temperature
dP	35.16	[kPa]	Pressure Drop
$Q_{Balance}$	183.07	[W]	Energy Balance
% Losses	19.21%	[-]	Energy Loss
$q''_{nominal}$	1.00	[MW/m^2]	Nominal Heat Flux
$q''_{experiment}$	0.89	[MW/m^2]	Measured Heat Flux
$q''_{FLUENT\ 1}$	0.83	[MW/m^2]	FLUENT Heat Flux at Ref. 1
$q''_{FLUENT\ 2}$	0.57	[MW/m^2]	FLUENT Heat Flux at Ref. 2
$q''_{FLUENT\ 3}$	0.43	[MW/m^2]	FLUENT Heat Flux at Ref. 3
$q''_{FLUENT\ 4}$	1.11	[MW/m^2]	FLUENT Heat Flux at Ref. 4
HTC 1	4901.64	[W/m^2-K]	Heat Transfer Coefficient at Ref. 1
HTC 2	3155.45	[W/m^2-K]	Heat Transfer Coefficient at Ref. 2
HTC 3	2305.38	[W/m^2-K]	Heat Transfer Coefficient at Ref. 3
HTC 4	5964.31	[W/m^2-K]	Heat Transfer Coefficient at Ref. 4
Nu 1	194.43	[-]	Nusselt Number at Ref. 1
Nu 2	125.17	[-]	Nusselt Number at Ref. 2
Nu 3	91.45	[-]	Nusselt Number at Ref. 3
Nu 4	236.59	[-]	Nusselt Number at Ref. 4

Table C.29 Experimentally measured data for Test 14

	Value	Units	Description
Q_{Heater}	227.6	[W]	Heater Input Power
MFR	6.20	[g/s]	Measured Mass Flow Rate
Θ	0.00	[°]	Azimuthal Position
T1	153.70	[°C]	Embedded TC Ref. 1 in brass
T2	167.10	[°C]	Embedded TC Ref. 2 in brass
T3	172.80	[°C]	Embedded TC Ref. 3 in brass
T4	174.70	[°C]	Embedded TC Ref. 4 in brass
T5	223.40	[°C]	TC Ref. 5 in copper "neck"
T6	236.70	[°C]	TC Ref. 6 in copper "neck"
T7	248.80	[°C]	TC Ref. 7 in copper "neck"
T8	299.90	[°C]	TC Ref. 8 in copper (maximum)
T9	299.90	[°C]	TC Ref. 9 in copper (maximum)
T_{in}	20.70	[°C]	Inlet Temperature
T_{out}	50.50	[°C]	Outlet Temperature
P_{in}	717.05	[kPa]	Inlet Pressure
P_{out}	632.94	[kPa]	Outlet Pressure

Table C.30 Calculated quantities for Test 14

	Value	Units	Description
$T1_{Surface}$	151.75	[°C]	Surface TC Ref. 1 in brass
$T2_{Surface}$	163.19	[°C]	Surface TC Ref. 2 in brass
$T3_{Surface}$	168.63	[°C]	Surface TC Ref. 3 in brass
$T4_{Surface}$	168.23	[°C]	Surface TC Ref. 4 in brass
$T_{Brazing}$	215.78	[°C]	Brazing Surface Temperature
dP	84.12	[kPa]	Pressure Drop
$Q_{Balance}$	186.42	[W]	Energy Balance
% Losses	18.09%	[-]	Energy Loss
$q''_{nominal}$	1.00	[MW/m^2]	Nominal Heat Flux
$q''_{experiment}$	0.90	[MW/m^2]	Measured Heat Flux
$q''_{FLUENT\ 1}$	0.93	[MW/m^2]	FLUENT Heat Flux at Ref. 1
$q''_{FLUENT\ 2}$	0.65	[MW/m^2]	FLUENT Heat Flux at Ref. 2
$q''_{FLUENT\ 3}$	0.48	[MW/m^2]	FLUENT Heat Flux at Ref. 3
$q''_{FLUENT\ 4}$	1.29	[MW/m^2]	FLUENT Heat Flux at Ref. 4
HTC 1	7096.64	[W/m^2-K]	Heat Transfer Coefficient at Ref. 1
HTC 2	4561.88	[W/m^2-K]	Heat Transfer Coefficient at Ref. 2
HTC 3	3244.76	[W/m^2-K]	Heat Transfer Coefficient at Ref. 3
HTC 4	8743.93	[W/m^2-K]	Heat Transfer Coefficient at Ref. 4
Nu 1	281.50	[-]	Nusselt Number at Ref. 1
Nu 2	180.96	[-]	Nusselt Number at Ref. 2
Nu 3	128.71	[-]	Nusselt Number at Ref. 3
Nu 4	346.84	[-]	Nusselt Number at Ref. 4

Table C.31 Experimentally measured data for Test 15

	Value	Units	Description
Q_{Heater}	227.9	[W]	Heater Input Power
MFR	8.18	[g/s]	Measured Mass Flow Rate
Θ	0.00	[°]	Azimuthal Position
T1	134.80	[°C]	Embedded TC Ref. 1 in brass
T2	148.20	[°C]	Embedded TC Ref. 2 in brass
T3	153.90	[°C]	Embedded TC Ref. 3 in brass
T4	155.70	[°C]	Embedded TC Ref. 4 in brass
T5	206.60	[°C]	TC Ref. 5 in copper "neck"
T6	220.30	[°C]	TC Ref. 6 in copper "neck"
T7	232.60	[°C]	TC Ref. 7 in copper "neck"
T8	284.60	[°C]	TC Ref. 8 in copper (maximum)
T9	284.60	[°C]	TC Ref. 9 in copper (maximum)
T_{in}	20.40	[°C]	Inlet Temperature
T_{out}	43.20	[°C]	Outlet Temperature
P_{in}	703.27	[kPa]	Inlet Pressure
P_{out}	537.10	[kPa]	Outlet Pressure

Table C.32 Calculated quantities for Test 15

	Value	Units	Description
$T1_{Surface}$	132.36	[°C]	Surface TC Ref. 1 in brass
$T2_{Surface}$	143.73	[°C]	Surface TC Ref. 2 in brass
$T3_{Surface}$	149.07	[°C]	Surface TC Ref. 3 in brass
$T4_{Surface}$	148.05	[°C]	Surface TC Ref. 4 in brass
$T_{Brazing}$	198.80	[°C]	Brazing Surface Temperature
dP	166.16	[kPa]	Pressure Drop
$Q_{Balance}$	188.18	[W]	Energy Balance
% Losses	17.43%	[-]	Energy Loss
$q''_{nominal}$	1.00	[MW/m^2]	Nominal Heat Flux
$q''_{experiment}$	0.92	[MW/m^2]	Measured Heat Flux
$q''_{FLUENT\ 1}$	1.11	[MW/m^2]	FLUENT Heat Flux at Ref. 1
$q''_{FLUENT\ 2}$	0.78	[MW/m^2]	FLUENT Heat Flux at Ref. 2
$q''_{FLUENT\ 3}$	0.58	[MW/m^2]	FLUENT Heat Flux at Ref. 3
$q''_{FLUENT\ 4}$	1.53	[MW/m^2]	FLUENT Heat Flux at Ref. 4
HTC 1	9913.99	[W/m^2-K]	Heat Transfer Coefficient at Ref. 1
HTC 2	6324.75	[W/m^2-K]	Heat Transfer Coefficient at Ref. 2
HTC 3	4507.66	[W/m^2-K]	Heat Transfer Coefficient at Ref. 3
HTC 4	11985.90	[W/m^2-K]	Heat Transfer Coefficient at Ref. 4
Nu 1	393.26	[-]	Nusselt Number at Ref. 1
Nu 2	250.88	[-]	Nusselt Number at Ref. 2
Nu 3	178.80	[-]	Nusselt Number at Ref. 3
Nu 4	475.44	[-]	Nusselt Number at Ref. 4

Table C.33 Experimentally measured data for Test 16

	Value	Units	Description
Q_{Heater}	228.4	[W]	Heater Input Power
MFR	2.07	[g/s]	Measured Mass Flow Rate
Θ	0.00	[°]	Azimuthal Position
T1	277.40	[°C]	Embedded TC Ref. 1 in brass
T2	291.00	[°C]	Embedded TC Ref. 2 in brass
T3	296.60	[°C]	Embedded TC Ref. 3 in brass
T4	298.50	[°C]	Embedded TC Ref. 4 in brass
T5	342.00	[°C]	TC Ref. 5 in copper "neck"
T6	354.90	[°C]	TC Ref. 6 in copper "neck"
T7	366.80	[°C]	TC Ref. 7 in copper "neck"
T8	417.50	[°C]	TC Ref. 8 in copper (maximum)
T9	417.50	[°C]	TC Ref. 9 in copper (maximum)
T_{in}	21.10	[°C]	Inlet Temperature
T_{out}	101.30	[°C]	Outlet Temperature
P_{in}	737.74	[kPa]	Inlet Pressure
P_{out}	726.02	[kPa]	Outlet Pressure

Table C.34 Calculated quantities for Test 16

	Value	Units	Description
$T1_{Surface}$	276.66	[°C]	Surface TC Ref. 1 in brass
$T2_{Surface}$	288.00	[°C]	Surface TC Ref. 2 in brass
$T3_{Surface}$	293.56	[°C]	Surface TC Ref. 3 in brass
$T4_{Surface}$	294.03	[°C]	Surface TC Ref. 4 in brass
$T_{Brazing}$	334.56	[°C]	Brazing Surface Temperature
dP	11.72	[kPa]	Pressure Drop
$Q_{Balance}$	167.51	[W]	Energy Balance
% Losses	26.66%	[-]	Energy Loss
$q''_{nominal}$	1.00	[MW/m^2]	Nominal Heat Flux
$q''_{experiment}$	0.88	[MW/m^2]	Measured Heat Flux
$q''_{FLUENT\ 1}$	0.61	[MW/m^2]	FLUENT Heat Flux at Ref. 1
$q''_{FLUENT\ 2}$	0.44	[MW/m^2]	FLUENT Heat Flux at Ref. 2
$q''_{FLUENT\ 3}$	0.35	[MW/m^2]	FLUENT Heat Flux at Ref. 3
$q''_{FLUENT\ 4}$	0.82	[MW/m^2]	FLUENT Heat Flux at Ref. 4
HTC 1	2386.89	[W/m^2-K]	Heat Transfer Coefficient at Ref. 1
HTC 2	1648.58	[W/m^2-K]	Heat Transfer Coefficient at Ref. 2
HTC 3	1284.58	[W/m^2-K]	Heat Transfer Coefficient at Ref. 3
HTC 4	3004.39	[W/m^2-K]	Heat Transfer Coefficient at Ref. 4
Nu 1	94.68	[-]	Nusselt Number at Ref. 1
Nu 2	65.39	[-]	Nusselt Number at Ref. 2
Nu 3	50.96	[-]	Nusselt Number at Ref. 3
Nu 4	119.17	[-]	Nusselt Number at Ref. 4

Table C.35 Experimentally measured data for Test 17

	Value	Units	Description
Q_{Heater}	228.2	[W]	Heater Input Power
MFR	2.06	[g/s]	Measured Mass Flow Rate
Θ	15.00	[°]	Azimuthal Position
T1	275.00	[°C]	Embedded TC Ref. 1 in brass
T2	288.90	[°C]	Embedded TC Ref. 2 in brass
T3	294.80	[°C]	Embedded TC Ref. 3 in brass
T4	296.80	[°C]	Embedded TC Ref. 4 in brass
T5	340.95	[°C]	TC Ref. 5 in copper "neck"
T6	354.10	[°C]	TC Ref. 6 in copper "neck"
T7	366.20	[°C]	TC Ref. 7 in copper "neck"
T8	417.60	[°C]	TC Ref. 8 in copper (maximum)
T9	417.60	[°C]	TC Ref. 9 in copper (maximum)
T_{in}	21.10	[°C]	Inlet Temperature
T_{out}	102.90	[°C]	Outlet Temperature
P_{in}	737.74	[kPa]	Inlet Pressure
P_{out}	725.33	[kPa]	Outlet Pressure

Table C.36 Calculated quantities for Test 17

	Value	Units	Description
$T1_{Surface}$	275.19	[°C]	Surface TC Ref. 1 in brass
$T2_{Surface}$	285.94	[°C]	Surface TC Ref. 2 in brass
$T3_{Surface}$	291.37	[°C]	Surface TC Ref. 3 in brass
$T4_{Surface}$	292.33	[°C]	Surface TC Ref. 4 in brass
$T_{Brazing}$	333.38	[°C]	Brazing Surface Temperature
dP	12.41	[kPa]	Pressure Drop
$Q_{Balance}$	170.02	[W]	Energy Balance
% Losses	25.50%	[-]	Energy Loss
$q''_{nominal}$	1.00	[MW/m^2]	Nominal Heat Flux
$q''_{experiment}$	0.90	[MW/m^2]	Measured Heat Flux
$q''_{FLUENT\ 1}$	0.20	[MW/m^2]	FLUENT Heat Flux at Ref. 1
$q''_{FLUENT\ 2}$	0.41	[MW/m^2]	FLUENT Heat Flux at Ref. 2
$q''_{FLUENT\ 3}$	0.46	[MW/m^2]	FLUENT Heat Flux at Ref. 3
$q''_{FLUENT\ 4}$	0.82	[MW/m^2]	FLUENT Heat Flux at Ref. 4
HTC 1	787.11	[W/m^2-K]	Heat Transfer Coefficient at Ref. 1
HTC 2	1548.10	[W/m^2-K]	Heat Transfer Coefficient at Ref. 2
HTC 3	1701.99	[W/m^2-K]	Heat Transfer Coefficient at Ref. 3
HTC 4	3023.22	[W/m^2-K]	Heat Transfer Coefficient at Ref. 4
Nu 1	31.22	[-]	Nusselt Number at Ref. 1
Nu 2	61.41	[-]	Nusselt Number at Ref. 2
Nu 3	67.51	[-]	Nusselt Number at Ref. 3
Nu 4	119.92	[-]	Nusselt Number at Ref. 4

Table C.37 Experimentally measured data for Test 18

	Value	Units	Description
Q_{Heater}	228.5	[W]	Heater Input Power
MFR	2.07	[g/s]	Measured Mass Flow Rate
Θ	30.00	[°]	Azimuthal Position
T1	272.50	[°C]	Embedded TC Ref. 1 in brass
T2	287.50	[°C]	Embedded TC Ref. 2 in brass
T3	293.40	[°C]	Embedded TC Ref. 3 in brass
T4	295.30	[°C]	Embedded TC Ref. 4 in brass
T5	339.30	[°C]	TC Ref. 5 in copper "neck"
T6	352.40	[°C]	TC Ref. 6 in copper "neck"
T7	365.40	[°C]	TC Ref. 7 in copper "neck"
T8	416.00	[°C]	TC Ref. 8 in copper (maximum)
T9	416.00	[°C]	TC Ref. 9 in copper (maximum)
T_{in}	20.90	[°C]	Inlet Temperature
T_{out}	102.90	[°C]	Outlet Temperature
P_{in}	737.74	[kPa]	Inlet Pressure
P_{out}	726.71	[kPa]	Outlet Pressure

Table C.38 Calculated quantities for Test 18

	Value	Units	Description
$T1_{Surface}$	272.38	[°C]	Surface TC Ref. 1 in brass
$T2_{Surface}$	283.98	[°C]	Surface TC Ref. 2 in brass
$T3_{Surface}$	289.58	[°C]	Surface TC Ref. 3 in brass
$T4_{Surface}$	290.83	[°C]	Surface TC Ref. 4 in brass
$T_{Brazing}$	331.47	[°C]	Brazing Surface Temperature
dP	11.03	[kPa]	Pressure Drop
$Q_{Balance}$	171.27	[W]	Energy Balance
% Losses	25.04%	[-]	Energy Loss
$q''_{nominal}$	1.00	[MW/m^2]	Nominal Heat Flux
$q''_{experiment}$	0.93	[MW/m^2]	Measured Heat Flux
$q''_{FLUENT\ 1}$	0.32	[MW/m^2]	FLUENT Heat Flux at Ref. 1
$q''_{FLUENT\ 2}$	0.52	[MW/m^2]	FLUENT Heat Flux at Ref. 2
$q''_{FLUENT\ 3}$	0.61	[MW/m^2]	FLUENT Heat Flux at Ref. 3
$q''_{FLUENT\ 4}$	0.82	[MW/m^2]	FLUENT Heat Flux at Ref. 4
HTC 1	1272.46	[W/m^2-K]	Heat Transfer Coefficient at Ref. 1
HTC 2	1976.59	[W/m^2-K]	Heat Transfer Coefficient at Ref. 2
HTC 3	2270.35	[W/m^2-K]	Heat Transfer Coefficient at Ref. 3
HTC 4	3037.78	[W/m^2-K]	Heat Transfer Coefficient at Ref. 4
Nu 1	50.47	[-]	Nusselt Number at Ref. 1
Nu 2	78.40	[-]	Nusselt Number at Ref. 2
Nu 3	90.06	[-]	Nusselt Number at Ref. 3
Nu 4	120.50	[-]	Nusselt Number at Ref. 4

Table C.39 Experimentally measured data for Test 19

	Value	Units	Description
Q_{Heater}	228.5	[W]	Heater Input Power
MFR	2.08	[g/s]	Measured Mass Flow Rate
Θ	45.00	[°]	Azimuthal Position
T1	275.10	[°C]	Embedded TC Ref. 1 in brass
T2	289.10	[°C]	Embedded TC Ref. 2 in brass
T3	294.80	[°C]	Embedded TC Ref. 3 in brass
T4	296.70	[°C]	Embedded TC Ref. 4 in brass
T5	340.10	[°C]	TC Ref. 5 in copper "neck"
T6	353.10	[°C]	TC Ref. 6 in copper "neck"
T7	365.00	[°C]	TC Ref. 7 in copper "neck"
T8	415.70	[°C]	TC Ref. 8 in copper (maximum)
T9	415.70	[°C]	TC Ref. 9 in copper (maximum)
T_{in}	20.80	[°C]	Inlet Temperature
T_{out}	103.70	[°C]	Outlet Temperature
P_{in}	737.74	[kPa]	Inlet Pressure
P_{out}	724.64	[kPa]	Outlet Pressure

Table C.40 Calculated quantities for Test 19

	Value	Units	Description
$T1_{Surface}$	275.29	[°C]	Surface TC Ref. 1 in brass
$T2_{Surface}$	286.19	[°C]	Surface TC Ref. 2 in brass
$T3_{Surface}$	291.27	[°C]	Surface TC Ref. 3 in brass
$T4_{Surface}$	292.23	[°C]	Surface TC Ref. 4 in brass
$T_{Brazing}$	332.63	[°C]	Brazing Surface Temperature
dP	13.10	[kPa]	Pressure Drop
$Q_{Balance}$	173.98	[W]	Energy Balance
% Losses	23.84%	[-]	Energy Loss
$q''_{nominal}$	1.00	[MW/m^2]	Nominal Heat Flux
$q''_{experiment}$	0.88	[MW/m^2]	Measured Heat Flux
$q''_{FLUENT\ 1}$	0.20	[MW/m^2]	FLUENT Heat Flux at Ref. 1
$q''_{FLUENT\ 2}$	0.41	[MW/m^2]	FLUENT Heat Flux at Ref. 2
$q''_{FLUENT\ 3}$	0.46	[MW/m^2]	FLUENT Heat Flux at Ref. 3
$q''_{FLUENT\ 4}$	0.82	[MW/m^2]	FLUENT Heat Flux at Ref. 4
HTC 1	785.88	[W/m^2-K]	Heat Transfer Coefficient at Ref. 1
HTC 2	1544.90	[W/m^2-K]	Heat Transfer Coefficient at Ref. 2
HTC 3	1700.74	[W/m^2-K]	Heat Transfer Coefficient at Ref. 3
HTC 4	3020.99	[W/m^2-K]	Heat Transfer Coefficient at Ref. 4
Nu 1	31.17	[-]	Nusselt Number at Ref. 1
Nu 2	61.28	[-]	Nusselt Number at Ref. 2
Nu 3	67.46	[-]	Nusselt Number at Ref. 3
Nu 4	119.83	[-]	Nusselt Number at Ref. 4

Table C.41 Experimentally measured data for Test 20

	Value	Units	Description
Q_{Heater}	228.5	[W]	Heater Input Power
MFR	2.07	[g/s]	Measured Mass Flow Rate
Θ	60.00	[°]	Azimuthal Position
T1	274.50	[°C]	Embedded TC Ref. 1 in brass
T2	288.20	[°C]	Embedded TC Ref. 2 in brass
T3	294.10	[°C]	Embedded TC Ref. 3 in brass
T4	296.00	[°C]	Embedded TC Ref. 4 in brass
T5	339.60	[°C]	TC Ref. 5 in copper "neck"
T6	352.60	[°C]	TC Ref. 6 in copper "neck"
T7	364.50	[°C]	TC Ref. 7 in copper "neck"
T8	415.50	[°C]	TC Ref. 8 in copper (maximum)
T9	415.50	[°C]	TC Ref. 9 in copper (maximum)
T_{in}	20.60	[°C]	Inlet Temperature
T_{out}	101.30	[°C]	Outlet Temperature
P_{in}	737.74	[kPa]	Inlet Pressure
P_{out}	724.64	[kPa]	Outlet Pressure

Table C.42 Calculated quantities for Test 20

	Value	Units	Description
$T1_{Surface}$	273.86	[°C]	Surface TC Ref. 1 in brass
$T2_{Surface}$	285.17	[°C]	Surface TC Ref. 2 in brass
$T3_{Surface}$	291.02	[°C]	Surface TC Ref. 3 in brass
$T4_{Surface}$	291.53	[°C]	Surface TC Ref. 4 in brass
$T_{Brazing}$	332.13	[°C]	Brazing Surface Temperature
dP	13.10	[kPa]	Pressure Drop
$Q_{Balance}$	168.55	[W]	Energy Balance
% Losses	26.22%	[-]	Energy Loss
$q''_{nominal}$	1.00	[MW/m^2]	Nominal Heat Flux
$q''_{experiment}$	0.88	[MW/m^2]	Measured Heat Flux
$q''_{FLUENT\ 1}$	0.61	[MW/m^2]	FLUENT Heat Flux at Ref. 1
$q''_{FLUENT\ 2}$	0.44	[MW/m^2]	FLUENT Heat Flux at Ref. 2
$q''_{FLUENT\ 3}$	0.35	[MW/m^2]	FLUENT Heat Flux at Ref. 3
$q''_{FLUENT\ 4}$	0.82	[MW/m^2]	FLUENT Heat Flux at Ref. 4
HTC 1	2408.56	[W/m^2-K]	Heat Transfer Coefficient at Ref. 1
HTC 2	1663.09	[W/m^2-K]	Heat Transfer Coefficient at Ref. 2
HTC 3	1294.27	[W/m^2-K]	Heat Transfer Coefficient at Ref. 3
HTC 4	3026.57	[W/m^2-K]	Heat Transfer Coefficient at Ref. 4
Nu 1	95.54	[-]	Nusselt Number at Ref. 1
Nu 2	65.97	[-]	Nusselt Number at Ref. 2
Nu 3	51.34	[-]	Nusselt Number at Ref. 3
Nu 4	120.05	[-]	Nusselt Number at Ref. 4

Table C.43 Experimentally measured data for Test 21

	Value	Units	Description
Q_{Heater}	228.4	[W]	Heater Input Power
MFR	2.07	[g/s]	Measured Mass Flow Rate
Θ	180.00	[°]	Azimuthal Position
T1	274.40	[°C]	Embedded TC Ref. 1 in brass
T2	288.20	[°C]	Embedded TC Ref. 2 in brass
T3	294.00	[°C]	Embedded TC Ref. 3 in brass
T4	295.90	[°C]	Embedded TC Ref. 4 in brass
T5	339.40	[°C]	TC Ref. 5 in copper "neck"
T6	352.40	[°C]	TC Ref. 6 in copper "neck"
T7	364.40	[°C]	TC Ref. 7 in copper "neck"
T8	415.30	[°C]	TC Ref. 8 in copper (maximum)
T9	415.30	[°C]	TC Ref. 9 in copper (maximum)
T_{in}	21.10	[°C]	Inlet Temperature
T_{out}	101.30	[°C]	Outlet Temperature
P_{in}	737.74	[kPa]	Inlet Pressure
P_{out}	724.64	[kPa]	Outlet Pressure

Table C.44 Calculated quantities for Test 21

	Value	Units	Description
$T1_{Surface}$	273.76	[°C]	Surface TC Ref. 1 in brass
$T2_{Surface}$	285.17	[°C]	Surface TC Ref. 2 in brass
$T3_{Surface}$	290.92	[°C]	Surface TC Ref. 3 in brass
$T4_{Surface}$	291.43	[°C]	Surface TC Ref. 4 in brass
$T_{Brazing}$	331.90	[°C]	Brazing Surface Temperature
dP	13.10	[kPa]	Pressure Drop
$Q_{Balance}$	167.51	[W]	Energy Balance
% Losses	26.66%	[-]	Energy Loss
$q''_{nominal}$	1.00	[MW/m^2]	Nominal Heat Flux
$q''_{experiment}$	0.89	[MW/m^2]	Measured Heat Flux
$q''_{FLUENT\ 1}$	0.61	[MW/m^2]	FLUENT Heat Flux at Ref. 1
$q''_{FLUENT\ 2}$	0.44	[MW/m^2]	FLUENT Heat Flux at Ref. 2
$q''_{FLUENT\ 3}$	0.35	[MW/m^2]	FLUENT Heat Flux at Ref. 3
$q''_{FLUENT\ 4}$	0.82	[MW/m^2]	FLUENT Heat Flux at Ref. 4
HTC 1	2414.28	[W/m^2-K]	Heat Transfer Coefficient at Ref. 1
HTC 2	1666.24	[W/m^2-K]	Heat Transfer Coefficient at Ref. 2
HTC 3	1297.15	[W/m^2-K]	Heat Transfer Coefficient at Ref. 3
HTC 4	3033.28	[W/m^2-K]	Heat Transfer Coefficient at Ref. 4
Nu 1	95.77	[-]	Nusselt Number at Ref. 1
Nu 2	66.09	[-]	Nusselt Number at Ref. 2
Nu 3	51.45	[-]	Nusselt Number at Ref. 3
Nu 4	120.32	[-]	Nusselt Number at Ref. 4

Table C.45 Experimentally measured data for Test 22

	Value	Units	Description
Q_{Heater}	228.8	[W]	Heater Input Power
MFR	2.07	[g/s]	Measured Mass Flow Rate
Θ	195.00	[°]	Azimuthal Position
T1	274.50	[°C]	Embedded TC Ref. 1 in brass
T2	288.00	[°C]	Embedded TC Ref. 2 in brass
T3	293.80	[°C]	Embedded TC Ref. 3 in brass
T4	295.80	[°C]	Embedded TC Ref. 4 in brass
T5	339.30	[°C]	TC Ref. 5 in copper "neck"
T6	352.30	[°C]	TC Ref. 6 in copper "neck"
T7	364.20	[°C]	TC Ref. 7 in copper "neck"
T8	415.10	[°C]	TC Ref. 8 in copper (maximum)
T9	415.10	[°C]	TC Ref. 9 in copper (maximum)
T_{in}	20.80	[°C]	Inlet Temperature
T_{out}	100.50	[°C]	Outlet Temperature
P_{in}	737.74	[kPa]	Inlet Pressure
P_{out}	726.02	[kPa]	Outlet Pressure

Table C.46 Calculated quantities for Test 22

	Value	Units	Description
$T1_{Surface}$	273.86	[°C]	Surface TC Ref. 1 in brass
$T2_{Surface}$	284.97	[°C]	Surface TC Ref. 2 in brass
$T3_{Surface}$	290.72	[°C]	Surface TC Ref. 3 in brass
$T4_{Surface}$	291.33	[°C]	Surface TC Ref. 4 in brass
$T_{Brazing}$	331.83	[°C]	Brazing Surface Temperature
dP	11.72	[kPa]	Pressure Drop
$Q_{Balance}$	166.46	[W]	Energy Balance
% Losses	27.24%	[-]	Energy Loss
$q''_{nominal}$	1.00	[MW/m^2]	Nominal Heat Flux
$q''_{experiment}$	0.88	[MW/m^2]	Measured Heat Flux
$q''_{FLUENT\ 1}$	0.20	[MW/m^2]	FLUENT Heat Flux at Ref. 1
$q''_{FLUENT\ 2}$	0.41	[MW/m^2]	FLUENT Heat Flux at Ref. 2
$q''_{FLUENT\ 3}$	0.46	[MW/m^2]	FLUENT Heat Flux at Ref. 3
$q''_{FLUENT\ 4}$	0.82	[MW/m^2]	FLUENT Heat Flux at Ref. 4
HTC 1	790.32	[W/m^2-K]	Heat Transfer Coefficient at Ref. 1
HTC 2	1552.04	[W/m^2-K]	Heat Transfer Coefficient at Ref. 2
HTC 3	1704.19	[W/m^2-K]	Heat Transfer Coefficient at Ref. 3
HTC 4	3031.04	[W/m^2-K]	Heat Transfer Coefficient at Ref. 4
Nu 1	31.35	[-]	Nusselt Number at Ref. 1
Nu 2	61.56	[-]	Nusselt Number at Ref. 2
Nu 3	67.60	[-]	Nusselt Number at Ref. 3
Nu 4	120.23	[-]	Nusselt Number at Ref. 4

Table C.47 Experimentally measured data for Test 23

	Value	Units	Description
Q_{Heater}	228.7	[W]	Heater Input Power
MFR	2.07	[g/s]	Measured Mass Flow Rate
Θ	210.00	[°]	Azimuthal Position
T1	274.00	[°C]	Embedded TC Ref. 1 in brass
T2	287.80	[°C]	Embedded TC Ref. 2 in brass
T3	293.50	[°C]	Embedded TC Ref. 3 in brass
T4	295.50	[°C]	Embedded TC Ref. 4 in brass
T5	339.00	[°C]	TC Ref. 5 in copper "neck"
T6	352.00	[°C]	TC Ref. 6 in copper "neck"
T7	364.00	[°C]	TC Ref. 7 in copper "neck"
T8	415.00	[°C]	TC Ref. 8 in copper (maximum)
T9	415.00	[°C]	TC Ref. 9 in copper (maximum)
T_{in}	20.60	[°C]	Inlet Temperature
T_{out}	100.20	[°C]	Outlet Temperature
P_{in}	737.74	[kPa]	Inlet Pressure
P_{out}	726.71	[kPa]	Outlet Pressure

Table C.48 Calculated quantities for Test 23

	Value	Units	Description
$T1_{Surface}$	273.36	[°C]	Surface TC Ref. 1 in brass
$T2_{Surface}$	284.77	[°C]	Surface TC Ref. 2 in brass
$T3_{Surface}$	290.42	[°C]	Surface TC Ref. 3 in brass
$T4_{Surface}$	291.03	[°C]	Surface TC Ref. 4 in brass
$T_{Brazing}$	331.50	[°C]	Brazing Surface Temperature
dP	11.03	[kPa]	Pressure Drop
$Q_{Balance}$	166.25	[W]	Energy Balance
% Losses	27.29%	[-]	Energy Loss
$q''_{nominal}$	1.00	[MW/m^2]	Nominal Heat Flux
$q''_{experiment}$	0.89	[MW/m^2]	Measured Heat Flux
$q''_{FLUENT\ 1}$	0.32	[MW/m^2]	FLUENT Heat Flux at Ref. 1
$q''_{FLUENT\ 2}$	0.52	[MW/m^2]	FLUENT Heat Flux at Ref. 2
$q''_{FLUENT\ 3}$	0.61	[MW/m^2]	FLUENT Heat Flux at Ref. 3
$q''_{FLUENT\ 4}$	0.82	[MW/m^2]	FLUENT Heat Flux at Ref. 4
HTC 1	1266.01	[W/m^2-K]	Heat Transfer Coefficient at Ref. 1
HTC 2	1968.44	[W/m^2-K]	Heat Transfer Coefficient at Ref. 2
HTC 3	2260.74	[W/m^2-K]	Heat Transfer Coefficient at Ref. 3
HTC 4	3032.16	[W/m^2-K]	Heat Transfer Coefficient at Ref. 4
Nu 1	50.22	[-]	Nusselt Number at Ref. 1
Nu 2	78.08	[-]	Nusselt Number at Ref. 2
Nu 3	89.68	[-]	Nusselt Number at Ref. 3
Nu 4	120.28	[-]	Nusselt Number at Ref. 4

Table C.49 Experimentally measured data for Test 24

	Value	Units	Description
Q_{Heater}	228.9	[W]	Heater Input Power
MFR	2.07	[g/s]	Measured Mass Flow Rate
Θ	225.00	[°]	Azimuthal Position
T1	274.20	[°C]	Embedded TC Ref. 1 in brass
T2	287.80	[°C]	Embedded TC Ref. 2 in brass
T3	293.60	[°C]	Embedded TC Ref. 3 in brass
T4	295.60	[°C]	Embedded TC Ref. 4 in brass
T5	339.00	[°C]	TC Ref. 5 in copper "neck"
T6	352.00	[°C]	TC Ref. 6 in copper "neck"
T7	364.00	[°C]	TC Ref. 7 in copper "neck"
T8	414.90	[°C]	TC Ref. 8 in copper (maximum)
T9	414.90	[°C]	TC Ref. 9 in copper (maximum)
T_{in}	20.60	[°C]	Inlet Temperature
T_{out}	100.20	[°C]	Outlet Temperature
P_{in}	737.74	[kPa]	Inlet Pressure
P_{out}	726.71	[kPa]	Outlet Pressure

Table C.50 Calculated quantities for Test 24

	Value	Units	Description
$T1_{Surface}$	273.56	[°C]	Surface TC Ref. 1 in brass
$T2_{Surface}$	284.77	[°C]	Surface TC Ref. 2 in brass
$T3_{Surface}$	290.52	[°C]	Surface TC Ref. 3 in brass
$T4_{Surface}$	291.13	[°C]	Surface TC Ref. 4 in brass
$T_{Brazing}$	331.50	[°C]	Brazing Surface Temperature
dP	11.03	[kPa]	Pressure Drop
$Q_{Balance}$	166.25	[W]	Energy Balance
% Losses	27.36%	[-]	Energy Loss
$q''_{nominal}$	1.00	[MW/m^2]	Nominal Heat Flux
$q''_{experiment}$	0.89	[MW/m^2]	Measured Heat Flux
$q''_{FLUENT\ 1}$	0.20	[MW/m^2]	FLUENT Heat Flux at Ref. 1
$q''_{FLUENT\ 2}$	0.41	[MW/m^2]	FLUENT Heat Flux at Ref. 2
$q''_{FLUENT\ 3}$	0.46	[MW/m^2]	FLUENT Heat Flux at Ref. 3
$q''_{FLUENT\ 4}$	0.82	[MW/m^2]	FLUENT Heat Flux at Ref. 4
HTC 1	790.63	[W/m^2-K]	Heat Transfer Coefficient at Ref. 1
HTC 2	1552.04	[W/m^2-K]	Heat Transfer Coefficient at Ref. 2
HTC 3	1704.19	[W/m^2-K]	Heat Transfer Coefficient at Ref. 3
HTC 4	3031.04	[W/m^2-K]	Heat Transfer Coefficient at Ref. 4
Nu 1	31.36	[-]	Nusselt Number at Ref. 1
Nu 2	61.56	[-]	Nusselt Number at Ref. 2
Nu 3	67.60	[-]	Nusselt Number at Ref. 3
Nu 4	120.23	[-]	Nusselt Number at Ref. 4

Table C.51 Experimentally measured data for Test 25

	Value	Units	Description
Q_{Heater}	228.9	[W]	Heater Input Power
MFR	2.07	[g/s]	Measured Mass Flow Rate
Θ	240.00	[°]	Azimuthal Position
T1	275.30	[°C]	Embedded TC Ref. 1 in brass
T2	288.40	[°C]	Embedded TC Ref. 2 in brass
T3	294.10	[°C]	Embedded TC Ref. 3 in brass
T4	296.10	[°C]	Embedded TC Ref. 4 in brass
T5	339.40	[°C]	TC Ref. 5 in copper "neck"
T6	352.40	[°C]	TC Ref. 6 in copper "neck"
T7	364.30	[°C]	TC Ref. 7 in copper "neck"
T8	414.90	[°C]	TC Ref. 8 in copper (maximum)
T9	414.90	[°C]	TC Ref. 9 in copper (maximum)
T_{in}	20.40	[°C]	Inlet Temperature
T_{out}	99.90	[°C]	Outlet Temperature
P_{in}	737.74	[kPa]	Inlet Pressure
P_{out}	726.71	[kPa]	Outlet Pressure

Table C.52 Calculated quantities for Test 25

	Value	Units	Description
$T1_{Surface}$	274.66	[°C]	Surface TC Ref. 1 in brass
$T2_{Surface}$	285.37	[°C]	Surface TC Ref. 2 in brass
$T3_{Surface}$	291.02	[°C]	Surface TC Ref. 3 in brass
$T4_{Surface}$	291.63	[°C]	Surface TC Ref. 4 in brass
$T_{Brazing}$	331.93	[°C]	Brazing Surface Temperature
dP	11.03	[kPa]	Pressure Drop
$Q_{Balance}$	166.05	[W]	Energy Balance
% Losses	27.47%	[-]	Energy Loss
$q''_{nominal}$	1.00	[MW/m^2]	Nominal Heat Flux
$q''_{experiment}$	0.88	[MW/m^2]	Measured Heat Flux
$q''_{FLUENT\ 1}$	0.61	[MW/m^2]	FLUENT Heat Flux at Ref. 1
$q''_{FLUENT\ 2}$	0.44	[MW/m^2]	FLUENT Heat Flux at Ref. 2
$q''_{FLUENT\ 3}$	0.35	[MW/m^2]	FLUENT Heat Flux at Ref. 3
$q''_{FLUENT\ 4}$	0.82	[MW/m^2]	FLUENT Heat Flux at Ref. 4
HTC 1	2399.09	[W/m^2-K]	Heat Transfer Coefficient at Ref. 1
HTC 2	1660.58	[W/m^2-K]	Heat Transfer Coefficient at Ref. 2
HTC 3	1293.31	[W/m^2-K]	Heat Transfer Coefficient at Ref. 3
HTC 4	3023.22	[W/m^2-K]	Heat Transfer Coefficient at Ref. 4
Nu 1	95.16	[-]	Nusselt Number at Ref. 1
Nu 2	65.87	[-]	Nusselt Number at Ref. 2
Nu 3	51.30	[-]	Nusselt Number at Ref. 3
Nu 4	119.92	[-]	Nusselt Number at Ref. 4

Table C.53 Experimentally measured data for Test 26

	Value	Units	Description
Q_{Heater}	182.8	[W]	Heater Input Power
MFR	3.03	[g/s]	Measured Mass Flow Rate
Θ	0.00	[°]	Azimuthal Position
T1	187.60	[°C]	Embedded TC Ref. 1 in brass
T2	198.70	[°C]	Embedded TC Ref. 2 in brass
T3	203.60	[°C]	Embedded TC Ref. 3 in brass
T4	205.20	[°C]	Embedded TC Ref. 4 in brass
T5	242.70	[°C]	TC Ref. 5 in copper "neck"
T6	253.10	[°C]	TC Ref. 6 in copper "neck"
T7	262.50	[°C]	TC Ref. 7 in copper "neck"
T8	303.00	[°C]	TC Ref. 8 in copper (maximum)
T9	303.00	[°C]	TC Ref. 9 in copper (maximum)
T_{in}	20.70	[°C]	Inlet Temperature
T_{out}	67.10	[°C]	Outlet Temperature
P_{in}	748.08	[kPa]	Inlet Pressure
P_{out}	730.15	[kPa]	Outlet Pressure

Table C.54 Calculated quantities for Test 26

	Value	Units	Description
$T1_{Surface}$	186.65	[°C]	Surface TC Ref. 1 in brass
$T2_{Surface}$	195.97	[°C]	Surface TC Ref. 2 in brass
$T3_{Surface}$	200.78	[°C]	Surface TC Ref. 3 in brass
$T4_{Surface}$	200.95	[°C]	Surface TC Ref. 4 in brass
$T_{Brazing}$	236.76	[°C]	Brazing Surface Temperature
dP	17.93	[kPa]	Pressure Drop
$Q_{Balance}$	141.86	[W]	Energy Balance
% Losses	22.40%	[-]	Energy Loss
$q''_{nominal}$	0.80	[MW/m^2]	Nominal Heat Flux
$q''_{experiment}$	0.70	[MW/m^2]	Measured Heat Flux
$q''_{FLUENT\ 1}$	0.63	[MW/m^2]	FLUENT Heat Flux at Ref. 1
$q''_{FLUENT\ 2}$	0.39	[MW/m^2]	FLUENT Heat Flux at Ref. 2
$q''_{FLUENT\ 3}$	0.37	[MW/m^2]	FLUENT Heat Flux at Ref. 3
$q''_{FLUENT\ 4}$	0.82	[MW/m^2]	FLUENT Heat Flux at Ref. 4
HTC 1	3796.26	[W/m^2-K]	Heat Transfer Coefficient at Ref. 1
HTC 2	2225.09	[W/m^2-K]	Heat Transfer Coefficient at Ref. 2
HTC 3	2054.68	[W/m^2-K]	Heat Transfer Coefficient at Ref. 3
HTC 4	4549.16	[W/m^2-K]	Heat Transfer Coefficient at Ref. 4
Nu 1	150.59	[-]	Nusselt Number at Ref. 1
Nu 2	88.26	[-]	Nusselt Number at Ref. 2
Nu 3	81.50	[-]	Nusselt Number at Ref. 3
Nu 4	180.45	[-]	Nusselt Number at Ref. 4

Table C.55 Experimentally measured data for Test 27

	Value	Units	Description
Q_{Heater}	182.7	[W]	Heater Input Power
MFR	3.03	[g/s]	Measured Mass Flow Rate
Θ	15.00	[°]	Azimuthal Position
T1	188.70	[°C]	Embedded TC Ref. 1 in brass
T2	199.60	[°C]	Embedded TC Ref. 2 in brass
T3	204.30	[°C]	Embedded TC Ref. 3 in brass
T4	206.00	[°C]	Embedded TC Ref. 4 in brass
T5	243.60	[°C]	TC Ref. 5 in copper "neck"
T6	254.00	[°C]	TC Ref. 6 in copper "neck"
T7	263.40	[°C]	TC Ref. 7 in copper "neck"
T8	304.00	[°C]	TC Ref. 8 in copper (maximum)
T9	303.90	[°C]	TC Ref. 9 in copper (maximum)
T_{in}	21.00	[°C]	Inlet Temperature
T_{out}	68.00	[°C]	Outlet Temperature
P_{in}	748.08	[kPa]	Inlet Pressure
P_{out}	733.60	[kPa]	Outlet Pressure

Table C.56 Calculated quantities for Test 27

	Value	Units	Description
$T1_{Surface}$	188.70	[°C]	Surface TC Ref. 1 in brass
$T2_{Surface}$	196.93	[°C]	Surface TC Ref. 2 in brass
$T3_{Surface}$	201.09	[°C]	Surface TC Ref. 3 in brass
$T4_{Surface}$	201.75	[°C]	Surface TC Ref. 4 in brass
$T_{Brazing}$	237.66	[°C]	Brazing Surface Temperature
dP	14.48	[kPa]	Pressure Drop
$Q_{Balance}$	143.69	[W]	Energy Balance
% Losses	21.37%	[-]	Energy Loss
$q''_{nominal}$	0.80	[MW/m^2]	Nominal Heat Flux
$q''_{experiment}$	0.70	[MW/m^2]	Measured Heat Flux
$q''_{FLUENT\ 1}$	0.21	[MW/m^2]	FLUENT Heat Flux at Ref. 1
$q''_{FLUENT\ 2}$	0.35	[MW/m^2]	FLUENT Heat Flux at Ref. 2
$q''_{FLUENT\ 3}$	0.45	[MW/m^2]	FLUENT Heat Flux at Ref. 3
$q''_{FLUENT\ 4}$	0.82	[MW/m^2]	FLUENT Heat Flux at Ref. 4
HTC 1	1252.27	[W/m^2-K]	Heat Transfer Coefficient at Ref. 1
HTC 2	1989.39	[W/m^2-K]	Heat Transfer Coefficient at Ref. 2
HTC 3	2498.81	[W/m^2-K]	Heat Transfer Coefficient at Ref. 3
HTC 4	4536.58	[W/m^2-K]	Heat Transfer Coefficient at Ref. 4
Nu 1	49.67	[-]	Nusselt Number at Ref. 1
Nu 2	78.91	[-]	Nusselt Number at Ref. 2
Nu 3	99.12	[-]	Nusselt Number at Ref. 3
Nu 4	179.95	[-]	Nusselt Number at Ref. 4

Table C.57 Experimentally measured data for Test 28

	Value	Units	Description
Q_{Heater}	182.3	[W]	Heater Input Power
MFR	3.03	[g/s]	Measured Mass Flow Rate
Θ	30.00	[°]	Azimuthal Position
T1	187.70	[°C]	Embedded TC Ref. 1 in brass
T2	198.80	[°C]	Embedded TC Ref. 2 in brass
T3	203.50	[°C]	Embedded TC Ref. 3 in brass
T4	205.30	[°C]	Embedded TC Ref. 4 in brass
T5	243.20	[°C]	TC Ref. 5 in copper "neck"
T6	253.70	[°C]	TC Ref. 6 in copper "neck"
T7	263.20	[°C]	TC Ref. 7 in copper "neck"
T8	304.10	[°C]	TC Ref. 8 in copper (maximum)
T9	304.00	[°C]	TC Ref. 9 in copper (maximum)
T_{in}	21.30	[°C]	Inlet Temperature
T_{out}	69.00	[°C]	Outlet Temperature
P_{in}	748.08	[kPa]	Inlet Pressure
P_{out}	730.84	[kPa]	Outlet Pressure

Table C.58 Calculated quantities for Test 28

	Value	Units	Description
$T1_{Surface}$	187.37	[°C]	Surface TC Ref. 1 in brass
$T2_{Surface}$	195.52	[°C]	Surface TC Ref. 2 in brass
$T3_{Surface}$	199.91	[°C]	Surface TC Ref. 3 in brass
$T4_{Surface}$	201.05	[°C]	Surface TC Ref. 4 in brass
$T_{Brazing}$	237.20	[°C]	Brazing Surface Temperature
dP	17.24	[kPa]	Pressure Drop
$Q_{Balance}$	145.83	[W]	Energy Balance
% Losses	20.01%	[-]	Energy Loss
$q''_{nominal}$	0.80	[MW/m^2]	Nominal Heat Flux
$q''_{experiment}$	0.71	[MW/m^2]	Measured Heat Flux
$q''_{FLUENT\ 1}$	0.32	[MW/m^2]	FLUENT Heat Flux at Ref. 1
$q''_{FLUENT\ 2}$	0.53	[MW/m^2]	FLUENT Heat Flux at Ref. 2
$q''_{FLUENT\ 3}$	0.62	[MW/m^2]	FLUENT Heat Flux at Ref. 3
$q''_{FLUENT\ 4}$	0.82	[MW/m^2]	FLUENT Heat Flux at Ref. 4
HTC 1	1926.94	[W/m^2-K]	Heat Transfer Coefficient at Ref. 1
HTC 2	3042.08	[W/m^2-K]	Heat Transfer Coefficient at Ref. 2
HTC 3	3471.35	[W/m^2-K]	Heat Transfer Coefficient at Ref. 3
HTC 4	4561.82	[W/m^2-K]	Heat Transfer Coefficient at Ref. 4
Nu 1	76.44	[-]	Nusselt Number at Ref. 1
Nu 2	120.67	[-]	Nusselt Number at Ref. 2
Nu 3	137.70	[-]	Nusselt Number at Ref. 3
Nu 4	180.95	[-]	Nusselt Number at Ref. 4

Table C.59 Experimentally measured data for Test 29

	Value	Units	Description
Q_{Heater}	183.0	[W]	Heater Input Power
MFR	3.03	[g/s]	Measured Mass Flow Rate
Θ	45.00	[°]	Azimuthal Position
T1	190.10	[°C]	Embedded TC Ref. 1 in brass
T2	200.90	[°C]	Embedded TC Ref. 2 in brass
T3	205.70	[°C]	Embedded TC Ref. 3 in brass
T4	207.30	[°C]	Embedded TC Ref. 4 in brass
T5	244.80	[°C]	TC Ref. 5 in copper "neck"
T6	255.20	[°C]	TC Ref. 6 in copper "neck"
T7	264.60	[°C]	TC Ref. 7 in copper "neck"
T8	305.10	[°C]	TC Ref. 8 in copper (maximum)
T9	305.00	[°C]	TC Ref. 9 in copper (maximum)
T_{in}	21.20	[°C]	Inlet Temperature
T_{out}	70.00	[°C]	Outlet Temperature
P_{in}	748.08	[kPa]	Inlet Pressure
P_{out}	727.40	[kPa]	Outlet Pressure

Table C.60 Calculated quantities for Test 29

	Value	Units	Description
$T1_{Surface}$	190.10	[°C]	Surface TC Ref. 1 in brass
$T2_{Surface}$	198.31	[°C]	Surface TC Ref. 2 in brass
$T3_{Surface}$	202.39	[°C]	Surface TC Ref. 3 in brass
$T4_{Surface}$	203.05	[°C]	Surface TC Ref. 4 in brass
$T_{Brazing}$	238.86	[°C]	Brazing Surface Temperature
dP	20.68	[kPa]	Pressure Drop
$Q_{Balance}$	149.19	[W]	Energy Balance
% Losses	18.49%	[-]	Energy Loss
$q''_{nominal}$	0.80	[MW/m^2]	Nominal Heat Flux
$q''_{experiment}$	0.70	[MW/m^2]	Measured Heat Flux
$q''_{FLUENT\ 1}$	0.21	[MW/m^2]	FLUENT Heat Flux at Ref. 1
$q''_{FLUENT\ 2}$	0.35	[MW/m^2]	FLUENT Heat Flux at Ref. 2
$q''_{FLUENT\ 3}$	0.45	[MW/m^2]	FLUENT Heat Flux at Ref. 3
$q''_{FLUENT\ 4}$	0.82	[MW/m^2]	FLUENT Heat Flux at Ref. 4
HTC 1	1243.38	[W/m^2-K]	Heat Transfer Coefficient at Ref. 1
HTC 2	1976.17	[W/m^2-K]	Heat Transfer Coefficient at Ref. 2
HTC 3	2483.65	[W/m^2-K]	Heat Transfer Coefficient at Ref. 3
HTC 4	4509.14	[W/m^2-K]	Heat Transfer Coefficient at Ref. 4
Nu 1	49.32	[-]	Nusselt Number at Ref. 1
Nu 2	78.39	[-]	Nusselt Number at Ref. 2
Nu 3	98.52	[-]	Nusselt Number at Ref. 3
Nu 4	178.86	[-]	Nusselt Number at Ref. 4

Table C.61 Experimentally measured data for Test 30

	Value	Units	Description
Q_{Heater}	182.7	[W]	Heater Input Power
MFR	3.03	[g/s]	Measured Mass Flow Rate
Θ	60.00	[°]	Azimuthal Position
T1	187.90	[°C]	Embedded TC Ref. 1 in brass
T2	199.00	[°C]	Embedded TC Ref. 2 in brass
T3	203.90	[°C]	Embedded TC Ref. 3 in brass
T4	205.60	[°C]	Embedded TC Ref. 4 in brass
T5	243.70	[°C]	TC Ref. 5 in copper "neck"
T6	254.30	[°C]	TC Ref. 6 in copper "neck"
T7	263.80	[°C]	TC Ref. 7 in copper "neck"
T8	305.00	[°C]	TC Ref. 8 in copper (maximum)
T9	305.00	[°C]	TC Ref. 9 in copper (maximum)
T_{in}	21.00	[°C]	Inlet Temperature
T_{out}	70.50	[°C]	Outlet Temperature
P_{in}	748.08	[kPa]	Inlet Pressure
P_{out}	730.84	[kPa]	Outlet Pressure

Table C.62 Calculated quantities for Test 30

	Value	Units	Description
$T1_{Surface}$	187.05	[°C]	Surface TC Ref. 1 in brass
$T2_{Surface}$	196.24	[°C]	Surface TC Ref. 2 in brass
$T3_{Surface}$	201.04	[°C]	Surface TC Ref. 3 in brass
$T4_{Surface}$	201.35	[°C]	Surface TC Ref. 4 in brass
$T_{Brazing}$	237.67	[°C]	Brazing Surface Temperature
dP	17.24	[kPa]	Pressure Drop
$Q_{Balance}$	151.33	[W]	Energy Balance
% Losses	17.19%	[-]	Energy Loss
$q''_{nominal}$	0.80	[MW/m^2]	Nominal Heat Flux
$q''_{experiment}$	0.71	[MW/m^2]	Measured Heat Flux
$q''_{FLUENT\ 1}$	0.63	[MW/m^2]	FLUENT Heat Flux at Ref. 1
$q''_{FLUENT\ 2}$	0.39	[MW/m^2]	FLUENT Heat Flux at Ref. 2
$q''_{FLUENT\ 3}$	0.37	[MW/m^2]	FLUENT Heat Flux at Ref. 3
$q''_{FLUENT\ 4}$	0.82	[MW/m^2]	FLUENT Heat Flux at Ref. 4
HTC 1	3794.08	[W/m^2-K]	Heat Transfer Coefficient at Ref. 1
HTC 2	2225.57	[W/m^2-K]	Heat Transfer Coefficient at Ref. 2
HTC 3	2055.14	[W/m^2-K]	Heat Transfer Coefficient at Ref. 3
HTC 4	4546.64	[W/m^2-K]	Heat Transfer Coefficient at Ref. 4
Nu 1	150.50	[-]	Nusselt Number at Ref. 1
Nu 2	88.28	[-]	Nusselt Number at Ref. 2
Nu 3	81.52	[-]	Nusselt Number at Ref. 3
Nu 4	180.35	[-]	Nusselt Number at Ref. 4

Table C.63 Experimentally measured data for Test 31

	Value	Units	Description
Q_{Heater}	227.0	[W]	Heater Input Power
MFR	3.03	[g/s]	Measured Mass Flow Rate
Θ	0.00	[°]	Azimuthal Position
T1	222.97	[°C]	Embedded TC Ref. 1 in brass
T2	236.93	[°C]	Embedded TC Ref. 2 in brass
T3	242.68	[°C]	Embedded TC Ref. 3 in brass
T4	244.81	[°C]	Embedded TC Ref. 4 in brass
T5	289.94	[°C]	TC Ref. 5 in copper "neck"
T6	303.27	[°C]	TC Ref. 6 in copper "neck"
T7	315.26	[°C]	TC Ref. 7 in copper "neck"
T8	366.56	[°C]	TC Ref. 8 in copper (maximum)
T9	366.57	[°C]	TC Ref. 9 in copper (maximum)
T_{in}	20.26	[°C]	Inlet Temperature
T_{out}	78.98	[°C]	Outlet Temperature
P_{in}	730.84	[kPa]	Inlet Pressure
P_{out}	712.92	[kPa]	Outlet Pressure

Table C.64 Calculated quantities for Test 31

	Value	Units	Description
$T1_{Surface}$	221.85	[°C]	Surface TC Ref. 1 in brass
$T2_{Surface}$	233.70	[°C]	Surface TC Ref. 2 in brass
$T3_{Surface}$	239.34	[°C]	Surface TC Ref. 3 in brass
$T4_{Surface}$	239.91	[°C]	Surface TC Ref. 4 in brass
$T_{Brazing}$	282.34	[°C]	Brazing Surface Temperature
dP	17.93	[kPa]	Pressure Drop
$Q_{Balance}$	179.52	[W]	Energy Balance
% Losses	20.90%	[-]	Energy Loss
$q''_{nominal}$	1.00	[MW/m^2]	Nominal Heat Flux
$q''_{experiment}$	0.90	[MW/m^2]	Measured Heat Flux
$q''_{FLUENT\ 1}$	0.72	[MW/m^2]	FLUENT Heat Flux at Ref. 1
$q''_{FLUENT\ 2}$	0.48	[MW/m^2]	FLUENT Heat Flux at Ref. 2
$q''_{FLUENT\ 3}$	0.40	[MW/m^2]	FLUENT Heat Flux at Ref. 3
$q''_{FLUENT\ 4}$	1.03	[MW/m^2]	FLUENT Heat Flux at Ref. 4
HTC 1	3571.59	[W/m^2-K]	Heat Transfer Coefficient at Ref. 1
HTC 2	2248.84	[W/m^2-K]	Heat Transfer Coefficient at Ref. 2
HTC 3	1825.86	[W/m^2-K]	Heat Transfer Coefficient at Ref. 3
HTC 4	4689.32	[W/m^2-K]	Heat Transfer Coefficient at Ref. 4
Nu 1	141.67	[-]	Nusselt Number at Ref. 1
Nu 2	89.20	[-]	Nusselt Number at Ref. 2
Nu 3	72.43	[-]	Nusselt Number at Ref. 3
Nu 4	186.01	[-]	Nusselt Number at Ref. 4

Table C.65 Experimentally measured data for Test 32

	Value	Units	Description
Q_{Heater}	226.9	[W]	Heater Input Power
MFR	3.03	[g/s]	Measured Mass Flow Rate
Θ	15.00	[°]	Azimuthal Position
T1	223.15	[°C]	Embedded TC Ref. 1 in brass
T2	236.91	[°C]	Embedded TC Ref. 2 in brass
T3	242.70	[°C]	Embedded TC Ref. 3 in brass
T4	244.83	[°C]	Embedded TC Ref. 4 in brass
T5	289.86	[°C]	TC Ref. 5 in copper "neck"
T6	303.15	[°C]	TC Ref. 6 in copper "neck"
T7	315.12	[°C]	TC Ref. 7 in copper "neck"
T8	366.29	[°C]	TC Ref. 8 in copper (maximum)
T9	366.31	[°C]	TC Ref. 9 in copper (maximum)
T_{in}	20.38	[°C]	Inlet Temperature
T_{out}	78.95	[°C]	Outlet Temperature
P_{in}	730.84	[kPa]	Inlet Pressure
P_{out}	690.17	[kPa]	Outlet Pressure

Table C.66 Calculated quantities for Test 32

	Value	Units	Description
$T1_{Surface}$	223.15	[°C]	Surface TC Ref. 1 in brass
$T2_{Surface}$	233.75	[°C]	Surface TC Ref. 2 in brass
$T3_{Surface}$	238.89	[°C]	Surface TC Ref. 3 in brass
$T4_{Surface}$	239.93	[°C]	Surface TC Ref. 4 in brass
$T_{Brazing}$	282.28	[°C]	Brazing Surface Temperature
dP	40.68	[kPa]	Pressure Drop
$Q_{Balance}$	179.06	[W]	Energy Balance
% Losses	21.09%	[-]	Energy Loss
$q''_{nominal}$	1.00	[MW/m^2]	Nominal Heat Flux
$q''_{experiment}$	0.90	[MW/m^2]	Measured Heat Flux
$q''_{FLUENT\ 1}$	0.22	[MW/m^2]	FLUENT Heat Flux at Ref. 1
$q''_{FLUENT\ 2}$	0.38	[MW/m^2]	FLUENT Heat Flux at Ref. 2
$q''_{FLUENT\ 3}$	0.61	[MW/m^2]	FLUENT Heat Flux at Ref. 3
$q''_{FLUENT\ 4}$	1.03	[MW/m^2]	FLUENT Heat Flux at Ref. 4
HTC 1	1084.96	[W/m^2-K]	Heat Transfer Coefficient at Ref. 1
HTC 2	1780.97	[W/m^2-K]	Heat Transfer Coefficient at Ref. 2
HTC 3	2791.67	[W/m^2-K]	Heat Transfer Coefficient at Ref. 3
HTC 4	4691.46	[W/m^2-K]	Heat Transfer Coefficient at Ref. 4
Nu 1	43.04	[-]	Nusselt Number at Ref. 1
Nu 2	70.65	[-]	Nusselt Number at Ref. 2
Nu 3	110.74	[-]	Nusselt Number at Ref. 3
Nu 4	186.10	[-]	Nusselt Number at Ref. 4

Table C.67 Experimentally measured data for Test 33

	Value	Units	Description
Q_{Heater}	227.0	[W]	Heater Input Power
MFR	3.03	[g/s]	Measured Mass Flow Rate
Θ	30.00	[°]	Azimuthal Position
T1	222.66	[°C]	Embedded TC Ref. 1 in brass
T2	236.74	[°C]	Embedded TC Ref. 2 in brass
T3	242.44	[°C]	Embedded TC Ref. 3 in brass
T4	244.56	[°C]	Embedded TC Ref. 4 in brass
T5	289.56	[°C]	TC Ref. 5 in copper "neck"
T6	302.86	[°C]	TC Ref. 6 in copper "neck"
T7	314.84	[°C]	TC Ref. 7 in copper "neck"
T8	365.96	[°C]	TC Ref. 8 in copper (maximum)
T9	365.97	[°C]	TC Ref. 9 in copper (maximum)
T_{in}	20.27	[°C]	Inlet Temperature
T_{out}	79.11	[°C]	Outlet Temperature
P_{in}	730.84	[kPa]	Inlet Pressure
P_{out}	691.54	[kPa]	Outlet Pressure

Table C.68 Calculated quantities for Test 33

	Value	Units	Description
$T1_{Surface}$	222.27	[°C]	Surface TC Ref. 1 in brass
$T2_{Surface}$	232.85	[°C]	Surface TC Ref. 2 in brass
$T3_{Surface}$	238.17	[°C]	Surface TC Ref. 3 in brass
$T4_{Surface}$	239.66	[°C]	Surface TC Ref. 4 in brass
$T_{Brazing}$	281.98	[°C]	Brazing Surface Temperature
dP	39.30	[kPa]	Pressure Drop
$Q_{Balance}$	179.89	[W]	Energy Balance
% Losses	20.74%	[-]	Energy Loss
$q''_{nominal}$	1.00	[MW/m^2]	Nominal Heat Flux
$q''_{experiment}$	0.90	[MW/m^2]	Measured Heat Flux
$q''_{FLUENT\ 1}$	0.38	[MW/m^2]	FLUENT Heat Flux at Ref. 1
$q''_{FLUENT\ 2}$	0.67	[MW/m^2]	FLUENT Heat Flux at Ref. 2
$q''_{FLUENT\ 3}$	0.77	[MW/m^2]	FLUENT Heat Flux at Ref. 3
$q''_{FLUENT\ 4}$	1.03	[MW/m^2]	FLUENT Heat Flux at Ref. 4
HTC 1	1881.20	[W/m^2-K]	Heat Transfer Coefficient at Ref. 1
HTC 2	3151.72	[W/m^2-K]	Heat Transfer Coefficient at Ref. 2
HTC 3	3533.68	[W/m^2-K]	Heat Transfer Coefficient at Ref. 3
HTC 4	4694.88	[W/m^2-K]	Heat Transfer Coefficient at Ref. 4
Nu 1	74.62	[-]	Nusselt Number at Ref. 1
Nu 2	125.02	[-]	Nusselt Number at Ref. 2
Nu 3	140.17	[-]	Nusselt Number at Ref. 3
Nu 4	186.23	[-]	Nusselt Number at Ref. 4

Table C.69 Experimentally measured data for Test 34

	Value	Units	Description
Q_{Heater}	227.0	[W]	Heater Input Power
MFR	3.03	[g/s]	Measured Mass Flow Rate
Θ	45.00	[°]	Azimuthal Position
T1	222.42	[°C]	Embedded TC Ref. 1 in brass
T2	236.42	[°C]	Embedded TC Ref. 2 in brass
T3	242.33	[°C]	Embedded TC Ref. 3 in brass
T4	244.40	[°C]	Embedded TC Ref. 4 in brass
T5	289.42	[°C]	TC Ref. 5 in copper "neck"
T6	302.71	[°C]	TC Ref. 6 in copper "neck"
T7	314.68	[°C]	TC Ref. 7 in copper "neck"
T8	365.79	[°C]	TC Ref. 8 in copper (maximum)
T9	365.83	[°C]	TC Ref. 9 in copper (maximum)
T_{in}	20.30	[°C]	Inlet Temperature
T_{out}	79.01	[°C]	Outlet Temperature
P_{in}	730.84	[kPa]	Inlet Pressure
P_{out}	714.16	[kPa]	Outlet Pressure

Table C.70 Calculated quantities for Test 34

	Value	Units	Description
$T1_{Surface}$	222.42	[°C]	Surface TC Ref. 1 in brass
$T2_{Surface}$	233.35	[°C]	Surface TC Ref. 2 in brass
$T3_{Surface}$	238.40	[°C]	Surface TC Ref. 3 in brass
$T4_{Surface}$	239.50	[°C]	Surface TC Ref. 4 in brass
$T_{Brazing}$	281.84	[°C]	Brazing Surface Temperature
dP	16.69	[kPa]	Pressure Drop
$Q_{Balance}$	179.49	[W]	Energy Balance
% Losses	20.94%	[-]	Energy Loss
$q''_{nominal}$	1.00	[MW/m^2]	Nominal Heat Flux
$q''_{experiment}$	0.90	[MW/m^2]	Measured Heat Flux
$q''_{FLUENT\ 1}$	0.22	[MW/m^2]	FLUENT Heat Flux at Ref. 1
$q''_{FLUENT\ 2}$	0.38	[MW/m^2]	FLUENT Heat Flux at Ref. 2
$q''_{FLUENT\ 3}$	0.61	[MW/m^2]	FLUENT Heat Flux at Ref. 3
$q''_{FLUENT\ 4}$	1.03	[MW/m^2]	FLUENT Heat Flux at Ref. 4
HTC 1	1088.46	[W/m^2-K]	Heat Transfer Coefficient at Ref. 1
HTC 2	1783.63	[W/m^2-K]	Heat Transfer Coefficient at Ref. 2
HTC 3	2796.92	[W/m^2-K]	Heat Transfer Coefficient at Ref. 3
HTC 4	4698.95	[W/m^2-K]	Heat Transfer Coefficient at Ref. 4
Nu 1	43.18	[-]	Nusselt Number at Ref. 1
Nu 2	70.75	[-]	Nusselt Number at Ref. 2
Nu 3	110.94	[-]	Nusselt Number at Ref. 3
Nu 4	186.39	[-]	Nusselt Number at Ref. 4

Table C.71 Experimentally measured data for Test 35

	Value	Units	Description
Q_{Heater}	227.1	[W]	Heater Input Power
MFR	3.03	[g/s]	Measured Mass Flow Rate
Θ	60.00	[°]	Azimuthal Position
T1	222.80	[°C]	Embedded TC Ref. 1 in brass
T2	236.37	[°C]	Embedded TC Ref. 2 in brass
T3	242.28	[°C]	Embedded TC Ref. 3 in brass
T4	244.36	[°C]	Embedded TC Ref. 4 in brass
T5	289.36	[°C]	TC Ref. 5 in copper "neck"
T6	302.65	[°C]	TC Ref. 6 in copper "neck"
T7	314.59	[°C]	TC Ref. 7 in copper "neck"
T8	365.70	[°C]	TC Ref. 8 in copper (maximum)
T9	365.70	[°C]	TC Ref. 9 in copper (maximum)
T_{in}	20.39	[°C]	Inlet Temperature
T_{out}	80.11	[°C]	Outlet Temperature
P_{in}	730.84	[kPa]	Inlet Pressure
P_{out}	714.64	[kPa]	Outlet Pressure

Table C.72 Calculated quantities for Test 35

	Value	Units	Description
$T1_{Surface}$	221.79	[°C]	Surface TC Ref. 1 in brass
$T2_{Surface}$	233.10	[°C]	Surface TC Ref. 2 in brass
$T3_{Surface}$	238.89	[°C]	Surface TC Ref. 3 in brass
$T4_{Surface}$	239.46	[°C]	Surface TC Ref. 4 in brass
$T_{Brazing}$	281.79	[°C]	Brazing Surface Temperature
dP	16.20	[kPa]	Pressure Drop
$Q_{Balance}$	182.58	[W]	Energy Balance
% Losses	19.60%	[-]	Energy Loss
$q''_{nominal}$	1.00	[MW/m^2]	Nominal Heat Flux
$q''_{experiment}$	0.90	[MW/m^2]	Measured Heat Flux
$q''_{FLUENT\ 1}$	0.72	[MW/m^2]	FLUENT Heat Flux at Ref. 1
$q''_{FLUENT\ 2}$	0.48	[MW/m^2]	FLUENT Heat Flux at Ref. 2
$q''_{FLUENT\ 3}$	0.40	[MW/m^2]	FLUENT Heat Flux at Ref. 3
$q''_{FLUENT\ 4}$	1.03	[MW/m^2]	FLUENT Heat Flux at Ref. 4
HTC 1	3574.90	[W/m^2-K]	Heat Transfer Coefficient at Ref. 1
HTC 2	2256.60	[W/m^2-K]	Heat Transfer Coefficient at Ref. 2
HTC 3	1830.69	[W/m^2-K]	Heat Transfer Coefficient at Ref. 3
HTC 4	4701.74	[W/m^2-K]	Heat Transfer Coefficient at Ref. 4
Nu 1	141.81	[-]	Nusselt Number at Ref. 1
Nu 2	89.51	[-]	Nusselt Number at Ref. 2
Nu 3	72.62	[-]	Nusselt Number at Ref. 3
Nu 4	186.50	[-]	Nusselt Number at Ref. 4

Table C.73 Experimentally measured data for Test 36

	Value	Units	Description
Q_{Heater}	226.7	[W]	Heater Input Power
MFR	3.03	[g/s]	Measured Mass Flow Rate
Θ	75.00	[°]	Azimuthal Position
T1	222.08	[°C]	Embedded TC Ref. 1 in brass
T2	235.65	[°C]	Embedded TC Ref. 2 in brass
T3	241.67	[°C]	Embedded TC Ref. 3 in brass
T4	243.75	[°C]	Embedded TC Ref. 4 in brass
T5	288.81	[°C]	TC Ref. 5 in copper "neck"
T6	302.11	[°C]	TC Ref. 6 in copper "neck"
T7	314.07	[°C]	TC Ref. 7 in copper "neck"
T8	365.20	[°C]	TC Ref. 8 in copper (maximum)
T9	365.20	[°C]	TC Ref. 9 in copper (maximum)
T_{in}	20.23	[°C]	Inlet Temperature
T_{out}	78.65	[°C]	Outlet Temperature
P_{in}	730.84	[kPa]	Inlet Pressure
P_{out}	716.16	[kPa]	Outlet Pressure

Table C.74 Calculated quantities for Test 36

	Value	Units	Description
$T1_{Surface}$	222.08	[°C]	Surface TC Ref. 1 in brass
$T2_{Surface}$	232.58	[°C]	Surface TC Ref. 2 in brass
$T3_{Surface}$	237.74	[°C]	Surface TC Ref. 3 in brass
$T4_{Surface}$	238.85	[°C]	Surface TC Ref. 4 in brass
$T_{Brazing}$	281.23	[°C]	Brazing Surface Temperature
dP	14.69	[kPa]	Pressure Drop
$Q_{Balance}$	178.61	[W]	Energy Balance
% Losses	21.20%	[-]	Energy Loss
$q''_{nominal}$	1.00	[MW/m^2]	Nominal Heat Flux
$q''_{experiment}$	0.90	[MW/m^2]	Measured Heat Flux
$q''_{FLUENT\ 1}$	0.22	[MW/m^2]	FLUENT Heat Flux at Ref. 1
$q''_{FLUENT\ 2}$	0.38	[MW/m^2]	FLUENT Heat Flux at Ref. 2
$q''_{FLUENT\ 3}$	0.61	[MW/m^2]	FLUENT Heat Flux at Ref. 3
$q''_{FLUENT\ 4}$	1.03	[MW/m^2]	FLUENT Heat Flux at Ref. 4
HTC 1	1089.91	[W/m^2-K]	Heat Transfer Coefficient at Ref. 1
HTC 2	1789.51	[W/m^2-K]	Heat Transfer Coefficient at Ref. 2
HTC 3	2804.51	[W/m^2-K]	Heat Transfer Coefficient at Ref. 3
HTC 4	4711.41	[W/m^2-K]	Heat Transfer Coefficient at Ref. 4
Nu 1	43.23	[-]	Nusselt Number at Ref. 1
Nu 2	70.98	[-]	Nusselt Number at Ref. 2
Nu 3	111.25	[-]	Nusselt Number at Ref. 3
Nu 4	186.89	[-]	Nusselt Number at Ref. 4

Table C.75 Experimentally measured data for Test 37

	Value	Units	Description
Q_{Heater}	226.9	[W]	Heater Input Power
MFR	3.03	[g/s]	Measured Mass Flow Rate
Θ	90.00	[°]	Azimuthal Position
T1	221.80	[°C]	Embedded TC Ref. 1 in brass
T2	235.75	[°C]	Embedded TC Ref. 2 in brass
T3	241.55	[°C]	Embedded TC Ref. 3 in brass
T4	243.62	[°C]	Embedded TC Ref. 4 in brass
T5	288.65	[°C]	TC Ref. 5 in copper "neck"
T6	301.92	[°C]	TC Ref. 6 in copper "neck"
T7	313.87	[°C]	TC Ref. 7 in copper "neck"
T8	364.96	[°C]	TC Ref. 8 in copper (maximum)
T9	365.00	[°C]	TC Ref. 9 in copper (maximum)
T_{in}	20.41	[°C]	Inlet Temperature
T_{out}	78.40	[°C]	Outlet Temperature
P_{in}	730.84	[kPa]	Inlet Pressure
P_{out}	716.43	[kPa]	Outlet Pressure

Table C.76 Calculated quantities for Test 37

	Value	Units	Description
$T1_{Surface}$	221.41	[°C]	Surface TC Ref. 1 in brass
$T2_{Surface}$	231.86	[°C]	Surface TC Ref. 2 in brass
$T3_{Surface}$	237.28	[°C]	Surface TC Ref. 3 in brass
$T4_{Surface}$	238.72	[°C]	Surface TC Ref. 4 in brass
$T_{Brazing}$	281.08	[°C]	Brazing Surface Temperature
dP	14.41	[kPa]	Pressure Drop
$Q_{Balance}$	177.29	[W]	Energy Balance
% Losses	21.87%	[-]	Energy Loss
$q''_{nominal}$	1.00	[MW/m^2]	Nominal Heat Flux
$q''_{experiment}$	0.89	[MW/m^2]	Measured Heat Flux
$q''_{FLUENT\ 1}$	0.38	[MW/m^2]	FLUENT Heat Flux at Ref. 1
$q''_{FLUENT\ 2}$	0.67	[MW/m^2]	FLUENT Heat Flux at Ref. 2
$q''_{FLUENT\ 3}$	0.77	[MW/m^2]	FLUENT Heat Flux at Ref. 3
$q''_{FLUENT\ 4}$	1.03	[MW/m^2]	FLUENT Heat Flux at Ref. 4
HTC 1	1890.56	[W/m^2-K]	Heat Transfer Coefficient at Ref. 1
HTC 2	3168.57	[W/m^2-K]	Heat Transfer Coefficient at Ref. 2
HTC 3	3550.47	[W/m^2-K]	Heat Transfer Coefficient at Ref. 3
HTC 4	4718.10	[W/m^2-K]	Heat Transfer Coefficient at Ref. 4
Nu 1	74.99	[-]	Nusselt Number at Ref. 1
Nu 2	125.69	[-]	Nusselt Number at Ref. 2
Nu 3	140.84	[-]	Nusselt Number at Ref. 3
Nu 4	187.15	[-]	Nusselt Number at Ref. 4

Table C.77 Experimentally measured data for Test 38

	Value	Units	Description
Q_{Heater}	226.8	[W]	Heater Input Power
MFR	3.03	[g/s]	Measured Mass Flow Rate
Θ	105.00	[°]	Azimuthal Position
T1	221.99	[°C]	Embedded TC Ref. 1 in brass
T2	235.80	[°C]	Embedded TC Ref. 2 in brass
T3	241.60	[°C]	Embedded TC Ref. 3 in brass
T4	243.66	[°C]	Embedded TC Ref. 4 in brass
T5	288.62	[°C]	TC Ref. 5 in copper "neck"
T6	301.88	[°C]	TC Ref. 6 in copper "neck"
T7	313.82	[°C]	TC Ref. 7 in copper "neck"
T8	364.85	[°C]	TC Ref. 8 in copper (maximum)
T9	364.86	[°C]	TC Ref. 9 in copper (maximum)
T_{in}	20.45	[°C]	Inlet Temperature
T_{out}	78.32	[°C]	Outlet Temperature
P_{in}	730.84	[kPa]	Inlet Pressure
P_{out}	714.50	[kPa]	Outlet Pressure

Table C.78 Calculated quantities for Test 38

	Value	Units	Description
$T1_{Surface}$	221.99	[°C]	Surface TC Ref. 1 in brass
$T2_{Surface}$	232.64	[°C]	Surface TC Ref. 2 in brass
$T3_{Surface}$	237.79	[°C]	Surface TC Ref. 3 in brass
$T4_{Surface}$	238.76	[°C]	Surface TC Ref. 4 in brass
$T_{Brazing}$	281.06	[°C]	Brazing Surface Temperature
dP	16.34	[kPa]	Pressure Drop
$Q_{Balance}$	176.92	[W]	Energy Balance
% Losses	22.00%	[-]	Energy Loss
$q''_{nominal}$	1.00	[MW/m^2]	Nominal Heat Flux
$q''_{experiment}$	0.89	[MW/m^2]	Measured Heat Flux
$q''_{FLUENT\ 1}$	0.22	[MW/m^2]	FLUENT Heat Flux at Ref. 1
$q''_{FLUENT\ 2}$	0.38	[MW/m^2]	FLUENT Heat Flux at Ref. 2
$q''_{FLUENT\ 3}$	0.61	[MW/m^2]	FLUENT Heat Flux at Ref. 3
$q''_{FLUENT\ 4}$	1.03	[MW/m^2]	FLUENT Heat Flux at Ref. 4
HTC 1	1091.58	[W/m^2-K]	Heat Transfer Coefficient at Ref. 1
HTC 2	1790.87	[W/m^2-K]	Heat Transfer Coefficient at Ref. 2
HTC 3	2806.70	[W/m^2-K]	Heat Transfer Coefficient at Ref. 3
HTC 4	4718.10	[W/m^2-K]	Heat Transfer Coefficient at Ref. 4
Nu 1	43.30	[-]	Nusselt Number at Ref. 1
Nu 2	71.04	[-]	Nusselt Number at Ref. 2
Nu 3	111.33	[-]	Nusselt Number at Ref. 3
Nu 4	187.15	[-]	Nusselt Number at Ref. 4

Table C.79 Experimentally measured data for Test 39

	Value	Units	Description
Q_{Heater}	227.1	[W]	Heater Input Power
MFR	3.03	[g/s]	Measured Mass Flow Rate
Θ	120.00	[°]	Azimuthal Position
T1	222.81	[°C]	Embedded TC Ref. 1 in brass
T2	236.19	[°C]	Embedded TC Ref. 2 in brass
T3	241.91	[°C]	Embedded TC Ref. 3 in brass
T4	243.96	[°C]	Embedded TC Ref. 4 in brass
T5	288.79	[°C]	TC Ref. 5 in copper "neck"
T6	302.02	[°C]	TC Ref. 6 in copper "neck"
T7	313.91	[°C]	TC Ref. 7 in copper "neck"
T8	364.85	[°C]	TC Ref. 8 in copper (maximum)
T9	364.86	[°C]	TC Ref. 9 in copper (maximum)
T_{in}	20.41	[°C]	Inlet Temperature
T_{out}	78.39	[°C]	Outlet Temperature
P_{in}	730.84	[kPa]	Inlet Pressure
P_{out}	711.33	[kPa]	Outlet Pressure

Table C.80 Calculated quantities for Test 39

	Value	Units	Description
$T1_{Surface}$	221.69	[°C]	Surface TC Ref. 1 in brass
$T2_{Surface}$	232.96	[°C]	Surface TC Ref. 2 in brass
$T3_{Surface}$	238.57	[°C]	Surface TC Ref. 3 in brass
$T4_{Surface}$	239.06	[°C]	Surface TC Ref. 4 in brass
$T_{Brazing}$	281.25	[°C]	Brazing Surface Temperature
dP	19.51	[kPa]	Pressure Drop
$Q_{Balance}$	177.26	[W]	Energy Balance
% Losses	21.93%	[-]	Energy Loss
$q''_{nominal}$	1.00	[MW/m^2]	Nominal Heat Flux
$q''_{experiment}$	0.89	[MW/m^2]	Measured Heat Flux
$q''_{FLUENT\ 1}$	0.72	[MW/m^2]	FLUENT Heat Flux at Ref. 1
$q''_{FLUENT\ 2}$	0.48	[MW/m^2]	FLUENT Heat Flux at Ref. 2
$q''_{FLUENT\ 3}$	0.40	[MW/m^2]	FLUENT Heat Flux at Ref. 3
$q''_{FLUENT\ 4}$	1.03	[MW/m^2]	FLUENT Heat Flux at Ref. 4
HTC 1	3577.09	[W/m^2-K]	Heat Transfer Coefficient at Ref. 1
HTC 2	2258.26	[W/m^2-K]	Heat Transfer Coefficient at Ref. 2
HTC 3	1833.56	[W/m^2-K]	Heat Transfer Coefficient at Ref. 3
HTC 4	4710.77	[W/m^2-K]	Heat Transfer Coefficient at Ref. 4
Nu 1	141.89	[-]	Nusselt Number at Ref. 1
Nu 2	89.58	[-]	Nusselt Number at Ref. 2
Nu 3	72.73	[-]	Nusselt Number at Ref. 3
Nu 4	186.86	[-]	Nusselt Number at Ref. 4

Table C.81 Experimentally measured data for Test 40

	Value	Units	Description
Q_{Heater}	226.6	[W]	Heater Input Power
MFR	4.05	[g/s]	Measured Mass Flow Rate
Θ	0.00	[°]	Azimuthal Position
T1	190.50	[°C]	Embedded TC Ref. 1 in brass
T2	204.10	[°C]	Embedded TC Ref. 2 in brass
T3	209.90	[°C]	Embedded TC Ref. 3 in brass
T4	211.90	[°C]	Embedded TC Ref. 4 in brass
T5	257.90	[°C]	TC Ref. 5 in copper "neck"
T6	271.10	[°C]	TC Ref. 6 in copper "neck"
T7	283.00	[°C]	TC Ref. 7 in copper "neck"
T8	333.50	[°C]	TC Ref. 8 in copper (maximum)
T9	333.50	[°C]	TC Ref. 9 in copper (maximum)
T_{in}	20.60	[°C]	Inlet Temperature
T_{out}	65.40	[°C]	Outlet Temperature
P_{in}	723.95	[kPa]	Inlet Pressure
P_{out}	688.79	[kPa]	Outlet Pressure

Table C.82 Calculated quantities for Test 40

	Value	Units	Description
$T1_{Surface}$	189.93	[°C]	Surface TC Ref. 1 in brass
$T2_{Surface}$	201.24	[°C]	Surface TC Ref. 2 in brass
$T3_{Surface}$	207.12	[°C]	Surface TC Ref. 3 in brass
$T4_{Surface}$	206.71	[°C]	Surface TC Ref. 4 in brass
$T_{Brazing}$	250.37	[°C]	Brazing Surface Temperature
dP	35.16	[kPa]	Pressure Drop
$Q_{Balance}$	183.07	[W]	Energy Balance
% Losses	19.21%	[-]	Energy Loss
$q''_{nominal}$	1.00	[MW/m^2]	Nominal Heat Flux
$q''_{experiment}$	0.89	[MW/m^2]	Measured Heat Flux
$q''_{FLUENT\ 1}$	0.81	[MW/m^2]	FLUENT Heat Flux at Ref. 1
$q''_{FLUENT\ 2}$	0.52	[MW/m^2]	FLUENT Heat Flux at Ref. 2
$q''_{FLUENT\ 3}$	0.47	[MW/m^2]	FLUENT Heat Flux at Ref. 3
$q''_{FLUENT\ 4}$	1.10	[MW/m^2]	FLUENT Heat Flux at Ref. 4
HTC 1	4797.70	[W/m^2-K]	Heat Transfer Coefficient at Ref. 1
HTC 2	2886.64	[W/m^2-K]	Heat Transfer Coefficient at Ref. 2
HTC 3	2526.61	[W/m^2-K]	Heat Transfer Coefficient at Ref. 3
HTC 4	5910.58	[W/m^2-K]	Heat Transfer Coefficient at Ref. 4
Nu 1	190.31	[-]	Nusselt Number at Ref. 1
Nu 2	114.50	[-]	Nusselt Number at Ref. 2
Nu 3	100.22	[-]	Nusselt Number at Ref. 3
Nu 4	234.45	[-]	Nusselt Number at Ref. 4

Table C.83 Experimentally measured data for Test 41

	Value	Units	Description
Q_{Heater}	226.6	[W]	Heater Input Power
MFR	4.05	[g/s]	Measured Mass Flow Rate
Θ	15.00	[°]	Azimuthal Position
T1	190.70	[°C]	Embedded TC Ref. 1 in brass
T2	204.30	[°C]	Embedded TC Ref. 2 in brass
T3	210.20	[°C]	Embedded TC Ref. 3 in brass
T4	212.20	[°C]	Embedded TC Ref. 4 in brass
T5	258.40	[°C]	TC Ref. 5 in copper "neck"
T6	271.50	[°C]	TC Ref. 6 in copper "neck"
T7	283.40	[°C]	TC Ref. 7 in copper "neck"
T8	334.00	[°C]	TC Ref. 8 in copper (maximum)
T9	334.00	[°C]	TC Ref. 9 in copper (maximum)
T_{in}	20.60	[°C]	Inlet Temperature
T_{out}	65.40	[°C]	Outlet Temperature
P_{in}	723.95	[kPa]	Inlet Pressure
P_{out}	690.17	[kPa]	Outlet Pressure

Table C.84 Calculated quantities for Test 41

	Value	Units	Description
$T1_{Surface}$	190.88	[°C]	Surface TC Ref. 1 in brass
$T2_{Surface}$	201.87	[°C]	Surface TC Ref. 2 in brass
$T3_{Surface}$	207.15	[°C]	Surface TC Ref. 3 in brass
$T4_{Surface}$	207.01	[°C]	Surface TC Ref. 4 in brass
$T_{Brazing}$	250.90	[°C]	Brazing Surface Temperature
dP	33.78	[kPa]	Pressure Drop
$Q_{Balance}$	183.07	[W]	Energy Balance
% Losses	19.21%	[-]	Energy Loss
$q''_{nominal}$	1.00	[MW/m^2]	Nominal Heat Flux
$q''_{experiment}$	0.89	[MW/m^2]	Measured Heat Flux
$q''_{FLUENT\ 1}$	0.26	[MW/m^2]	FLUENT Heat Flux at Ref. 1
$q''_{FLUENT\ 2}$	0.44	[MW/m^2]	FLUENT Heat Flux at Ref. 2
$q''_{FLUENT\ 3}$	0.60	[MW/m^2]	FLUENT Heat Flux at Ref. 3
$q''_{FLUENT\ 4}$	1.10	[MW/m^2]	FLUENT Heat Flux at Ref. 4
HTC 1	1497.51	[W/m^2-K]	Heat Transfer Coefficient at Ref. 1
HTC 2	2427.26	[W/m^2-K]	Heat Transfer Coefficient at Ref. 2
HTC 3	3216.35	[W/m^2-K]	Heat Transfer Coefficient at Ref. 3
HTC 4	5901.07	[W/m^2-K]	Heat Transfer Coefficient at Ref. 4
Nu 1	59.40	[-]	Nusselt Number at Ref. 1
Nu 2	96.28	[-]	Nusselt Number at Ref. 2
Nu 3	127.58	[-]	Nusselt Number at Ref. 3
Nu 4	234.08	[-]	Nusselt Number at Ref. 4

Table C.85 Experimentally measured data for Test 42

	Value	Units	Description
Q_{Heater}	226.1	[W]	Heater Input Power
MFR	4.05	[g/s]	Measured Mass Flow Rate
Θ	30.00	[°]	Azimuthal Position
T1	191.00	[°C]	Embedded TC Ref. 1 in brass
T2	204.90	[°C]	Embedded TC Ref. 2 in brass
T3	210.50	[°C]	Embedded TC Ref. 3 in brass
T4	212.50	[°C]	Embedded TC Ref. 4 in brass
T5	258.70	[°C]	TC Ref. 5 in copper "neck"
T6	271.80	[°C]	TC Ref. 6 in copper "neck"
T7	283.80	[°C]	TC Ref. 7 in copper "neck"
T8	334.40	[°C]	TC Ref. 8 in copper (maximum)
T9	334.40	[°C]	TC Ref. 9 in copper (maximum)
T_{in}	20.60	[°C]	Inlet Temperature
T_{out}	65.40	[°C]	Outlet Temperature
P_{in}	723.95	[kPa]	Inlet Pressure
P_{out}	691.54	[kPa]	Outlet Pressure

Table C.86 Calculated quantities for Test 42

	Value	Units	Description
$T1_{Surface}$	190.71	[°C]	Surface TC Ref. 1 in brass
$T2_{Surface}$	201.80	[°C]	Surface TC Ref. 2 in brass
$T3_{Surface}$	207.08	[°C]	Surface TC Ref. 3 in brass
$T4_{Surface}$	207.31	[°C]	Surface TC Ref. 4 in brass
$T_{Brazing}$	251.17	[°C]	Brazing Surface Temperature
dP	32.41	[kPa]	Pressure Drop
$Q_{Balance}$	183.07	[W]	Energy Balance
% Losses	19.03%	[-]	Energy Loss
$q''_{nominal}$	1.00	[MW/m^2]	Nominal Heat Flux
$q''_{experiment}$	0.89	[MW/m^2]	Measured Heat Flux
$q''_{FLUENT\ 1}$	0.41	[MW/m^2]	FLUENT Heat Flux at Ref. 1
$q''_{FLUENT\ 2}$	0.68	[MW/m^2]	FLUENT Heat Flux at Ref. 2
$q''_{FLUENT\ 3}$	0.79	[MW/m^2]	FLUENT Heat Flux at Ref. 3
$q''_{FLUENT\ 4}$	1.10	[MW/m^2]	FLUENT Heat Flux at Ref. 4
HTC 1	2410.23	[W/m^2-K]	Heat Transfer Coefficient at Ref. 1
HTC 2	3752.84	[W/m^2-K]	Heat Transfer Coefficient at Ref. 2
HTC 3	4236.49	[W/m^2-K]	Heat Transfer Coefficient at Ref. 3
HTC 4	5891.58	[W/m^2-K]	Heat Transfer Coefficient at Ref. 4
Nu 1	95.61	[-]	Nusselt Number at Ref. 1
Nu 2	148.86	[-]	Nusselt Number at Ref. 2
Nu 3	168.05	[-]	Nusselt Number at Ref. 3
Nu 4	233.70	[-]	Nusselt Number at Ref. 4

Table C.87 Experimentally measured data for Test 43

	Value	Units	Description
Q_{Heater}	227.3	[W]	Heater Input Power
MFR	4.05	[g/s]	Measured Mass Flow Rate
Θ	45.00	[°]	Azimuthal Position
T1	190.90	[°C]	Embedded TC Ref. 1 in brass
T2	204.80	[°C]	Embedded TC Ref. 2 in brass
T3	210.60	[°C]	Embedded TC Ref. 3 in brass
T4	212.50	[°C]	Embedded TC Ref. 4 in brass
T5	258.80	[°C]	TC Ref. 5 in copper "neck"
T6	272.00	[°C]	TC Ref. 6 in copper "neck"
T7	283.90	[°C]	TC Ref. 7 in copper "neck"
T8	334.70	[°C]	TC Ref. 8 in copper (maximum)
T9	334.70	[°C]	TC Ref. 9 in copper (maximum)
T_{in}	20.60	[°C]	Inlet Temperature
T_{out}	65.30	[°C]	Outlet Temperature
P_{in}	723.95	[kPa]	Inlet Pressure
P_{out}	691.54	[kPa]	Outlet Pressure

Table C.88 Calculated quantities for Test 43

	Value	Units	Description
$T1_{Surface}$	191.08	[°C]	Surface TC Ref. 1 in brass
$T2_{Surface}$	202.05	[°C]	Surface TC Ref. 2 in brass
$T3_{Surface}$	207.20	[°C]	Surface TC Ref. 3 in brass
$T4_{Surface}$	207.31	[°C]	Surface TC Ref. 4 in brass
$T_{Brazing}$	251.27	[°C]	Brazing Surface Temperature
dP	32.41	[kPa]	Pressure Drop
$Q_{Balance}$	182.66	[W]	Energy Balance
% Losses	19.64%	[-]	Energy Loss
$q''_{nominal}$	1.00	[MW/m^2]	Nominal Heat Flux
$q''_{experiment}$	0.89	[MW/m^2]	Measured Heat Flux
$q''_{FLUENT\ 1}$	0.26	[MW/m^2]	FLUENT Heat Flux at Ref. 1
$q''_{FLUENT\ 2}$	0.44	[MW/m^2]	FLUENT Heat Flux at Ref. 2
$q''_{FLUENT\ 3}$	0.60	[MW/m^2]	FLUENT Heat Flux at Ref. 3
$q''_{FLUENT\ 4}$	1.10	[MW/m^2]	FLUENT Heat Flux at Ref. 4
HTC 1	1495.75	[W/m^2-K]	Heat Transfer Coefficient at Ref. 1
HTC 2	2424.87	[W/m^2-K]	Heat Transfer Coefficient at Ref. 2
HTC 3	3215.43	[W/m^2-K]	Heat Transfer Coefficient at Ref. 3
HTC 4	5891.58	[W/m^2-K]	Heat Transfer Coefficient at Ref. 4
Nu 1	59.33	[-]	Nusselt Number at Ref. 1
Nu 2	96.19	[-]	Nusselt Number at Ref. 2
Nu 3	127.55	[-]	Nusselt Number at Ref. 3
Nu 4	233.70	[-]	Nusselt Number at Ref. 4

Table C.89 Experimentally measured data for Test 44

	Value	Units	Description
Q_{Heater}	227.3	[W]	Heater Input Power
MFR	4.05	[g/s]	Measured Mass Flow Rate
Θ	60.00	[°]	Azimuthal Position
T1	191.30	[°C]	Embedded TC Ref. 1 in brass
T2	204.70	[°C]	Embedded TC Ref. 2 in brass
T3	210.70	[°C]	Embedded TC Ref. 3 in brass
T4	212.60	[°C]	Embedded TC Ref. 4 in brass
T5	259.00	[°C]	TC Ref. 5 in copper "neck"
T6	272.20	[°C]	TC Ref. 6 in copper "neck"
T7	284.10	[°C]	TC Ref. 7 in copper "neck"
T8	335.00	[°C]	TC Ref. 8 in copper (maximum)
T9	335.00	[°C]	TC Ref. 9 in copper (maximum)
T_{in}	20.50	[°C]	Inlet Temperature
T_{out}	66.00	[°C]	Outlet Temperature
P_{in}	723.95	[kPa]	Inlet Pressure
P_{out}	692.23	[kPa]	Outlet Pressure

Table C.90 Calculated quantities for Test 44

	Value	Units	Description
$T1_{Surface}$	190.47	[°C]	Surface TC Ref. 1 in brass
$T2_{Surface}$	201.63	[°C]	Surface TC Ref. 2 in brass
$T3_{Surface}$	207.82	[°C]	Surface TC Ref. 3 in brass
$T4_{Surface}$	207.41	[°C]	Surface TC Ref. 4 in brass
$T_{Brazing}$	251.47	[°C]	Brazing Surface Temperature
dP	31.72	[kPa]	Pressure Drop
$Q_{Balance}$	185.93	[W]	Energy Balance
% Losses	18.20%	[-]	Energy Loss
$q''_{nominal}$	1.00	[MW/m^2]	Nominal Heat Flux
$q''_{experiment}$	0.89	[MW/m^2]	Measured Heat Flux
$q''_{FLUENT\ 1}$	0.81	[MW/m^2]	FLUENT Heat Flux at Ref. 1
$q''_{FLUENT\ 2}$	0.52	[MW/m^2]	FLUENT Heat Flux at Ref. 2
$q''_{FLUENT\ 3}$	0.47	[MW/m^2]	FLUENT Heat Flux at Ref. 3
$q''_{FLUENT\ 4}$	1.10	[MW/m^2]	FLUENT Heat Flux at Ref. 4
HTC 1	4765.49	[W/m^2-K]	Heat Transfer Coefficient at Ref. 1
HTC 2	2870.90	[W/m^2-K]	Heat Transfer Coefficient at Ref. 2
HTC 3	2509.04	[W/m^2-K]	Heat Transfer Coefficient at Ref. 3
HTC 4	5885.28	[W/m^2-K]	Heat Transfer Coefficient at Ref. 4
Nu 1	189.03	[-]	Nusselt Number at Ref. 1
Nu 2	113.88	[-]	Nusselt Number at Ref. 2
Nu 3	99.53	[-]	Nusselt Number at Ref. 3
Nu 4	233.45	[-]	Nusselt Number at Ref. 4

Table C.91 Experimentally measured data for Test 45

	Value	Units	Description
Q_{Heater}	226.0	[W]	Heater Input Power
MFR	4.05	[g/s]	Measured Mass Flow Rate
Θ	75.00	[°]	Azimuthal Position
T1	191.80	[°C]	Embedded TC Ref. 1 in brass
T2	205.00	[°C]	Embedded TC Ref. 2 in brass
T3	211.00	[°C]	Embedded TC Ref. 3 in brass
T4	213.00	[°C]	Embedded TC Ref. 4 in brass
T5	259.30	[°C]	TC Ref. 5 in copper "neck"
T6	272.50	[°C]	TC Ref. 6 in copper "neck"
T7	284.50	[°C]	TC Ref. 7 in copper "neck"
T8	335.30	[°C]	TC Ref. 8 in copper (maximum)
T9	335.30	[°C]	TC Ref. 9 in copper (maximum)
T_{in}	20.30	[°C]	Inlet Temperature
T_{out}	65.10	[°C]	Outlet Temperature
P_{in}	723.95	[kPa]	Inlet Pressure
P_{out}	692.92	[kPa]	Outlet Pressure

Table C.92 Calculated quantities for Test 45

	Value	Units	Description
$T1_{Surface}$	191.98	[°C]	Surface TC Ref. 1 in brass
$T2_{Surface}$	202.25	[°C]	Surface TC Ref. 2 in brass
$T3_{Surface}$	207.60	[°C]	Surface TC Ref. 3 in brass
$T4_{Surface}$	207.81	[°C]	Surface TC Ref. 4 in brass
$T_{Brazing}$	251.74	[°C]	Brazing Surface Temperature
dP	31.03	[kPa]	Pressure Drop
$Q_{Balance}$	183.07	[W]	Energy Balance
% Losses	18.99%	[-]	Energy Loss
$q''_{nominal}$	1.00	[MW/m^2]	Nominal Heat Flux
$q''_{experiment}$	0.89	[MW/m^2]	Measured Heat Flux
$q''_{FLUENT\ 1}$	0.26	[MW/m^2]	FLUENT Heat Flux at Ref. 1
$q''_{FLUENT\ 2}$	0.44	[MW/m^2]	FLUENT Heat Flux at Ref. 2
$q''_{FLUENT\ 3}$	0.60	[MW/m^2]	FLUENT Heat Flux at Ref. 3
$q''_{FLUENT\ 4}$	1.10	[MW/m^2]	FLUENT Heat Flux at Ref. 4
HTC 1	1485.30	[W/m^2-K]	Heat Transfer Coefficient at Ref. 1
HTC 2	2418.21	[W/m^2-K]	Heat Transfer Coefficient at Ref. 2
HTC 3	3203.42	[W/m^2-K]	Heat Transfer Coefficient at Ref. 3
HTC 4	5866.45	[W/m^2-K]	Heat Transfer Coefficient at Ref. 4
Nu 1	58.92	[-]	Nusselt Number at Ref. 1
Nu 2	95.92	[-]	Nusselt Number at Ref. 2
Nu 3	127.07	[-]	Nusselt Number at Ref. 3
Nu 4	232.70	[-]	Nusselt Number at Ref. 4

Table C.93 Experimentally measured data for Test 46

	Value	Units	Description
Q_{Heater}	226.3	[W]	Heater Input Power
MFR	4.05	[g/s]	Measured Mass Flow Rate
Θ	90.00	[°]	Azimuthal Position
T1	191.40	[°C]	Embedded TC Ref. 1 in brass
T2	205.10	[°C]	Embedded TC Ref. 2 in brass
T3	210.90	[°C]	Embedded TC Ref. 3 in brass
T4	212.90	[°C]	Embedded TC Ref. 4 in brass
T5	259.30	[°C]	TC Ref. 5 in copper "neck"
T6	272.50	[°C]	TC Ref. 6 in copper "neck"
T7	284.50	[°C]	TC Ref. 7 in copper "neck"
T8	335.40	[°C]	TC Ref. 8 in copper (maximum)
T9	335.40	[°C]	TC Ref. 9 in copper (maximum)
T_{in}	20.30	[°C]	Inlet Temperature
T_{out}	64.90	[°C]	Outlet Temperature
P_{in}	723.95	[kPa]	Inlet Pressure
P_{out}	693.61	[kPa]	Outlet Pressure

Table C.94 Calculated quantities for Test 46

	Value	Units	Description
$T1_{Surface}$	191.11	[°C]	Surface TC Ref. 1 in brass
$T2_{Surface}$	202.00	[°C]	Surface TC Ref. 2 in brass
$T3_{Surface}$	207.48	[°C]	Surface TC Ref. 3 in brass
$T4_{Surface}$	207.71	[°C]	Surface TC Ref. 4 in brass
$T_{Brazing}$	251.74	[°C]	Brazing Surface Temperature
dP	30.34	[kPa]	Pressure Drop
$Q_{Balance}$	182.26	[W]	Energy Balance
% Losses	19.46%	[-]	Energy Loss
$q''_{nominal}$	1.00	[MW/m^2]	Nominal Heat Flux
$q''_{experiment}$	0.89	[MW/m^2]	Measured Heat Flux
$q''_{FLUENT\ 1}$	0.41	[MW/m^2]	FLUENT Heat Flux at Ref. 1
$q''_{FLUENT\ 2}$	0.68	[MW/m^2]	FLUENT Heat Flux at Ref. 2
$q''_{FLUENT\ 3}$	0.79	[MW/m^2]	FLUENT Heat Flux at Ref. 3
$q''_{FLUENT\ 4}$	1.10	[MW/m^2]	FLUENT Heat Flux at Ref. 4
HTC 1	2400.36	[W/m^2-K]	Heat Transfer Coefficient at Ref. 1
HTC 2	3742.51	[W/m^2-K]	Heat Transfer Coefficient at Ref. 2
HTC 3	4220.65	[W/m^2-K]	Heat Transfer Coefficient at Ref. 3
HTC 4	5869.58	[W/m^2-K]	Heat Transfer Coefficient at Ref. 4
Nu 1	95.21	[-]	Nusselt Number at Ref. 1
Nu 2	148.45	[-]	Nusselt Number at Ref. 2
Nu 3	167.42	[-]	Nusselt Number at Ref. 3
Nu 4	232.83	[-]	Nusselt Number at Ref. 4

Table C.95 Experimentally measured data for Test 47

	Value	Units	Description
Q_{Heater}	227.0	[W]	Heater Input Power
MFR	4.05	[g/s]	Measured Mass Flow Rate
Θ	105.00	[°]	Azimuthal Position
T1	192.20	[°C]	Embedded TC Ref. 1 in brass
T2	205.70	[°C]	Embedded TC Ref. 2 in brass
T3	211.50	[°C]	Embedded TC Ref. 3 in brass
T4	213.50	[°C]	Embedded TC Ref. 4 in brass
T5	259.80	[°C]	TC Ref. 5 in copper "neck"
T6	273.00	[°C]	TC Ref. 6 in copper "neck"
T7	284.90	[°C]	TC Ref. 7 in copper "neck"
T8	335.70	[°C]	TC Ref. 8 in copper (maximum)
T9	335.70	[°C]	TC Ref. 9 in copper (maximum)
T_{in}	20.30	[°C]	Inlet Temperature
T_{out}	64.80	[°C]	Outlet Temperature
P_{in}	723.95	[kPa]	Inlet Pressure
P_{out}	690.17	[kPa]	Outlet Pressure

Table C.96 Calculated quantities for Test 47

	Value	Units	Description
$T1_{Surface}$	192.38	[°C]	Surface TC Ref. 1 in brass
$T2_{Surface}$	203.27	[°C]	Surface TC Ref. 2 in brass
$T3_{Surface}$	208.45	[°C]	Surface TC Ref. 3 in brass
$T4_{Surface}$	208.31	[°C]	Surface TC Ref. 4 in brass
$T_{Brazing}$	252.27	[°C]	Brazing Surface Temperature
dP	33.78	[kPa]	Pressure Drop
$Q_{Balance}$	181.85	[W]	Energy Balance
% Losses	19.89%	[-]	Energy Loss
$q''_{nominal}$	1.00	[MW/m^2]	Nominal Heat Flux
$q''_{experiment}$	0.89	[MW/m^2]	Measured Heat Flux
$q''_{FLUENT\ 1}$	0.26	[MW/m^2]	FLUENT Heat Flux at Ref. 1
$q''_{FLUENT\ 2}$	0.44	[MW/m^2]	FLUENT Heat Flux at Ref. 2
$q''_{FLUENT\ 3}$	0.60	[MW/m^2]	FLUENT Heat Flux at Ref. 3
$q''_{FLUENT\ 4}$	1.10	[MW/m^2]	FLUENT Heat Flux at Ref. 4
HTC 1	1481.84	[W/m^2-K]	Heat Transfer Coefficient at Ref. 1
HTC 2	2404.71	[W/m^2-K]	Heat Transfer Coefficient at Ref. 2
HTC 3	3189.00	[W/m^2-K]	Heat Transfer Coefficient at Ref. 3
HTC 4	5850.85	[W/m^2-K]	Heat Transfer Coefficient at Ref. 4
Nu 1	58.78	[-]	Nusselt Number at Ref. 1
Nu 2	95.39	[-]	Nusselt Number at Ref. 2
Nu 3	126.50	[-]	Nusselt Number at Ref. 3
Nu 4	232.08	[-]	Nusselt Number at Ref. 4

Table C.97 Experimentally measured data for Test 48

	Value	Units	Description
Q_{Heater}	226.3	[W]	Heater Input Power
MFR	4.05	[g/s]	Measured Mass Flow Rate
Θ	120.00	[°]	Azimuthal Position
T1	192.80	[°C]	Embedded TC Ref. 1 in brass
T2	205.80	[°C]	Embedded TC Ref. 2 in brass
T3	211.60	[°C]	Embedded TC Ref. 3 in brass
T4	213.60	[°C]	Embedded TC Ref. 4 in brass
T5	259.90	[°C]	TC Ref. 5 in copper "neck"
T6	273.10	[°C]	TC Ref. 6 in copper "neck"
T7	285.00	[°C]	TC Ref. 7 in copper "neck"
T8	335.80	[°C]	TC Ref. 8 in copper (maximum)
T9	335.80	[°C]	TC Ref. 9 in copper (maximum)
T_{in}	20.30	[°C]	Inlet Temperature
T_{out}	64.80	[°C]	Outlet Temperature
P_{in}	723.95	[kPa]	Inlet Pressure
P_{out}	690.17	[kPa]	Outlet Pressure

Table C.98 Calculated quantities for Test 48

	Value	Units	Description
$T1_{Surface}$	192.23	[°C]	Surface TC Ref. 1 in brass
$T2_{Surface}$	202.94	[°C]	Surface TC Ref. 2 in brass
$T3_{Surface}$	208.82	[°C]	Surface TC Ref. 3 in brass
$T4_{Surface}$	208.41	[°C]	Surface TC Ref. 4 in brass
$T_{Brazing}$	252.37	[°C]	Brazing Surface Temperature
dP	33.78	[kPa]	Pressure Drop
$Q_{Balance}$	181.85	[W]	Energy Balance
% Losses	19.64%	[-]	Energy Loss
$q''_{nominal}$	1.00	[MW/m^2]	Nominal Heat Flux
$q''_{experiment}$	0.89	[MW/m^2]	Measured Heat Flux
$q''_{FLUENT\ 1}$	0.81	[MW/m^2]	FLUENT Heat Flux at Ref. 1
$q''_{FLUENT\ 2}$	0.52	[MW/m^2]	FLUENT Heat Flux at Ref. 2
$q''_{FLUENT\ 3}$	0.47	[MW/m^2]	FLUENT Heat Flux at Ref. 3
$q''_{FLUENT\ 4}$	1.10	[MW/m^2]	FLUENT Heat Flux at Ref. 4
HTC 1	4711.19	[W/m^2-K]	Heat Transfer Coefficient at Ref. 1
HTC 2	2847.13	[W/m^2-K]	Heat Transfer Coefficient at Ref. 2
HTC 3	2493.10	[W/m^2-K]	Heat Transfer Coefficient at Ref. 3
HTC 4	5847.74	[W/m^2-K]	Heat Transfer Coefficient at Ref. 4
Nu 1	186.88	[-]	Nusselt Number at Ref. 1
Nu 2	112.94	[-]	Nusselt Number at Ref. 2
Nu 3	98.89	[-]	Nusselt Number at Ref. 3
Nu 4	231.96	[-]	Nusselt Number at Ref. 4

BIBLIOGRAPHY

1. W. Meier, F. Najmabadi, J. Schmidt, and J. Sheffield, "Role of fusion energy in a sustainable global energy strategy," 2001, http://fire.pppl.gove/energy_us_wec01.pdf

2. B. T. Shellabarger, "Experimental Studies of High-speed Liquid Films on Flat and Curved Downward-facing Surfaces for IFE Applications," 2003, Master's thesis, Georgia Institute of Technology.

3. L. Crosatti, et. al, "Experimental and Numerical Investigation of the Thermal Performance of Gas-Cooled T-Tube Divertor Modules," 17th TOFE Meeting, Albuquerque, NM, 11/14/2006.

4. T. Ihli, "He-cooled Divertor Development in the EU: The Helium Jet cooled Divertor HEMJ," ARIES Meeting, General Atomics, San Diego, CA, 24-25 Feb. 2005.

5. P. Norajitra, et. al, "Status of He-cooled Divertor Development (PPCS Subtask TW4-TRP-001-D2, FZKA 7100, 2005.

6. C. B. Baxi and C.P.C. Wong, "Review of Helium Cooling for Fusion Reactor Applications," Fusion Engineering and Design 51 – 52, p 319-324, 2000.

7. D. Maisonnier et. al, "A Conceptual Study of Commercial Fusion Power Plants," EFDA, EFDA-RP-RE-5.0, April, 2005.

8. S. Hermsmeyer and K. Kleefeldt, "Review and Comparative Assessment of Helium-cooled Divertor Concepts." FZKA 6597, 2001.

9. S. Hermsmeyer and S. Malang, "Gas-cooled High Performance Divertor for a Power Plant," Fusion Engineering and Design, 61-62, 2002, p. 197-202

10. S. Malang and S. Hermsmeyer, "FZK-Concept of Helium-cooled Divertor Plates for Power Plants," PPCS Design Review Meeting He-cooled Divertor, Garching, 21 Nov, 2001.

11. L.V. Boccaccini et. al, "He-Cooled Divertor Concepts," US-Japan Workshop on Fusion Power Plants and Related Advanced Technologies, Tokyo, Japan, 11-13 Jan., 2005.

12. K. Kleefeldt and S. Gordeev, "Performance Limits of a Helium-Cooled Divertor (Unconventional Design)," FZKA 6401, 2000.

13. R. Kruessmann, P. Norajitra, et. al, "Conceptual Design of a He-cooled Divertor with Integrated Flow and Heat Transfer Promoters (PPCS Subtask TW3-TRP-001-D2, Part II Detailed Version, FZKA 6975, 2004.

14. F. Incropera and D. DeWitt, *Fundamentals of Heat and Mass Transfer*, p. 434, 5th Ed., John Wiley & Sons, Hoboken, NJ, 2002.

15. T. Ihli and A.R. Raffray, "He-cooled Divertor Design Approach," ARIES Meeting, General Atomics, Sand Diego, CA, 24-25 Feb. 2005.

16. P. Norajitra et al, "European Development of He-cooled Divertors for Fusion Power Plants," FZK

17. P.J. Karditsas and N.P. Taylor, "Thermal Fluid Finite Element Calculations for the European PPCS Divertor Concepts," 15th TOFE, 17-21 Nov. 2002, Washington DC.

18. P. Norajitra, et al, "Development of a Helium-cooled Divertor Concept: Design-Related Requirements on Material and Fabrication Technology," FZK

19. L. Crosatti, "Private Communication," 2007

20. B.R. Munson, D. F. Young, and T. H. Okiishi, *Fundamentals of Fluid Mechanics*, 4th Ed., John Wiley & Sons, Hoboken, NJ 2002.

21. Fluent, Version 6.2, "Computational Fluid Dynamics", Fluent Inc. 2004.

22. P. R. Bevington and D. Keith Robinson, *Data Reduction and Error Analysis for the Physical Sciences*, 3rd Ed., McGraw-Hill, New York City, 2003.

10/4/50
#2
Para 2 & 2

Elsevier Editorial System(tm) for Fusion Engineering and Design

Manuscript Draft

Manuscript Number:

Title: Development of Modular Helium-cooled Divertor for DEMO Based on the Multi-Jet Impingement (HEMJ) Concept: Experimental Validation of Thermal Performance

Article Type: ISFNT-8 Special Issue

Section/Category:

Keywords: Helium-cooled divertor, HEMJ concept, impingement cooling, experimental validation, CFD

Corresponding Author: Dr. Regina Kruessmann,

Corresponding Author's Institution: Forschungszentrum Karlsruhe

First Author: James B Weathers

Order of Authors: James B Weathers; Lorenzo Crosatti; Regina Kruessmann; Dennis L Sadowski; Said I Abdel-Khalik

Abstract: A modular helium-cooled divertor design based on the multi-jet impingement concept (HEMJ) that is capable of accommodating a surface heat flux of at least 10 MW/m2 has been developed at the Forschungszentrum Karlsruhe [1]. Thermal-hydraulic simulations used in the original design optimization process predicted extremely high local heat transfer coefficients (~50 kW/(m2-K)) [2]. This prompted an experimental investigation to validate the numerical results. A one-to-one scale test section of the HEMJ divertor reference geometry has undergone testing in an air flow loop under a wide range of operating conditions that include the Reynolds number of the actual helium-cooled HEMJ design. The temperature distribution and local heat transfer coefficients have been measured and compared to numerical predictions of the FLUENT CFD software package [3]. The experimental data closely match the numerical predictions. This comparison provides confidence in using the numerical model for the design of the HEMJ divertor, as

well as other gas-cooled high heat flux components. Future experiments will be performed using the same test module with helium cooling at prototypical Reynolds numbers.

ID #88 Kruessmann

Development of Modular Helium-cooled Divertor for DEMO Based on the Multi-Jet Impingement (HEMJ) Concept: Experimental Validation of Thermal Performance

J. B. Weathers[1], L. Crosatti[1], R. Kruessmann[2], D. L. Sadowski[1], S. I. Abdel-Khalik[1]

[1]G. W. Woodruff School of Mechanical Engineering, Georgia Institute of Technology, Atlanta, GA 30332-0405, USA
[2]Forschungszentrum Karlsruhe GmbH, Institut fuer Materialforschung III, P.O. Box 3640, 76021 Karlsruhe, Germany

Abstract

A modular helium-cooled divertor design based on the multi-jet impingement concept (HEMJ) that is capable of accommodating a surface heat flux of at least 10 MW/m^2 has been developed at the Forschungszentrum Karlsruhe [1]. Thermal-hydraulic simulations used in the original design optimization process predicted extremely high local heat transfer coefficients (~50 kW/(m^2-K)) [2]. This prompted an experimental investigation to validate the numerical results. A one-to-one scale test section of the HEMJ divertor reference geometry has undergone testing in an air flow loop under a wide range of operating conditions that include the Reynolds number of the actual helium-cooled HEMJ design. The temperature distribution and local heat transfer coefficients have been measured and compared to numerical predictions of the FLUENT CFD software package [3]. The experimental data closely match the numerical predictions. This comparison provides confidence in using the numerical model for the design of the HEMJ divertor, as well as other gas-cooled high heat flux components. Future experiments will be performed using the same test module with helium cooling at prototypical Reynolds numbers.

Keywords:

Helium-cooled divertor, HEMJ concept, impingement cooling, experimental validation, CFD

1 INTRODUCTION

The Helium-cooled Multi-Jet (HEMJ) divertor design relies on enhancement of the convective heat transfer coefficient through the use of multiple impinging jets. Predictions indicate that it is capable of withstanding the required incident heat load of 10 MW/m^2 on the divertor surface using helium with an inlet temperature of 634 °C and a pressure of 10.0 MPa [1].

According to the latest design studies for the "post-ITER" demonstration reactor (DEMO), the entire divertor is split into 48 cassettes which are separately cooled [4]. The plasma facing surfaces of the cassettes are divided into a number of cooling fingers to minimize the thermal stresses. Each cooling finger (Fig. 1) consists of a plasma-facing tungsten armor tile which is attached to a tungsten-alloy W-La_2O_3 (WL10) cap. A cylindrical steel cartridge that has twenty-four 0.6 mm diameter holes surrounding a single 1.0 mm diameter hole in its center is secured below the cap. Helium enters the cartridge and is accelerated through the holes to create jets which impinge on the capped inner surface of the tungsten alloy. Downstream of the jet impingement location, the helium forms a turbulent wall jet along the surface of the cap before it exits the cooling finger at approximately 700 °C.

Numerical and experimental analyses have been performed at FZK to characterize the divertor geometry, select appropriate materials, simulate heat removal capability, and develop manufacturing processes of the proposed HEMJ divertor [5]. Experimental tests of the HEMJ divertor are needed to validate the heat removal capability predicted by computational fluid dynamics (CFD) software packages, because the predicted values of the local convective heat transfer coefficient (~50 $kW/(m^2-K)$) near the impinging jets are "out of the experience base" for high power density gas-cooled engineering systems.

The experimental investigation is the focus of this paper. It will describe the experimental planning, apparatus, procedures, and numerical model used for this purpose. A comparison of the experimental and numerical results will be presented along with the conclusions obtained from this investigation.

A 1:1 test module that closely simulates the geometry and thermal-hydraulic behavior of the helium-cooled HEMJ divertor was designed, constructed, and instrumented for testing in an air flow loop at the Georgia Institute of Technology. The operating conditions of the air flow loop were selected to match the non-dimensional parameters expected for the DEMO reactor. The most important of these is the Reynolds number based on the 1.0 mm diameter central jet. It is defined as:

$$\mathrm{Re}_{jet} = \frac{\dot{m} D_{jet}}{A_{jets} \mu_{in}} \qquad (1)$$

Here, $\dot{m}$ is the mass flow rate, D_{jet} is the diameter of the central jet, A_{jet} is the cross section area of the jets, and μ_{in} is the coolant dynamic viscosity at the inlet.

The expected Reynolds number of the central jet corresponding to the nominal operating conditions is 21,600. An air mass flow rate of 3.03 g/s corresponds to it. Table 1 details the nominal operating conditions of the HEMJ divertor in the DEMO reactor and the air flow loop at the Georgia Institute of Technology. The difference between the Prandtl numbers of air (0.74) and helium (0.66) is deemed to have a small effect on the measured and predicted values of the convective heat transfer coefficient. Hence, validating the code using air data (and calculations) should adequately reflect the code's validity for the actual, helium-cooled case.

The air flow loop experiments spanned a range of mass flow rates from 2.0 g/s to 8.0 g/s (Reynolds number range 14,100 to 56,500). Experiments were performed with nominal incident heat fluxes of 0.8 MW/m^2 and 1.0 MW/m^2.

2 EXPERIMENTAL APPARATUS AND PROCEDURES

2.A Experimental Test Section

A test section design which yields a uniform surface heat flux on the armor top was constructed (Fig. 2). The test section combines the armor and cap pieces of the HEMJ divertor into a single unit of brass, called the thimble. The thermal conductivity of brass nearly matches that of WL10.

The uniform incident heat flux was achieved by using a 117 mm long cylindrical copper heater block which contracts from a 50 mm diameter region, containing an electric heater, to a 17 mm diameter "neck" region. In the "neck" region of the copper heater block, a very uniform radial temperature distribution and thus axial heat flux is created. The Magnesium-Oxide cartridge heater (Fast-Heat®) has a maximum output of 750 W. It is slip-fitted within a 15.9 mm diameter, 76.2 mm deep hole in the copper block. The power input to the heater (i.e., the heat flux incident on the thimble) is controlled by controlling the voltage to the heater with a variable autotransformer (Staco Energy Products 3PN1010V). The voltage and the current are measured with multimeters (Hewlett Packard 34401 A and Fluke 25). The 17 mm diameter end of the copper heater block is brazed to the top of the thimble using silver.

The jet cartridge (Fig. 3) was constructed from free machining brass C36000. Three 2.0 mm sectors extend from the bottom of the jet cartridge and are used to secure it in the 2.0 mm thimble indention to ensure a 0.9 mm gap between the top of the jet cartridge and the thimble. The jet cartridge is connected to the end of a 150 mm long tube made of 10.0 mm OD thin-walled SS 316 tubing using a high temperature epoxy.

The thimble is instrumented with four 0.5 mm diameter OMEGA Type-E thermocouples (TCs). The TCs are offset by 90° from each other (Fig. 3) to allow measurements of the cooled

surface temperature distribution. TC 1 (R = 6.4 mm, z = 8.26 mm) is aligned with a jet on the outermost "bolt" circle at the 0^{o} angular position. The remaining TCs are positioned at: TC 2 (R = 4.3 mm, z = 6.88mm), TC 3 (R = 2.1 mm, z = 6.36 mm), and TC 4 (R = 0 mm, z = 6.25 mm). All four TCs have a 0.5 mm distance between their embedded location and the convection-cooled surface of the thimble. The TC probes were secured by placing a thin layer of Rockwool™ insulation around the test section and tightly winding a nickel wire over the insulation. The thimble was screwed into a SS ½ inch diameter tee (Parker #8-8-8 FT) through which the jet cartridge and inlet tube were inserted.

Fig. 4 shows the jet cartridge (left) and test section (right) consisting of the tee, thimble, and copper heater block. The assembled HEMJ divertor test section is insulated with a 12.5 cm diameter cylinder of Rockwool™ that has the test section's profile carved out of its center. The insulation extends 5 cm beyond the height of the copper heater block.

2.B Air Flow Loop

The test section was placed in an air flow loop (Fig. 5). Air from a compressed-air line enters the flow loop at a controlled pressure of ~724 kPa. Temperature and pressure measurements are made at the inlet and exit of the test section. A needle valve is used to control the mass flow rate through the flow loop, which is determined by measuring the volumetric flow rate and density (pressure and temperature). The inlet and exit pressures are measured with an analog test gauge (Ashcroft AMC-4291) and a pressure transducer (Omega PX302-300AV), respectively. Two OMEGA Type-E TCs (EMQSS-020G-6) are used to measure the inlet and exit temperatures. The SS inlet tube and thus the jet cartridge are capable of rotating relative to the thimble and its fixed location TC probes. An angular scale and reference steel wire are used to indicate the angular position θ of the jet cartridge.

The air flows through a copper heat transfer coil before entering a positive displacement gas flowmeter (Rockwell International R-315). The temperature and pressure are measured at the inlet of the gas flowmeter with a TC (OMEGA Type-E) and a pressure transducer (OMEGA PX180-015GV) before being vented directly to the atmosphere.

The data acquisition system consists of a 60-channel data acquisition unit (Agilent 34970) which has three, 20-channels each, A/D cards (Agilent 34901A). It is connected to a PC through a RS-232 serial cable. The Agilent Bench Link Data Logger 3 software is used to configure the unit and monitor the data on the PC. Only steady state data are stored for each experiment.

3 NUMERICAL MODEL

The HEMJ divertor test section model (Fig. 6) used for the numerical studies includes all pertinent features of the experimental test section. The symmetry of the test section was used to reduce it to a half-model. The mesh was created using GAMBIT® 2.2 [6] and consists of nearly 1,500,000 cells (700,000 nodes). In regions of complex geometry, such as the jet cartridge head and tee, a tetragonal/hybrid mesh was used (Fig. 7). The computational fluid dynamics software package FLUENT® 6.2 [3] was used to perform the simulations.

All material parameters are given in Table 2. The heater power input, inlet mass flow rate, and outlet pressure are specified as boundary conditions based on their experimentally measured values for each test. Convective heat transfer coefficients based on natural convection between the outer insulation surface and the ambient were imposed to account for heat losses: 5 W/(m^2-K) with an ambient temperature of 20 °C on the outer insulation surface and 15 W/(m^2-K) and an ambient temperature of 68 °C on the insulation surface above the copper block were assumed. The boundary of the cartridge heater top and the ambient was given a constant temperature which was measured during each experiment.

The standard k- ε turbulence model with standard wall functions was used for the simulations. Convergence was determined when the order of magnitude for the residuals was at least 10^{-3} (10^{-7} for the energy equation). On average it took 6 hours for the solution to converge on a Pentium® IV 3.4 GHz workstation with 2 GB of RAM.

4 RESULTS AND DISCUSSION

A comparison between the experimental and numerical pressure drop across the test section is shown in Fig. 8. The solid line is the FLUENT® predicted pressure drop and the experimental data points represent power inputs of 182 W (◆) and 227 W (■). They correspond to a nominal heat flux incident on the thimble of 0.8 MW/m^2 and 1.0 MW/m^2, respectively. There is good agreement between the experimental and numerical pressure drop across the entire range of mass flow rates spanned in this investigation.

The local experimental jet impingement surface temperatures are calculated by correcting the embedded TC values for the temperature drop due to conduction between the embedded locations and the jet impingement surface. The temperature drop due to conduction is obtained from the FLUENT® model. Fig. 9 shows the agreement between the FLUENT® (dashed lines) and experimental surface temperatures for TC 1 (■), TC 2 (◆), TC 3 (▲), and TC 4 (●) over an angular extent of 60°. The experimental data shown was collected in 15° increments for a mass flow rate of 3.03 g/s (Re = 21,600) and a power input of 227 W. The results show that the jet impingement surface temperature remains nearly constant and is thus not affected by the location of the jets.

The local experimental heat transfer coefficient was calculated for the four surface locations corresponding to the four TC probes in the thimble. The experimentally calculated surface temperatures described above were used in this calculation along with the experimental

air inlet temperature. The heat flux on the jet impingement surface was determined from the numerical simulation by manually obtaining an average heat flux value in the vicinity of the desired surface point. The convective heat transfer coefficient was then calculated in the following manner:

$$h = \frac{q''_{surface}}{T_{surface} - T_{inlet}} \tag{2}$$

$$T_{surface} = T_{embedded} - \Delta T_{conduction} \tag{3}$$

The calculated values of heat flux were used to evaluate the experimental heat transfer coefficient since it is impossible to experimentally measure the local heat flux at each instrumented location. While this argument seems somewhat "circular," the fact remains that matching between the experimental and numerical surface temperatures is, by itself, a confirmation of the matching between the local heat transfer coefficients. Fig. 10 displays the experimental heat transfer coefficients for the locations of TC 1 (■), TC 2 (◆), TC 3 (▲), and TC 4 (●) with dashed lines representing the heat transfer coefficients based solely on numerical values for a mass flow rate of 3.03 g/s (Re = 21,600) and a power input of 227 W. The large variation in the heat transfer coefficient over the 60° angular extent shows that the local heat flux and thus the heat transfer coefficient is very sensitive to the location of the jets, while the surface temperatures are nearly independent of the angular position (Fig. 9). The agreement of the experimental and numerical heat transfer coefficient is strong for the full range of mass flow rates studied.

Fig. 11 represents experiments performed with a power input of 227 W and at the 0° angular position. The heat transfer coefficient is the highest near the surface under TC 4 (●) due to the central jet impinging directly upon it. In the 0° angular position, a jet is also directly

impinging on the surface immediately opposite to TC 1 (■), while TC 2 (◆) and TC 3 (▲) are positioned between the jets.

The ratio of conductivities between the helium and air operating conditions is approximately 13. Due to this difference in conductivity, a comparison under equal Nusselt numbers would yield an expected helium-cooled heat transfer coefficient on the order of 60,000 W/(m^2-K) for the reference location of TC 4 (●) with a mass flow rate 3.03 g/s (Re = 21,600) and a nominal incident heat flux of 1.0 MW/m^2.

5 CONCLUSIONS

This paper detailed the experimental heat transfer performance validation study of the Helium-cooled Multi-jet (HEMJ) divertor. The convective heat transfer coefficient predicted by computational fluid dynamics software packages with helium cooling at prototypical operating conditions is on the order of 50,000 W/(m^2-K), which necessitated experimental validation.

A 1 : 1 test section which simulates the thermal performance of the HEMJ divertor was designed, constructed, and instrumented for testing in an air flow loop. The operating conditions of the air flow loop were chosen to match the non-dimensional operating conditions expected for the HEMJ divertor in the "post-ITER" fusion power plant (DEMO). The air flow loop experiments were performed for mass flow rates of 2.0 g/s to 8.0 g/s and with incident nominal heat fluxes of 0.8 MW/m^2 and 1.0 MW/m^2. The angular variation of the heat transfer coefficient was also investigated. Numerical simulations which matched the experimental operating conditions were performed using the computational fluid dynamics software package, FLUENT® 6.2. Comparisons of the experimental and numerical pressure drop, temperature, and heat transfer coefficient were made. The experimental results agreed with the numerical predictions for all

operating conditions in this investigation. This provides a strong degree of confidence in using the FLUENT® software package to analyze the HEMJ divertor design.

ACKNOWLEDGEMENTS

This work, supported by the European Communities under the contract of association between EURATOM and Forschungszentrum Karlsruhe, was carried out within the framework of the European Fusion Development Agreement. The views and opinions expressed herein do not necessarily reflect those of the European Commission.

REFERENCES

[1] P. Norajitra et al., He-cooled Divertor for DEMO: Experimental Verification of the Conceptual Modular Design, Proceeding of the ISFTNT-7, May 22-27, 2005, Tokyo, Japan. Fusion Engineering and Design, 81 (1-7) 2006 341-346.

[2] FLUENT® 6.2.16, FLUENT Inc., 2005.

[3] R. Kruessmann, Parametric study to evaluate the design options of the HEMJ divertor cooling concept by CFD simulations (Task TW4-TRP-001). Internal Report, Forschungszentrum Karlsruhe, July 2006.

[4] P. Norajitra et al., Conceptual design of a He-cooled divertor with integrated flow and heat transfer promoters (PPCS subtask TW3-TRP-001-D2), Part II: Detailed Version. Forschungszentrum Karlsruhe, Wissenschaftliche Berichte, FZKA 6975, April 2004.

[5] P. Norajitra, et al, Status of He-cooled Divertor Development, PPCS Subtask TW4-TRP-001-D2, Forschungszentrum Karlsruhe, Wissenschaftliche Berichte, FZKA 7100, 2005.

[6] GAMBIT® 2.2.30, FLUENT Inc., 2006.

Corresponding Author:

Regina Kruessmann, Forschungszentrum Karlsruhe GmbH, Institute for Materials Research III, P. O. Box 36 40, 76021 Karlsruhe, Germany, regina.kruessmann@imf.fzk.de, Tel. +49 72 47 / 82 54 57, Fax +49 72 47 / 82 20 95

Figure captions

Fig. 1. The HEMJ layout [5].

Fig. 2. The HEMJ divertor test section.

Fig. 3. Thermocouple and jet locations for 0° (left) and 45° (right) rotations of the jet cartridge and in the brass thimble.

Fig. 4. Constructed jet cartridge (left) and test section (right) consisting of the tee, thimble, and copper heater block with a five dollarcent coin for scale.

Fig. 5. Diagram of the air flow loop.

Fig. 6. Cross-sectional view of the numerical model.

Fig. 7. Mesh of the jet cartridge head.

Fig. 8. Experimental and numerically predicted pressure drop across the test section. Solid line: FLUENT® prediction; experimental results for 182 W (◆) and 227 W (■) power input.

Fig. 9. Experimental (symbols) and numerical (dashed lines) results for the surface temperature (3.03 g/s and 227 W).

Fig. 10. Experimental (symbols) and numerical (dashed lines) results for h(θ) (3.03 g/s and 227 W).

Fig. 11. Mass flow rate versus h (0° angular position and 227 W power input), TC 1 (■), TC 2 (◆), TC 3 (▲), and TC 4 (●).

Figure

ID #88 Kruessmann

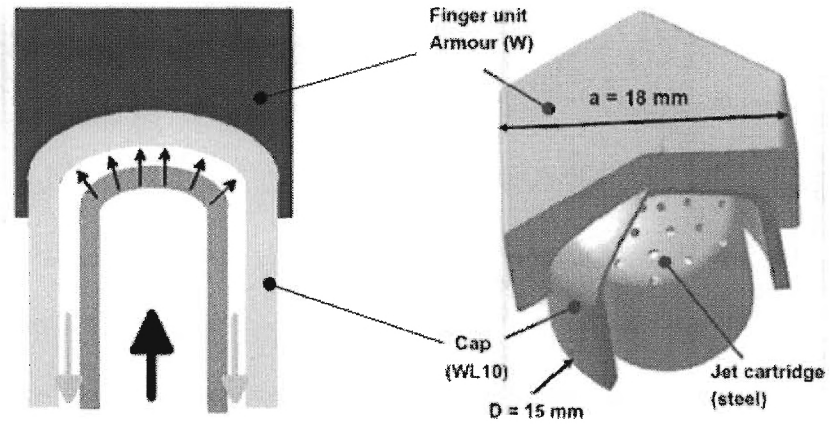

Fig. 1. The HEMJ layout [5]. (1/6)

Figure

ID #88 Kruessmann

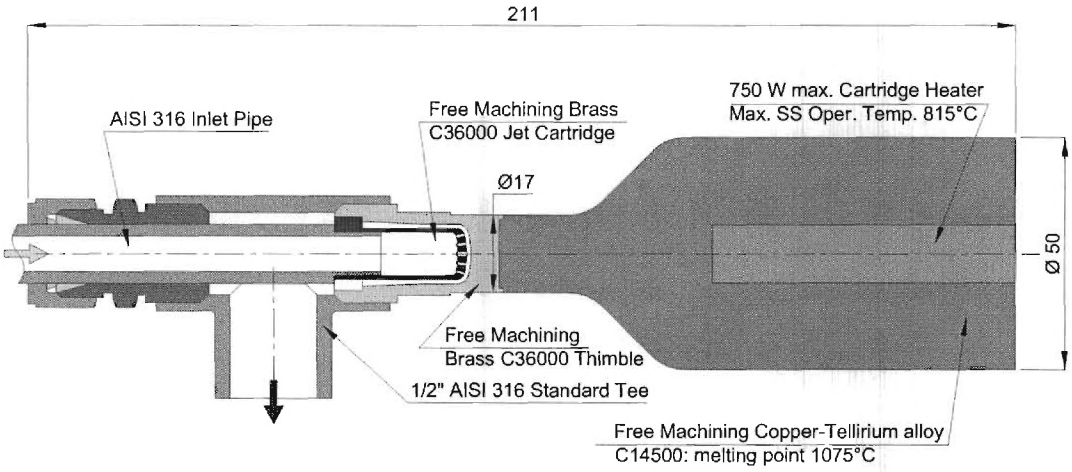

Fig. 2. The HEMJ divertor test section. (1/6)

Figure

#88 Kruessmann

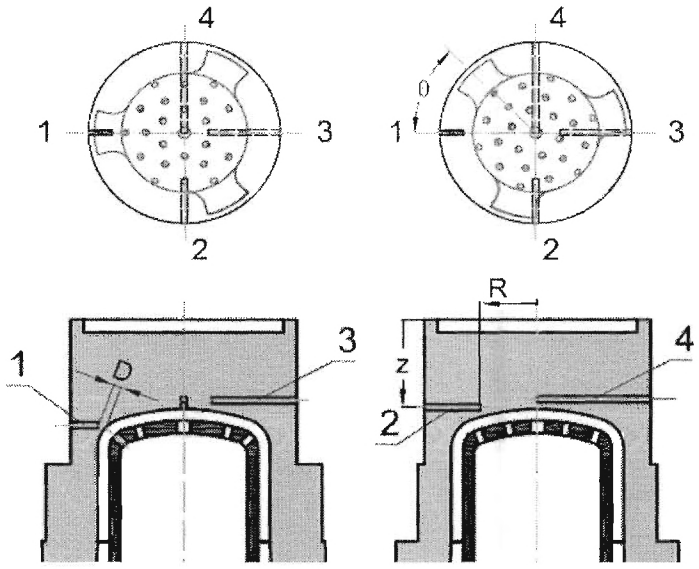

Fig. 3. Thermocouple and jet locations for 0° (left) and 45° (right) rotations of the jet cartridge and in the brass thimble. (1/6)

#88 Kruessmann

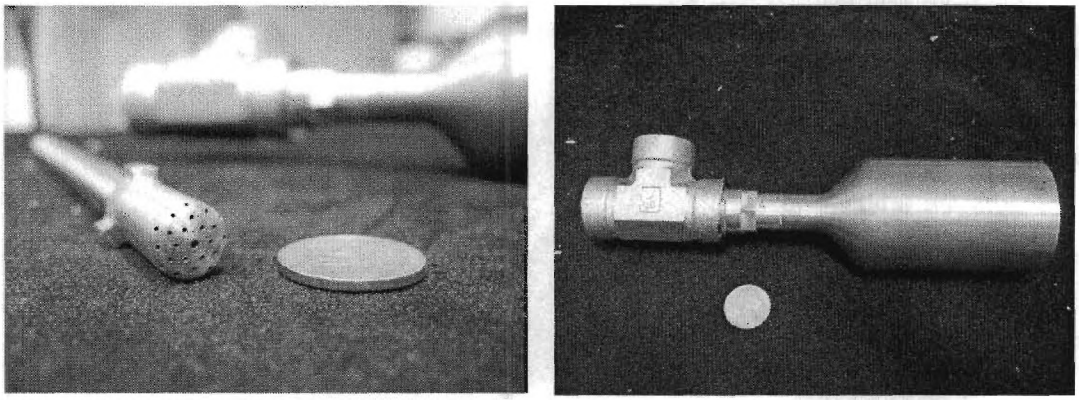

Fig. 4. Constructed jet cartridge (left) and test section (right) consisting of the tee, thimble, and copper heater block with a five cents coin for scale. (1/6)

Figure

#88 Kruessmann

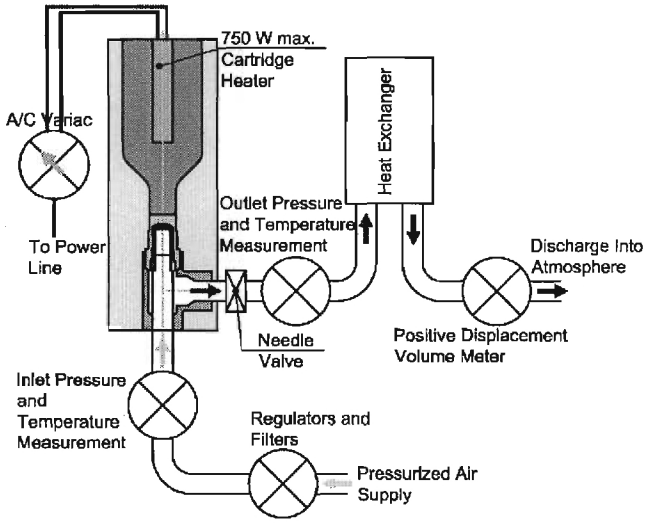

Fig. 5. Diagram of the air flow loop. (1/6)

Figure

#88 Kruessmann

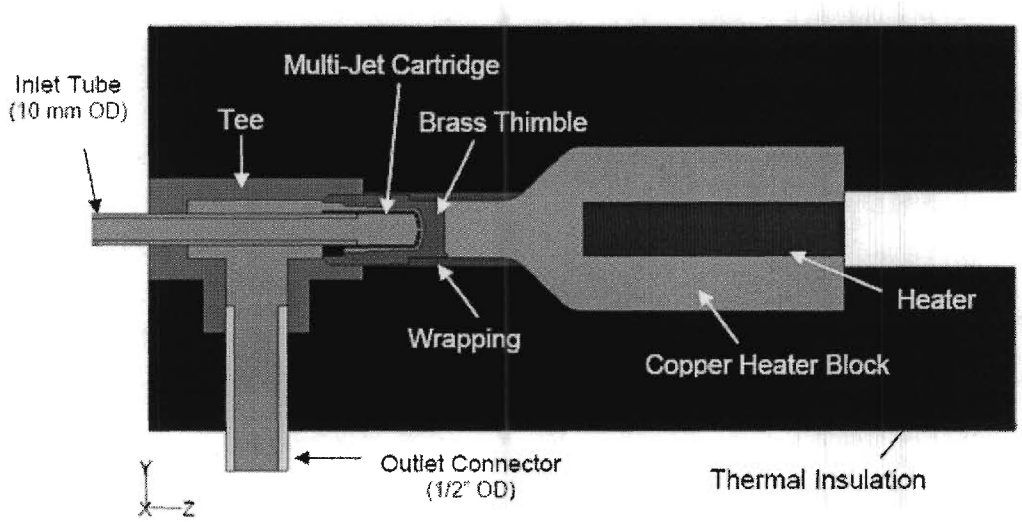

Fig. 6. Cross-sectional view of the numerical model. (1/6)

#88 Kruessmann

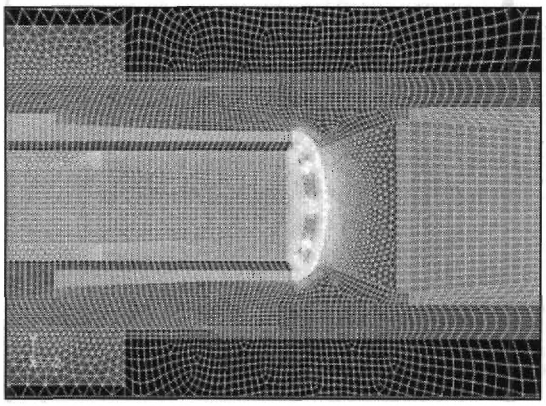

Fig. 7. Mesh of the jet cartridge head. (1/6)

Figure

#88 Kruessmann

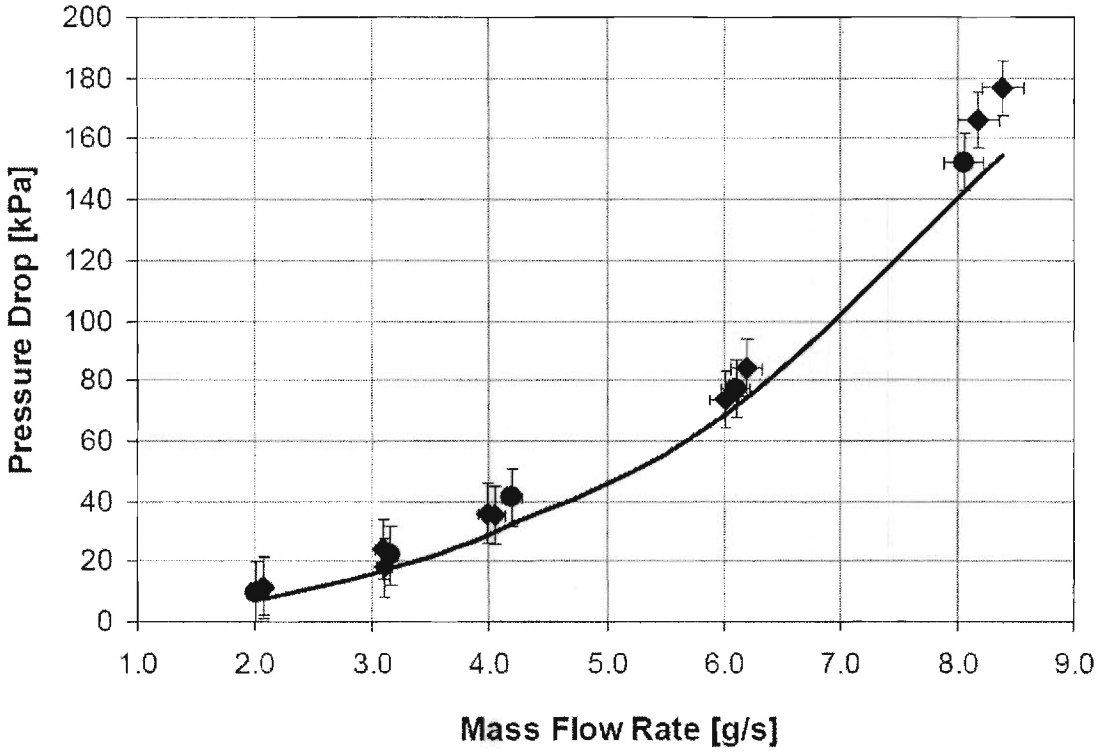

Fig. 8. Experimental and numerically predicted pressure drop across the test section. Solid line: FLUENT® prediction; experimental results for 182 W (◆) and 227 W (■) power input. (1/4)

Figure

#88 Kruessmann

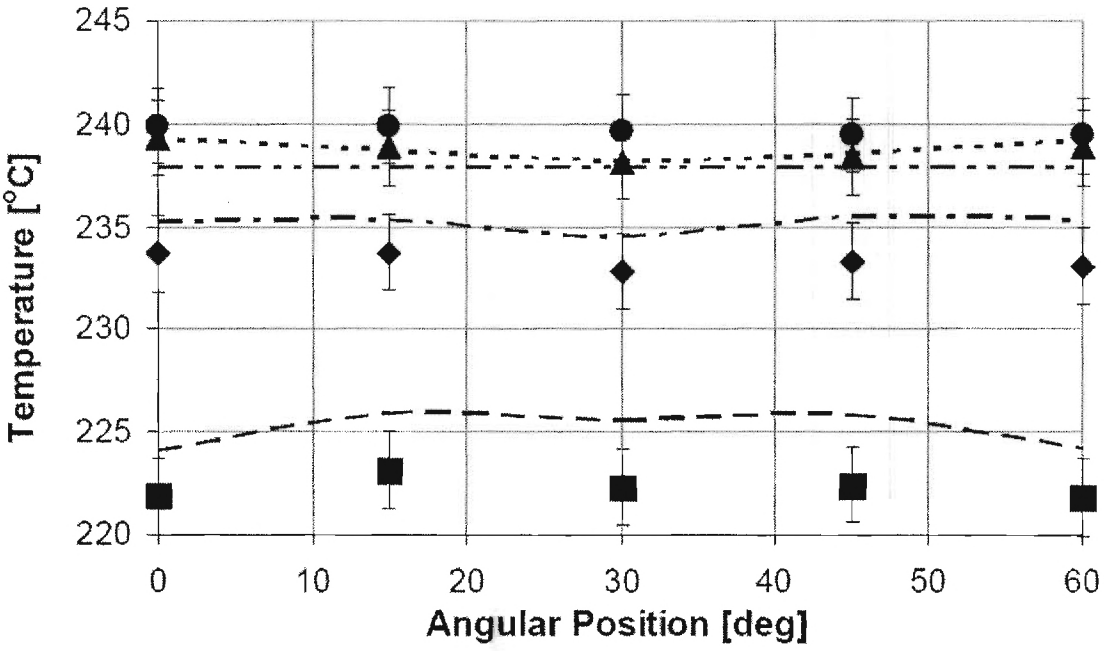

Fig. 9. Experimental (symbols) and numerical (dashed lines) results for the surface temperature (3.03 g/s and 227 W). (1/4)

Figure

#88 Kruessmann

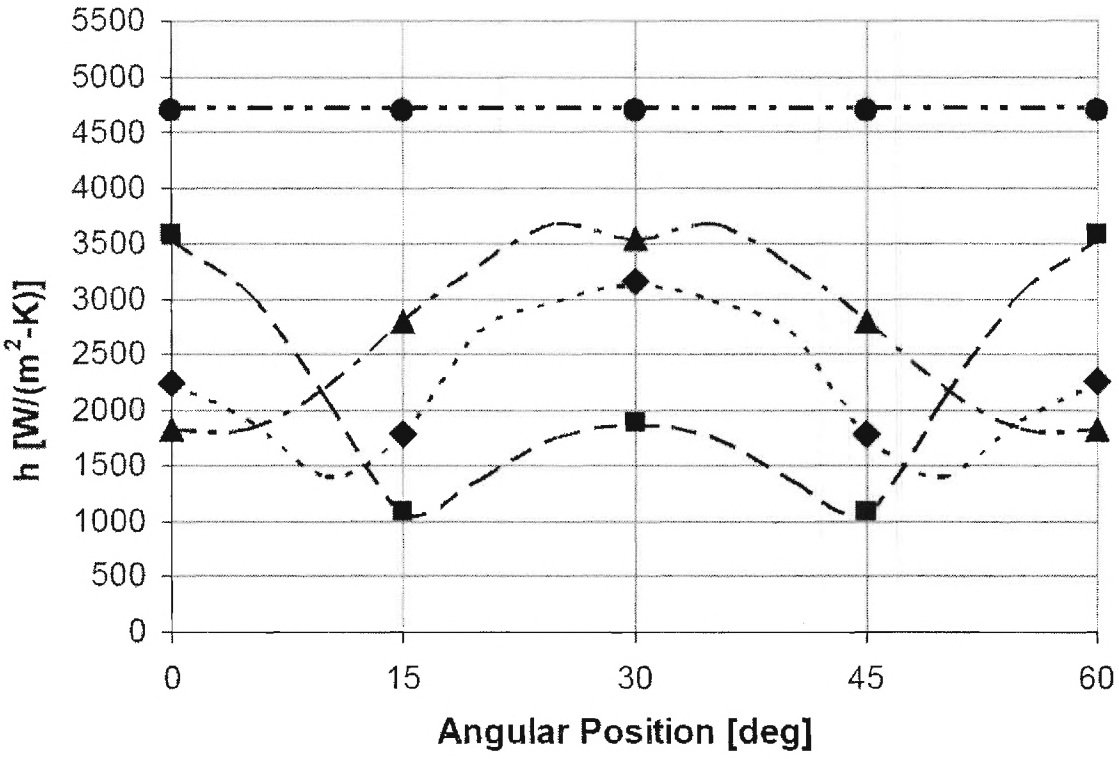

Fig. 10. Experimental (symbols) and numerical (dashed lines) results for h(θ) (3.03 g/s and 227 W). (1/4)

Figure

#88 Kruessmann

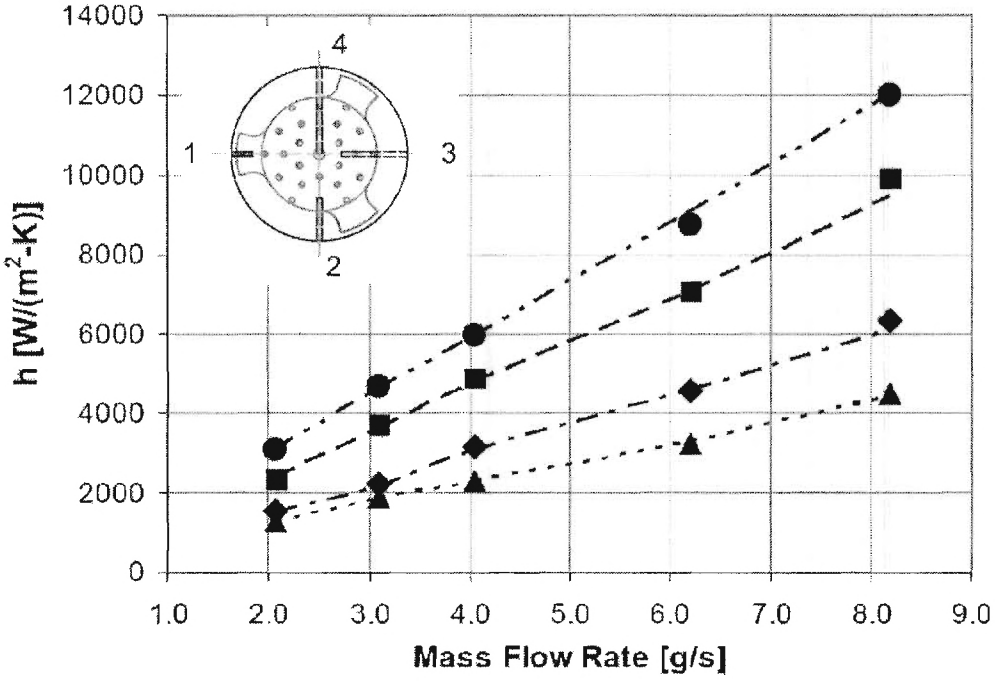

Fig. 11. Mass flow rate versus h (0° angular position and 227 W power input), TC 1 (■), TC 2 (◆), TC 3 (▲), and TC 4 (●). (1/4)

ID #88 Kruessmann

TABLE 1. Comparison of thermal-hydraulic parameters for the HEMJ Divertor. (1/6)

Parameter	DEMO (He)	Air
Inlet Temperature [°C]	634	20
Pressure [bar]	100	7.24
Dynamic Viscosity [kg/m-s x10^{-5}]	4.16	1.85
Re number [10^3]	21.6	14.1– 56.5
Pr number [-]	0.66	0.71
Mass Flow Rate [g/s]	6.8	2.0 – 8.0
Heat Flux [MW/m^2]	10.0	0.8 – 1.0

Table

ID #88 Kruessmann

TABLE 2. Material parameters. (1/6)

Material	**Density ρ**	**Thermal conductivity k**		**Specific heat c_p**
	[kg/m³]	[W/m-K]		[J/kg-K]
Steel AISI 316 SS (tee, inlet tube)	8027	16.26		502
Brass C36000 (thimble, outlet connector, jet cartridge)	8500	116		380
Rockwool, Rockwool Wrapping (insulation)	130	$0.0407-10^{-4}*T+3*10^{-7}*T^2$		840
Copper C14500 (bottle)	8940	354.8		376.8
Magnesium oxide (heater)	3580	T [K]	k [W/m-K]	877
		273	42	
		400	29	
		600	20	
		800	14	
		1000	11	